DESIGN AND OPTIMIZATION OF THERMAL MANAGEMENT APPROACHES IN DATA CENTER APPLICATIONS

by

RAJESH KASUKURTHY

DISSERTATION

Submitted in Partial Fulfillment of the Requirements
for the Degree of Doctor of Philosophy at
The University of Texas at Arlington
December 2019
Arlington, Texas

Supervising Committee:

Dereje Agonafer, Supervising Professor
Abdolhossein Haji-Sheikh
Miguel Amaya
Saket Karajgikar
Zeynep Celik- Butler

Acknowledgements

I would like to thank Dr. Dereje Agonafer for his continued support and guidance over the course of my doctoral degree at UTA. Without his resources and knowledge this would not have been possible. He is primarily responsible for encouraging me to work on industry-funded projects and understanding the importance of networking by attending conferences and workshops.

I would like to thank Dr. Abdolhossein Haji Sheikh, Dr. Miguel Amaya, and Dr. Zeynep Çelik-Butler for being on my committee and giving their valuable time in reviewing my work. I owe a great deal of gratitude to Dr. Saket Karajgikar of Facebook Inc. for not only serving as an external committee member, but also being my mentor when I did my internship at Facebook Inc. twice. As a former member of the EMNSPC, he was a constant source of encouragement. I would like to take this opportunity to thank industry mentors Mark Seymour, Steven Schon, Andrew Cole and others from ES2 I/UCRC who helped me develop my industrial pace and apply theoretical knowledge to present day industrial applications.

I would like to acknowledge my family (Mother: Siva Nagendramma Kasukurthy, Sister: Mukunda Priya Kasukurthy) for believing in me and send overseas for my studies. I would not be who I am today without your love and support. My Father (Subbaiah Kasukurthy), who is no longer with us, is responsible for who I am today.

I would like to thank all the people I met at EMNSPC and for their support during my time at UTA. Special thanks to Sally Thompson, Janet Gober, Lanie Gordon, Flora Pinegar, Ayesha Fatima, Wendy Ryan, Kathy Priester, Debi Barton, Catherine Gruebbel, and many others for assisting me in almost everything. You all have been wonderful. Mike Baker thanks for giving me a hard time, I learned a lot.

I would like to thank my friends, for their support and valuable advices throughout my time at UTA.

November 7, 2019

I would like to dedicate my Ph.D.
Dissertation

To

My Mother

For her unconditional love, endless support and encouragement, I know how much you worked hard to see me in this position, I am always grateful to you.

My sister

I always wanted to be a role model for her. She always supported me on my journey. I know she is always proud of me as I am proud of her being my sister.

November 7, 2019

Abstract

DESIGN AND OPTIMIZATION OF THERMAL MANAGEMENT APPROACHES IN DATA CENTER APPLICATIONS

Rajesh Kasukurthy, Ph.D.

The University of Texas at Arlington, 2019

Supervising Professor: Dereje Agonafer

In the present day to day life, Internet of Things (IOT) is everything, i.e., Internet and telecommunication is needed for almost every task of our life, which require data centers. These data centers provide various facilities such as, data processing, storage, transmission, maintenance, operations etc., To perform these tasks, a huge amount of power is consumed, which in turn generates large amount of heat. As these data centers are to be made operational throughout the year, cooling of data centers is of utmost importance. The continued increase in heat flux at the chip level due to new and robust technology nodes following Moore's law is starting to push the boundaries of existing cooling technologies especially for high end servers. Electronics cooling research is facing the challenges of high heat flux removal and increased pumping power. Not much attention has been focused on server and module level cooling. Present study focuses on two innovative methods in cooling:

- Dynamic cold plates at the server level
- Air flow path optimization at data center level.

Dynamic cold plates can be very efficient means of heat reduction and uniform distribution for high power electronics like servers. When high-power electronics with non-uniform temperature distribution are cooled using traditional cooling methods, they give rise to localized regions of high temperature known as 'hot spots', the main failure regions of the devices. Novel techniques which bring uniform cooling need to be investigated and employed. One such solution is dynamic cooling, which employs a self-regulated flow control device to regular the flow of the liquid coolant towards different sections of the electronic device according to cooling requirements. This approach eliminates actuators, sensors, transducer and control module which make the system complex and reduce its reliability. The proposed Flow Control Device (FCD) uses a one-way nitinol spring coupled with stainless-steel spring that can sense the heat load and change the flow rate of coolant to each section of the electronic device.

One of the major issues of data centers is non uniform cooling of its server racks owing many reasons like the position of cooling air guiding shafts and their angles, fan power and pressure drop across the air flow path. Optimization of air flow path results in uniform cooling of server racks as well as significantly low power consumption of the cooling system. The present study focuses on a data center model, identifying the changes in flow of air from 6SigmaRoom simulation of it. Different design changes to bring uniformity in air flow across the racks have been proposed. Modifying and introducing different flow guiding features into the design such as the angle of the cooling air guide shaft and employing a porous plate are tested using CFD to bring uniformity in air flow.

Table of Contents

Table of Illustrations

List of Tables

CHAPTER 1

INTRODUCTION

1.1 Internet of Things

A data center is a facility that houses IT equipment used for data processing, storage and transmission. Data that is used in day to day activities of Internet of Things. A thing, in the Internet of Things, can be a person with a heart monitor implant, a farm animal with a biochip transponder, an automobile that has built-in sensors to alert the driver when tire pressure is low or any other natural or man-made object that can be assigned an IP address and provided with the ability to transfer data over a network [1].

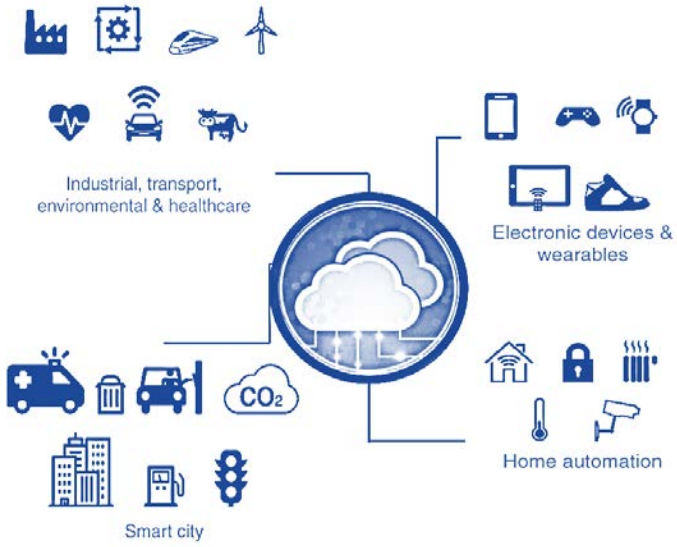

Figure 1-1: Internet of Things in our daily life

These data centers are kept secured in tightly controlled environment to make it run throughout the year. To maintain the controlled environment a lot of energy is used by the air conditioning systems.

1.2 Data Center

The data center industry has experienced significant growth over the past decade with the introduction, expansion and wide use of on-line banking, cloud computing, internet entertainment and social networking services. It was reported that data centers account for around 2% of the total national electricity consumption in 2016 [2].

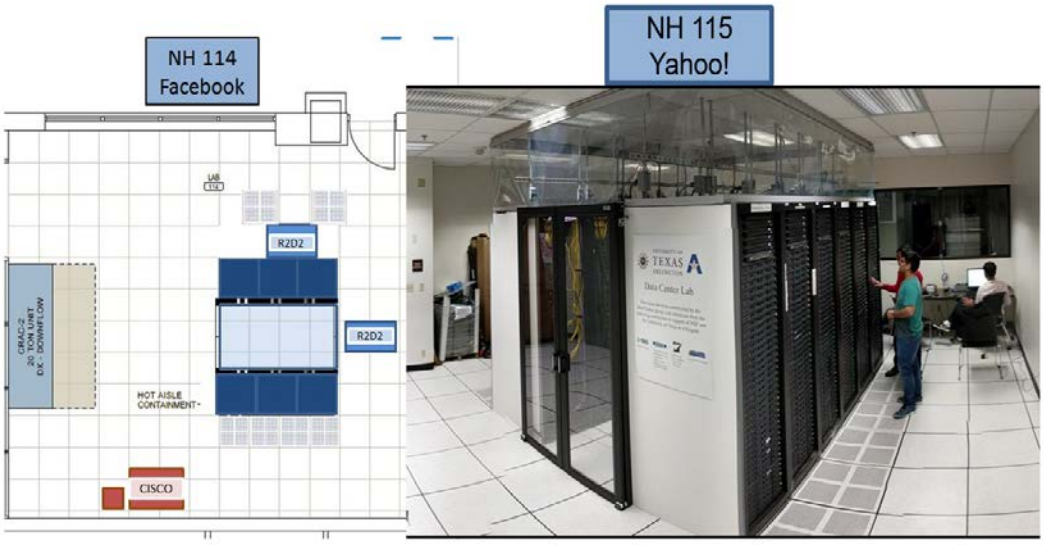

Figure 1-2: Data Center facilities at UTA

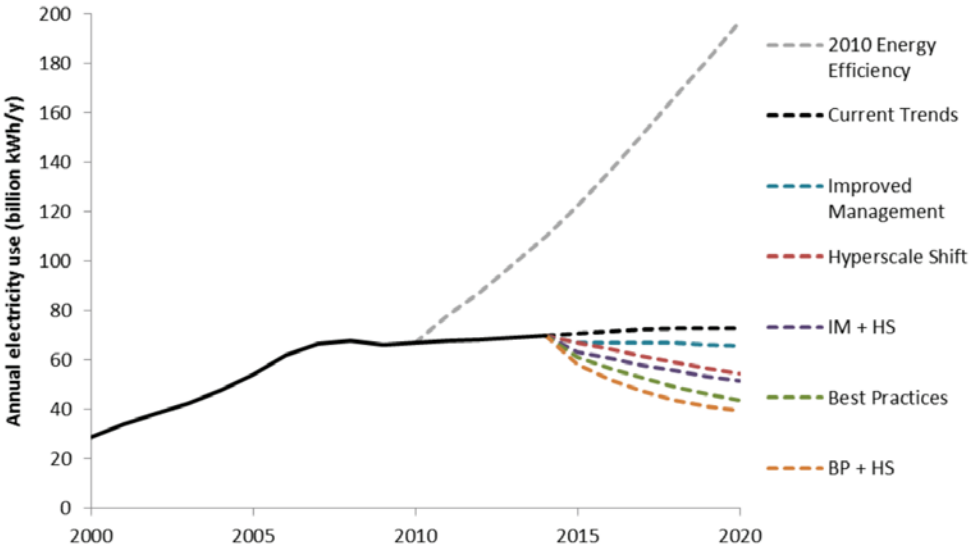

Figure 1-3 Present trends in data center energy consumption [2]

The parasitic loads namely cooling and power distribution account for a considerable amount of whole data center power consumption. It has become imperative that energy savings and efficiencies be pursued in the cooling and power distribution components at various levels within the data center facility. The need for energy-efficiency has coincided with continuing trends of increasing microprocessor power densities and non-uniform temperature distributions which pose a significant challenge to the cooling requirements of high-power devices. These devices have non-uniform power distribution at the die with power densities assigned to different functional units. This gives rise to localized regions of high temperature known as 'hot spots'. These hot spots and maximum junction temperatures will determine the performance and reliability of the equipment. The

existing solutions have been designed to cool these high temperature regions which increase the thermal budget and in-turn reduce the cost of cooling these devices.

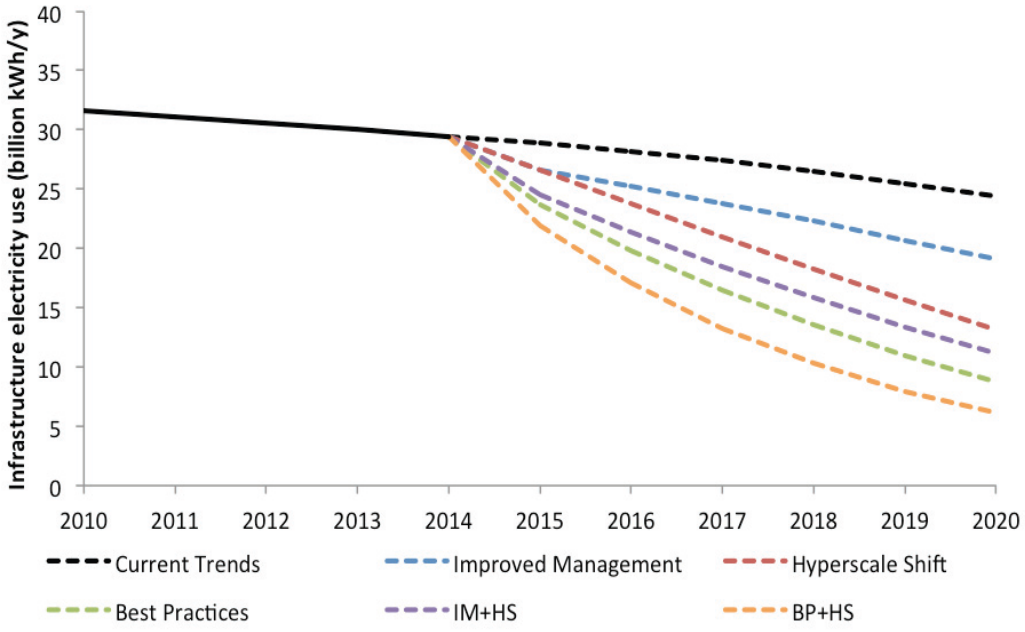

Figure 1-4 Infrastructure energy consumption trends [2]

1.3 Thermal Management

Data center holds the IT equipment to maintain the safe environment and provide adequate cooling while maintaining the reliability of the equipment. Cooling technologies applied in data centers varies based on the type of the equipment, power, density, and geo location. These techniques include air cooling, indirect and direct liquid cooling with appropriate fluid movers. All this aim to achieve a single result of keeping the equipment in safe temperature and humidity

limits. The common approach used is to deploy an overly conservative thermal management system which leads to squandered cooling resources.

A significant number of existing data centers i.e. small / medium and multi-tenant data centers which constitute of around 95% of electricity share in data center market are in compelling need for energy efficiency [3]. A typical data center consumes 45-55% of energy for IT equipment and around 30-40% of energy is consumed by cooling systems. In terms of energy costs, cooling and electricity infrastructure contribute to 70-80% of the capital costs [4]. In order to track the data center energy efficiency, the Green Grid Association (GGA) has introduced metrics such as Power Usage Effectiveness (PUE) [5]. PUE provides the sum of IT and Cooling energy as a fraction of IT power consumption from data centers. In addition to PUE, GGA has later introduced metric known as Data Center Energy Productivity (DCeP) [6]. This serves as a metric to quantify the useful work the data center produces based on the energy it consumed. Improvements in data center facility energy efficiency have flattened out and even deteriorated slightly in the past two years. The average PUE for 2019 is 1.67 [7].

$$\text{PUE} = \frac{\text{Total Facility Energy}}{\text{IT Equipment Energy}}$$

$$DCeP = \frac{\text{Useful work produced}}{\text{Data center energy consumed to produce this work}}$$

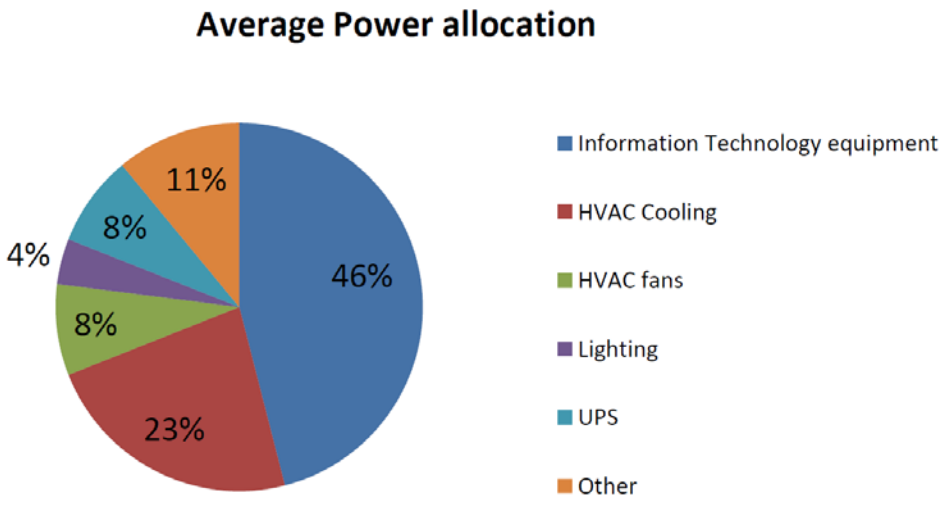

Figure 1-5:Energy consumption impact of mechanical equipment and systems [8]

American Society of Heating, Refrigeration and Air-Conditioning Engineers (ASHRAE) TC 9.9 chapter conducts extensive work in analyzing and defining the model codes, standards and guidelines for data center and mission critical facilities [8].

Table 1-1: ASHRAE IT Equipment Classification and Corresponding Environmental Control [9]

2011 classes	2008 classes	Applications	IT Equipment	Environmental Control
A1	1	Datacenter	Enterprise servers, storage products	Tightly controlled
A2	2		Volume servers, storage products, personal computers, workstations	Some control
A3	NA		Volume servers, storage products, personal computers, workstations	Some control
A4	NA		Volume servers, storage products, personal computers, workstations	Some control
B	3	Office, home, transportable environment, etc.	Personal computers, workstations, laptops, and printers	Minimal control
C	4	Point-of-sale, industrial, factory, etc.	Point-of-sale equipment, ruggedized controllers, or computers and PDAs	No control

Different types of equipment need a different environmental condition. ASHRAE developed different temperature ranges called recommended and allowable ranges. The recommended envelope has the limitations of operating the IT equipment with utmost reliability and sensible energy efficiency. As the data center environment envelope is expanded from A1, A2 towards A3 and A4 higher energy efficiency can be achieved, however, considerable trade-off exists in terms of operation and reliability of the equipment.

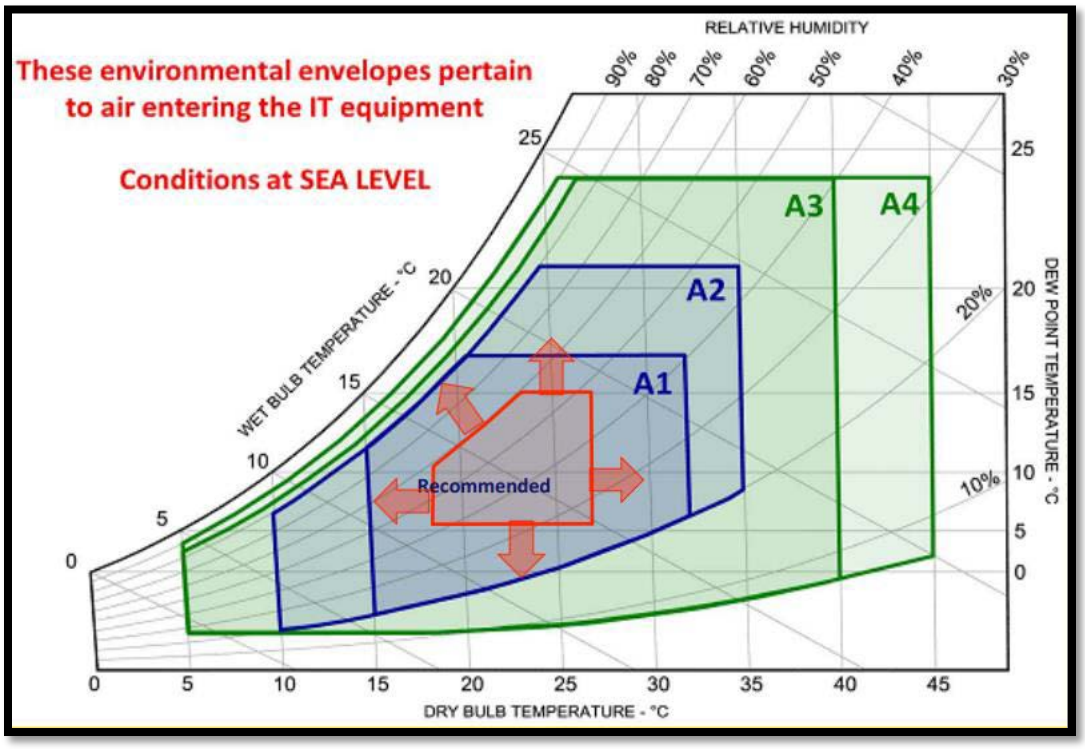

Figure 1-6: ASHRAE TC 9.9 2011 Thermal Guidelines for Air Cooled IT [9]

Since the use of liquid cooling at module and rack level has been wide-spreading, ASHRAE TC 9.9 has introduced liquid cooling classes as well with

varying coolant temperature ranges as shown in [9]. Based on the type of infrastructure cooling design that needs to be used, the facility supply side water temperature ranges are defined as shown in [9].

Table 1-2: ASHRAE Liquid Cooled Thermal Guidelines [9]

<table>
<tr><th rowspan="2">Classes</th><th colspan="2">Typical Infrastructure Design</th><th rowspan="2">Facility Supply Water Temp (C)</th><th rowspan="2">IT Equipment Availability</th></tr>
<tr><th>Main Cooling Equipment</th><th>Supplemental Cooling Equipment</th></tr>
<tr><td>W1</td><td rowspan="2">Chiller/Cooling Tower</td><td rowspan="2">Water-side Economizer Chiller</td><td>2 – 17</td><td rowspan="2">Now available</td></tr>
<tr><td>W2</td><td>2 – 27</td></tr>
<tr><td>W3</td><td>Cooling Tower</td><td>Chiller</td><td>2 – 32</td><td rowspan="2">Not generally available, dependent on future demand</td></tr>
<tr><td>W4</td><td>Water-side Economizer (with drycooler or cooling tower)</td><td>Nothing</td><td>2 – 45</td></tr>
<tr><td>W5</td><td>Building Heating System</td><td>Cooling Tower</td><td>> 45</td><td>Specialized systems</td></tr>
</table>

Several efforts are being made by IT industry for years in order to achieve the improved energy efficiency. Thermal management in data center is of multi-scale nature [14]. The thermal architecture needs to be coupled at different sizes or scales such that the overall energy management can be effectively designed and monitored. The multiple cooling scales can be divided as chip level, server level, chassis level, cabinet level, room level and plenum level [14]. In the context of current study, the cooling scales that are studied are module level i.e. the chip level cooling using heat sinks or cold plates, server/chassis level i.e. thermal transport

across the IT server using fans or heat exchangers, room-level i.e. cooling configuration with Computer Room Air Handling/Conditioning (CRAH/CRAC) or Air Handling Unit (AHU) units.

CHAPTER 2

LITERATURE REVIEW

The advancements in technology have led to the development of high-powered robust micro electronic devices, which call the use of liquid cooling to maintain high-power densities [10]. Water is one of the most versatile liquid coolants, Water cooling has various advantages like greater heat carrying capacity, targeted delivery and lower transport power requirement over air cooling. Also, according to Barroso and Holzle [11] the servers are more energy-efficient when operating at higher utilization, making liquids more appropriate for heat transfer while maintaining desired operating temperatures. Water cooling uses cold plate as the heat exchanger attached to the module. IBM started using computers incorporated with water cooled thermal conduction modules, the earliest direct to chip liquid cooling [12]. Cold plates are capable of removing heat up to 2000W power module [13]. Chu et al. wrote a comprehensive review on cold plates employed for thermal management of high-power density servers [14].

Though cold plates are efficient over air cooling mediums, there is lots of room for improvement. A methodology for multi-design variable optimization of a water-cooled cold plate is mentioned by Fernandes et al. which employed Computational Fluid Dynamic analysis with embedded user defined functions to reduce the pressure drop to improve the pumping power consumption [15].

Furthermore, Fernandes compared his optimized thermal resistance from Computational Fluid Dynamic analysis with Hwang et al. experimental results which are in excellent agreement [16]. There are many researches like Fernandes et al. who has previewed novel designs to extend performance of cold plates [17]. But the need for energy-efficiency has coincided with continuing trends of increasing microprocessor power densities and non-uniform temperature distributions which pose a significant challenge to the cooling requirements of high-power devices. At this power densities the processor die experiences a local elevated temperatures known as hot spots [18]. Therefore, a substantially large temperature difference can be observed across the surface of the device which is detrimental to its performance and reliability. As a result, conventional static cooling solutions are not capable to cool these high temperature regions which increase the thermal budget and in-turn the cost of cooling these devices.

The cooling cost is proportional to the maximum junction temperature of the module. To reduce the maximum temperature cooling solutions employed pumps at the cold plate level for every cold plate. But according to Sahini et al. observations distributed pumping consumes a lot of energy when compared to centralized pumping [19]. This concludes that aforementioned challenges and advancements could not solve the problem of high energy consumption of pumping the coolant. This issue can be answered with the proposed novel dynamic cooling

solution employing the self-regulated flow control device. This enables the target delivery of the coolant lowering the maximum junction temperature there by reducing the overall pumping power.

The emergence of Liquid Cooling in thermal management of electronic devices has been studied in various literature. Tuckerman and Pease [20] experimented the idea of cooling a chip by forcing coolant through the closed channels etched on the backside of the silicon wafer. They reported that the heat transfer coefficient is inversely proportional to the channel width in case of a laminar flow. This idea has influenced various researchers working in the design and optimization of heat sinks especially for electronics. Zhang et al. [21] stepped further by experimentally characterizing the performance of a liquid cooled heat sink populated by microchannels made of Aluminum with the dimensions of 15mm x 12.2mm. This experiment was also carried out on two different chip footprints, 12mm x 12mm and 10mm x 10mm. Thermal resistance curves were obtained in the range of 0.44 to 0.32 ˚C/W for the hip footprint of 12mm x 12mm and 0.59 ˚C/W to 0.44 ˚C/W for the chip with footprint of 10mm x 10mm. Higher heat spreading results in higher thermal resistance for the chip with a footprint of 10mm x 10mm. Both the analytical and experimental results are well matched while considering the respective thermal resistance elements.

Madhusudan developed a thermal resistance-based network model to characterize microchannel cooling system for electronics thermal management. Spreading/constriction resistances are developed from the model given by Lee et al. [22]. This literature based thermal resistance model predicted that the thermally optimal design can dissipate 24% more than the practical design thus addressing the manufacturability gap. Experimental and numerical investigation of liquid cooled heat sinks containing microchannels were carried out by Qu et al. [23] by varying the porosity, aspect ratio and imposed pressure drop. It was reported that the Nusselt number decreases with increasing aspect ratio. The heat transfer enhancement due to the rising pressure drop is significant on microchannels with high aspect ratio and hence thinner channels are reported to be advantageous.

The cooling power consumption should be reduced, and temperature uniformity should be maintained across the die. The objective of this project is to design the dynamic cooling solution to improve device performance and reliability and minimization of system power consumption and further develop a control strategy and instrumentation to promote smarter systems with better performance and reduce facility cooling power. Promoting the warm water cooling will reduce the cooling power consumption. The research in dynamic cooling solution and implementation enables the smart and energy-efficient approach to thermal management of high-density interconnect devices (module level), power

consumption at the data center level. This reduces the power consumption which is increasingly becoming a noticeable load on the national electrical grid. This results in a broader environmental impact by reducing the carbon footprint of the facility. The designed self-regulating flow control device regulates the flow of the coolant with respect to the temperature variation across the element, without any energy consumption. This method can largely eliminate the hot spots.

In present work result in generation of detailed guidelines for the design, testing and validation of a dynamic water-cooled cold plate for the energy-efficient operation of high-power microelectronic platforms. Key experimental data will result in accurate prediction of the magnitude of energy savings available through reduction in operating temperature and static power dissipation. The proposed work will also assist in outlining the requirements of control systems at the server and rack levels for seamless deployment of the dynamic solution in a data center environment.

The designed cooling solution will employ the novel dynamic cooling concept to target delivery cooling resources to counteract non-uniform power distribution in electronic devices, which is crucial for increasing their reliability and performance. This research will serve to define industry standards for numerical modeling of such solutions, and to understand how those solutions can be extended over multiple generations of the device. The energy savings by the dynamic cooling solution will

save the cooling cost of the data center cooling. This will solve the problem of non-uniform distribution of temperature for high power devices and boost the overall efficiency of the data center.

Cooling energy consumption in data centers accounts for approximately 40% of the total data center power, which can be reduced with effective optimization of equipment and cooling technologies. The existing cooling solution of the data center are not energy efficient due to mechanical losses. As the processor is the major heat emitting component in the equipment this can be cooled with a direct heat exchanger like cold plate. In order to have a better performance and reliability these processors should be maintained at uniform low temperatures. According to Barroso and Holzle the servers are energy efficient at higher utilization [11], which compel us to remove large amount of heat from the processor.

- Analyze the designed cold plate experimentally and analytically for its performance.
- Implement smarter cooling and instrumentation for improved performance.
- Introduce the control strategy for system and rack level cooling to boost the overall performance of the data center.

Distributed pumping consumes a lot of energy compared to centralized pumping [19]. Employing the self-regulating flow control devices at component and rack

level with a cauterized pump and dynamic control strategy will achieve the desired power savings. Furthermore, it becomes necessary to remove the hot spots and maintain non-uniform temperatures across the module, when the increase of performance and reliability with reduced cooling cost are the objectives.

2.1 Scope of the work

The objectives of this dissertation are as fallowing:

- Module-level: Dynamic liquid cooling for high power devices
  - Dynamic cold plate and requirement of FCD
  - FCD material selection and characterization
  - Design and test an FCD prototype for proof of concept
  - Characterize the cold plat used to test the FCD
  - CFD analysis of the FCD miniaturization
- Server-level: Server level FCD and dynamic cooling at rack and data center
  - Develop a control strategy for implementing FCD in the data centers
  - Use CFD to test the control strategy and report the savings
  - Outline components and procedures for experimental testing of the Control strategy and FCD reliability
- Data center-level: Energy optimizations of air-cooled data center
  - Optimization of supply shaft for better airflow distribution
  - Outline the future work for better solutions

CHAPTER 3

DYNAMIC COLD PLATE

The need for energy-efficiency in data centers has coincided with the increasing microprocessor power densities and non-uniform power distributions, which pose a challenge to the existing cooling technologies in high-power devices. As a result, conventional single section cold plate cooling solutions must be designed to cool these high temperature regions which spikes the thermal budget and in-turn cost of cooling these devices. In addition, rackmount servers are the most efficient when operate close to maximum utilization [11]. Therefore, the next-generation solution for high power cooling should have selective distribution of resources for promotion of uniform device temperatures. This requires a detailed understanding and incorporation of microprocessor architecture, electronic packaging, and control systems to produce a robust solution.

3.1 Concept of Dynamic Cold Plate

To meet the necessary requirements, conventional single section cold plate designs require integration of control devices and schemes to enable targeted delivery of cooling resources based on requirement. The layout and operation of the dynamic cold plate can be easily visualized as seen in Figure 3-5. Depending on the power map, the footprint of the cold plate is divided into several individual channel sections, as shown in Figure. Each section has a different inlet conduit (see

Figure 3-5) that is fed by the main inlet manifold to the cold plate, making each of them independent from the others. In order to accommodate different power dissipations beneath the active region of each section, the introduction of sensing and control is necessary at each section level.

3.2 MCM Experimental Testing

In order to apply the preceding concept, a reference platform is required for design of such a dynamic solution. A high-power mutli-chip module (MCM), provided by Endicott Interconnect Technologies Inc. (now i3 Electronics, Inc.[24]) that serves this purpose.

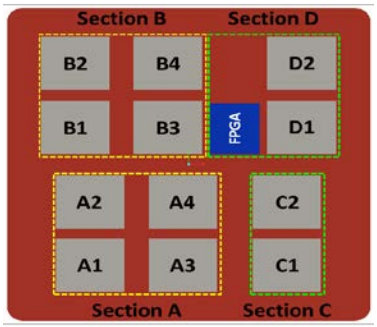

Figure 3-1 Multi-chip module divided into 4 sections

Table 3-1 Details of MCM components

Component	Quantity	Power (W)
Base	1	-
ASIC	12	40
FPGA	1	5

The module is populated with an array of surface mounted components (ASICs, LICAs and a FPGA) and setup to have a maximum power dissipation of 485 watts over a 78mm by 78mm footprint. A list of component power specifications can be found in Table 3-1. Heat generating components of the MCM

(13 in total) were grouped into four sections based on proximity as seen in *Figure 3-1*. A cold plate was designed by Fernandes with four sections and it is called as dynamic cold plate[15]. This dynamic cold plate is analyzed using CFD and proven that pumping power reduction in orders of magnitude [25]. This cold plate is impingement style cold plate with perpendicular channels to the direction of the flow. Sony changed the fin orientation to parallel fins and was able to reduce the pumping power by 28% more [26].

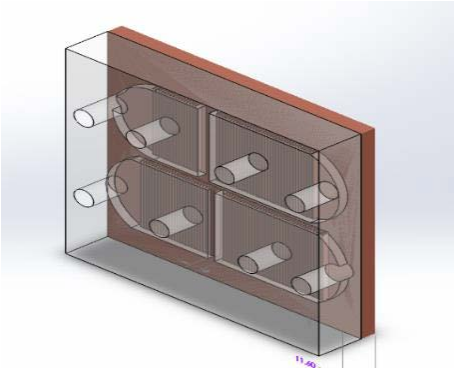

Figure 3-2 DCP model [25]

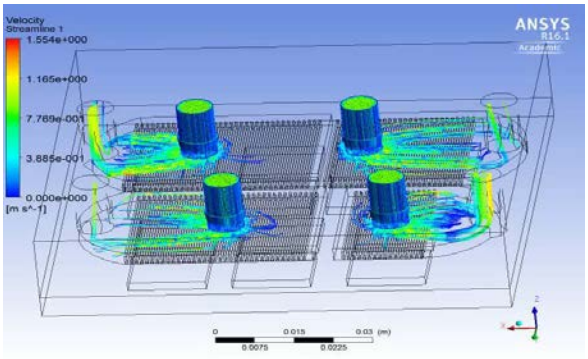

Figure 3-3 CFD simulation of dynamic cold plate [26]

This dynamic cold plate is manufactured by and tested by Kokate using four pumps for the four sections [27]. Experimental testes on the dynamic cold plate proved that the 30% of pumping power could be reduced when compared with the original single section cold plate (OCP). Pumping power with OCP is 3.85W at flow rate of 4lpm and ΔT of 12.87°. Whereas DCP pumping power is 2.76W at flow rate of 4lpm and ΔT of 6.13°, which is 28% reduction in pumping power and 52% reduction in temperature difference.

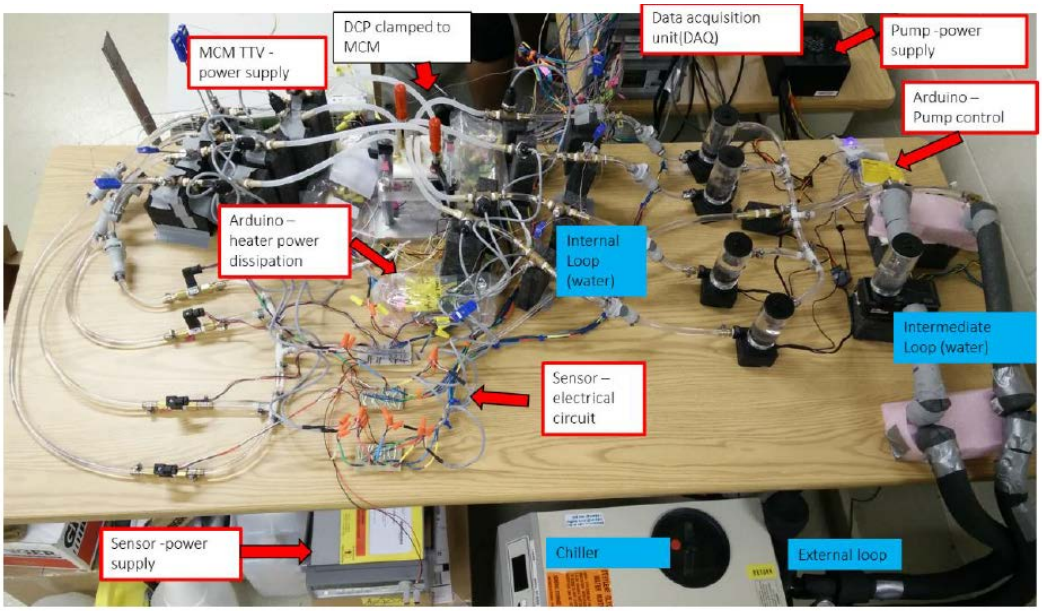

Figure 3-4 Experimental setup for DCP testing [27]

The Experiment showed the proof of the dynamic cold plate concept, in this experiment a pump is used for each section of the cold plate as a flow control device. This is inefficient considering the efficiency of the pump it is proven by Manasa that centralized pump is more efficient than a distributed pumping [19][28]. This necessity gave birth to a self-sensing and self-controlling flow control device.

3.3 Purpose of a flow control device

Self-regulated Flow control device (FCD) when attached to the outlets of Dynamic Cold plate (DCP) sections, can vary flow rate as a function of temperature of the coolant (water) flowing through each one of them. This allows for sections of the DCP at high temperatures to receive more coolant as compared to cooler

sections of the DCP. An array of FCDs essentially distribute flow between each other, thereby negating the need for individual pumps for each DCP section.

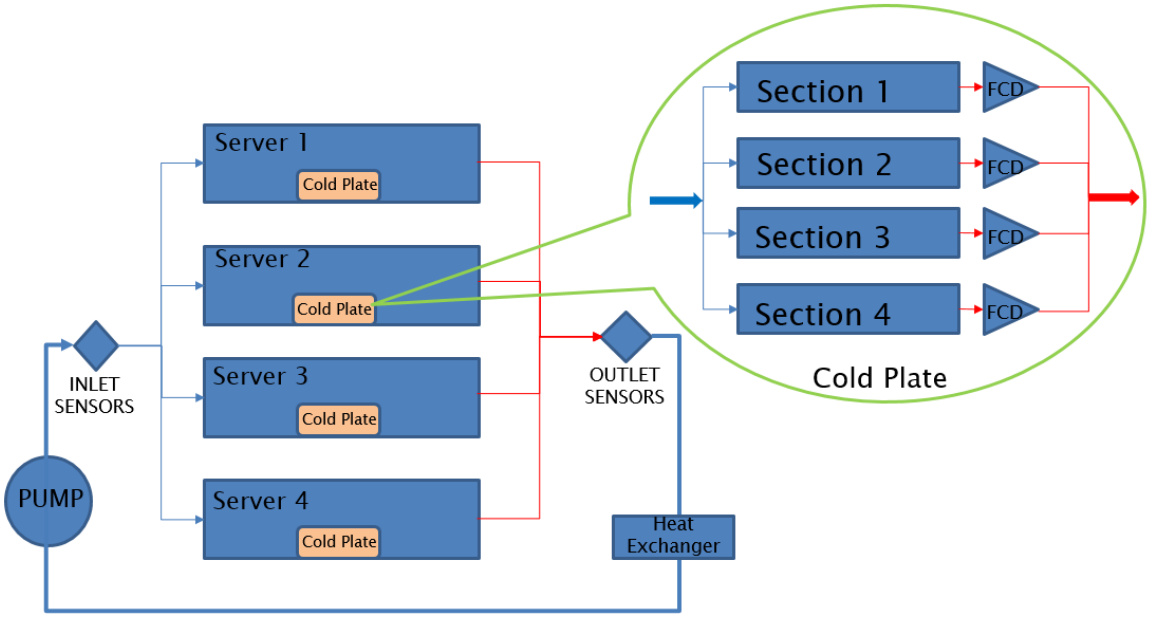

Figure 3-5 Dynamic Cold Plate schematic

In a scenario where all DCP sections require maximum flowrates (100% utilization), the FCDs would provide least resistance to coolant flow and the pressure across the DCP would be minimum..Figure 3-5 If this value of pressure difference across the DCP at 100% utilization is perpetually maintained across the DCP for all utilizations by reducing flow delivery from the pump, significant savings in pumping power can be made. It is also to be noted that the use of an array of FCDs allows for centralized pumping rather than having individual pumps for each section.

Table 3-2: Material Selection Criteria table

Materials and Selection Criteria	TM5	Treated Shape Memory Polymers	Nitinol @ 65C	Soft Polymer coating over deflecting material	NiTi @ 35C, 45C, 55C	R-Phase NiTi at standard and body temperature
Composition of the Material	80% MnCuNi + 20% NiFe	Polycaprolactones, Poltlactides, Polyester uerthane	NiTiCu	NiTi Coated with PES or PEEK	NiTi	R – Phase is the operating Region
Deflection	1	5	4	3	4	3
Cost	5	1	3	3	2	4
Corrosion	3	5	4	5	4	4
Energy consumed for deflection	0	5	0	3	5	5
Energy transferred to water	2	5	2	5	5	5
Relaxation time	4	0	5	2	3	3
Repeatability of N number of cycles	4	0	5	2	4	5
Ease of developing and availability in market	5	1	4	3	4	1
Flexibility in operation	2	1	3	3	3	3
thermal gradient within the pipe	5	3	5	5	3	3
Effect of Cooling and Heating Hysteresis	3	1	3	3	3	
Delta T required for Deflection			25 Degree Celsius		10 Degree Celsius	3 to 7 Degree Celsius
Total	34	27	38	37	39	36
Passive usage in application	No	Yes	No	No	Yes	Yes

Fail criteria	Worse	Bad	Moderate	Good	Excellent
0	1	2	3	4	5

3.4 FCD material selection

The actuator used in the FCD must be capable of reacting to change in coolant (water) temperature. The actuator material is also constantly in contact with water and hence must be resistant to corrosion. Deflection produced per unit rise in temperature and repeatability over several cycles of use are the highest priorities during material selection for the FCD. Several other factors exclusive to the FCD use-case are also considered during material selection. The material of choice after comparing numerous materials based on several criteria is Nitinol shape memory alloy. The table validates Nitinol over the various criteria that were considered during material selection.

Selected material	NiTi
Deflection	Very good
Cost	Average
Corrosion Resistance	Very good
Energy consumed for deflection	Exceptional
Relaxation time	Good
Repeatability of n number of cycles	Exceptional
Ease of developing and availability in market	Very good
Flexibility in operation as per aging and changing need	Good
Can thermal gradient within the pipe create issues	No

Effect of cooling and heating hysteresis curve on performance Can be minimized in several ways It can be used passively for given application.

3.5 Nitinol Properties

Table 3-3 : Properties of Nitinol

Young's Modulus	Austenite	approx. 83 GPa
	Martensite	approx. 28 to 41 GPa
Yield Strength	Austenite	195 to 690 MPa
	Martensite	70 to 140 MPa
Ultimate Tensile Strength		895 MPa

Nitinol is a shape memory alloy that reacts to application of heat with a change in its shape. Nitinol has two phases, a low temperature martensite phase and a high temperature austenite phase. Nitinol undergoes a phase change from martensite to austenite on heating accompanied by an increase in its young's modulus and shear modulus. This implies that in its high temperature austenite phase, nitinol is much stiffer compared to its low temperature martensite phase, in which it can more readily be deformed. Nitinol phase change does not occur at fixed temperatures. Rather, the phase change occurs over a range of temperature. Nitinol

also exhibits a difference in the transformation temperatures upon heating from martensite to austenite and cooling from austenite to martensite. This difference results in a lag during the cooling cycle. This lag between the heating and cooling cycles is called thermal hysteresis. Several alloying methods can be employed to manipulate the hysteresis of Nitinol and ensure that the lag is acceptably small.

3.5.1 Two-way Nitinol

Two-way Nitinol can remember two different shapes: one at low temperatures, and one at the high temperature. This means nitinol has fixed shapes for 100% Martensite and 100% Austenite compositions. Two-way nitinol can freely transform between its high temperature and low temperature phases purely by thermal loading and unloading. A two-way nitinol helical spring was experimentally tested by thermal cycling in a thermal chamber. The plot below shows a large hysteresis between the heating and cooling curves.

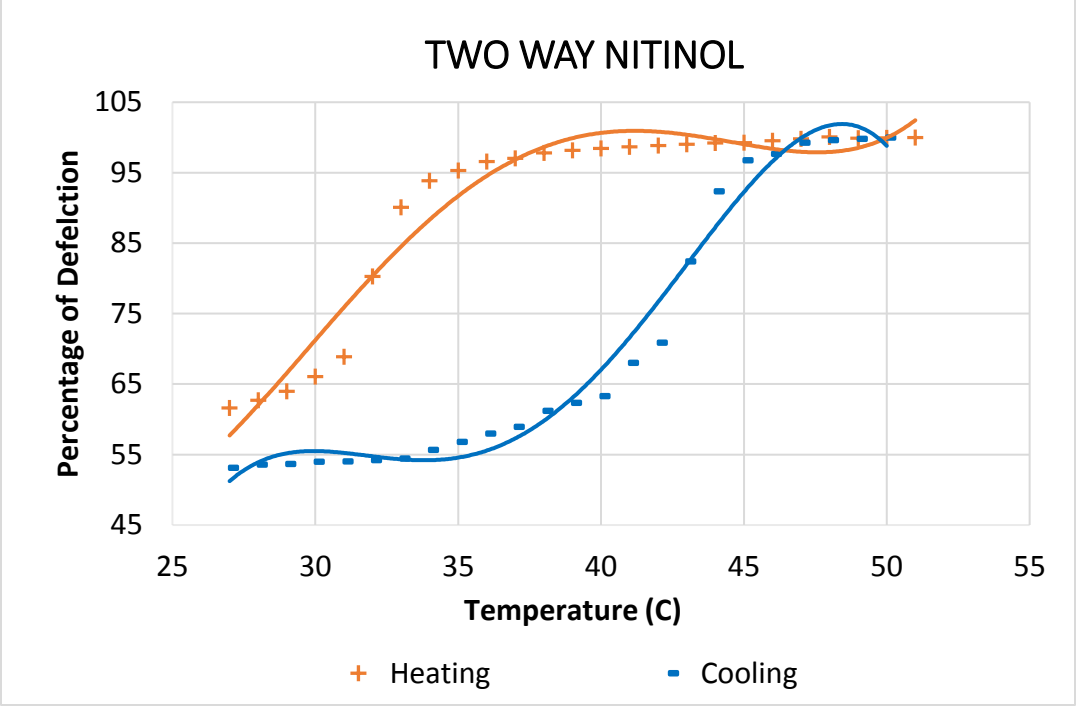

Figure 3-6 Hysteresis curve for two-way nitinol

3.5.2 One-way Nitinol

One-way nitinol remembers only one unique shape. When Nitinol is in its low temperature state, it can be deformed owing to its low stiffness at this phase and will stay deformed until heated above its transition temperature. Upon heating, it changes back to its original shape. Experimental testing shows one-way nitinol has appreciably low hysteresis when compared to two-way nitinol. But one-way nitinol requires an external force to deform it at its low temperature martensite phase. For effective functioning of the FCD and best dynamic response times, low hysteresis is essential. Hence one-way nitinol is preferred over two-way nitinol. To

address the need for external loading to initially deform one-way nitinol, a novel dual spring setup is used. A helical nitinol spring is coupled with a stainless-steel tension spring. The force exerted by the tension spring can deflect the nitinol spring when it is in martensite form. Since the tension spring is non-reactive to heat, with the increase in temperature, the tensile force generated by the nitinol spring becomes more than that of the stainless-steel spring.

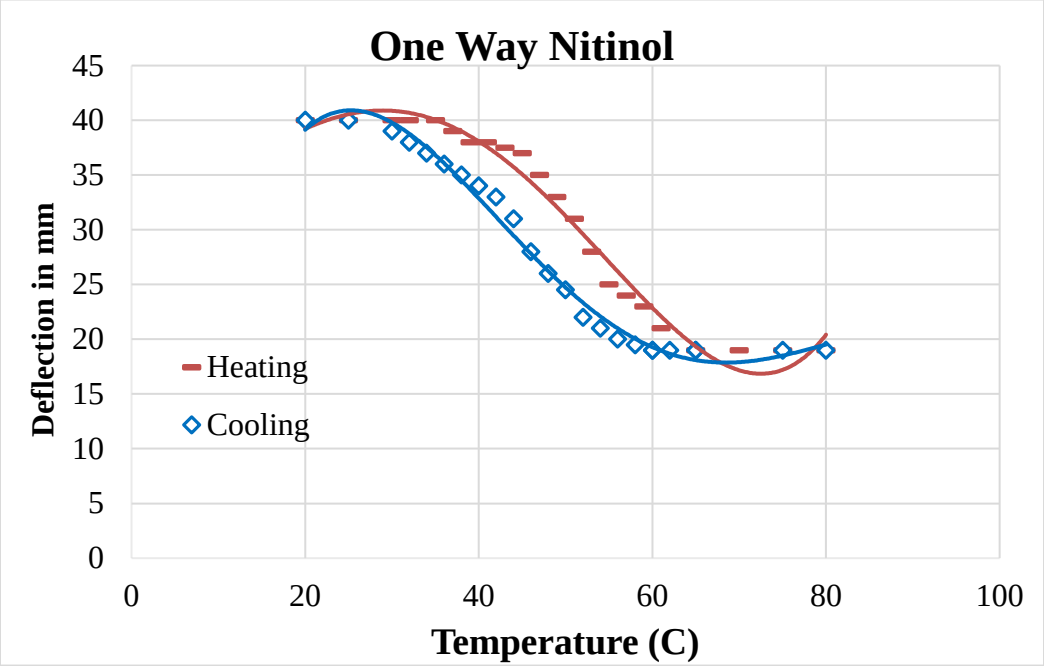

Figure 3-7 Hysteresis curve for one-way nithinol

3.6 Nitinol Characterization

To design the heat sensitive actuator for the FCD it is essential to completely understand the behavior of Nitinol helical springs. The main parameters of interest are:

1. Force Generated with respect to Spring Dimensions
2. Displacement with respect to Temperature
3. Hysteresis Curve

To understand the behavior of nitinol springs, an assortment of springs was experimentally tested. All springs are of the same standard temperature Nitinol, purchased from the same vendor.

Table 3-4 Dimensions of nitinol samples

S. No	Mandrel Size (mm)	Wire Diameter(mm)	Spring length (mm)
1	4.75	0.25	15
2	4.75	0.25	25
3	4.75	0.25	35
4	4.75	0.5	15
5	4.75	0.5	25
6	4.75	0.5	35
7	4.75	1	15
8	4.75	1	25
9	4.75	1	35

It is to be noted that all the springs tested were one-way nitinol and hence all of them had to be coupled to a suitable stainless-steel spring to be tested. The experimental testing procedure of choice was performing thermal cycling on the dual spring system in a thermal chamber. A properly calibrated thermocouple was attached to the Nitinol spring to monitor its temperature. As a preliminary test, thermal cycling of one arbitrary spring was done from 20°C to 80°C and back. This allowed for the overall hysteresis curve to be documented. The phase transition temperatures were also identified. As the nitinol spring in martensite phase is easily deformed, it is important to ensure that the deformation is purely due to the stainless-steel spring. To ensure that this is always the case, one or two thermal cycles are done for each spring combination before data is logged. After preliminary testing, nitinol springs of various wire diameters and lengths were coupled with suitable stainless-steel springs, making sure that the stainless-steel spring is capable of producing required deformation of the nitinol spring at room temperature. All stainless-steel springs used were standard springs of known dimensions and hence were used for force measurement as well.

$T_f = I_t + (D \times K)$

Where:

T_f = Total Force exerted on spring (N)

I_t = Initial tension force on spring

D = Deflection

K = Spring Constant

Displacement was another parameter to be documented. Image processing was used to measure the exact deflection produced by nitinol spring. The total distance between the ends of both the springs was used as scale for displacement measurements as this value is known and kept constant during the entire thermal cycling process.

In practical use cases of the FCD, the temperatures might not always be high enough to enable complete phase change of Nitinol to its Austenite phase. It is hence important to understand how nitinol behaves in the intermediate zone below its transition temperature. Experimental testing was done between various temperature ranges below the transition temperature of nitinol to better understand its behavior in this region.

3.7 Nitinol Test setup

Nitinol and stainless steel are arranged as shown in the figure below acting against each other. A Vernier calipers scale is used to compare the changes in the indicator. This setup is then put into a thermal cycling chamber where the temperatures are varied at a low ramping rates to look at the nitinol behavior. These changes are

captured by a digital camera and processed to get the required deflection data of the nitinol springs.

Table 3-5: Nitinol Spring Setup for testing

3.8 Characterization of Nitinol Helical Springs

Force as a function of spring dimensions is plotted from data recorded by experimental testing. The dual spring setup is placed in a thermal chamber where thermal cycling is done. Note that only heating cycles are plotted below. Nitinol springs of various wire diameters and lengths are coupled with suitable stainless-steel springs, making sure that the stainless-steel spring can produce required deformation of the nitinol spring at room temperature.

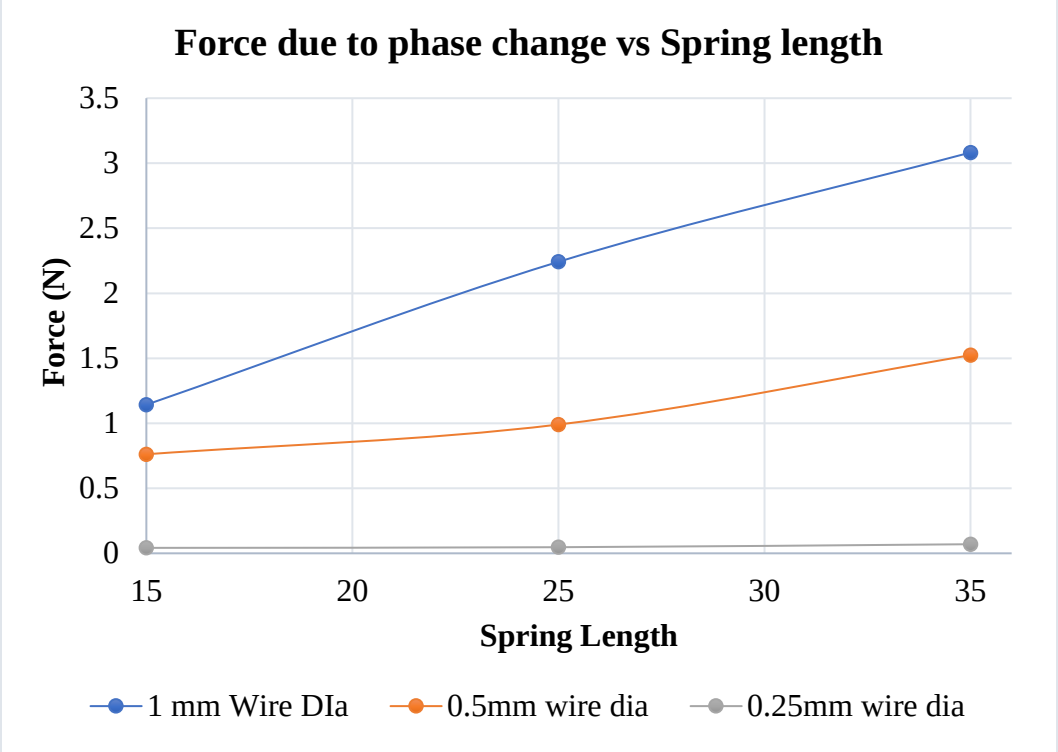

Figure 3-8 Force generated by nitinol

The stainless-steel springs used are all standard springs of known dimensions and hence they can be used for force measurement as well. The forces observed in plot shows sum of structural and phase transformation forces. The above graph in the Figure 3-8 has nine individual data points that represent force generated due to phase change for nine unique nitinol springs of different dimensions. From the plot it is clear that the springs with larger wire diameters and solid spring lengths can generate more force compared to springs with smaller wire diameters and solid

spring lengths. The forces plotted are purely due to phase change and do not include structural resistance.

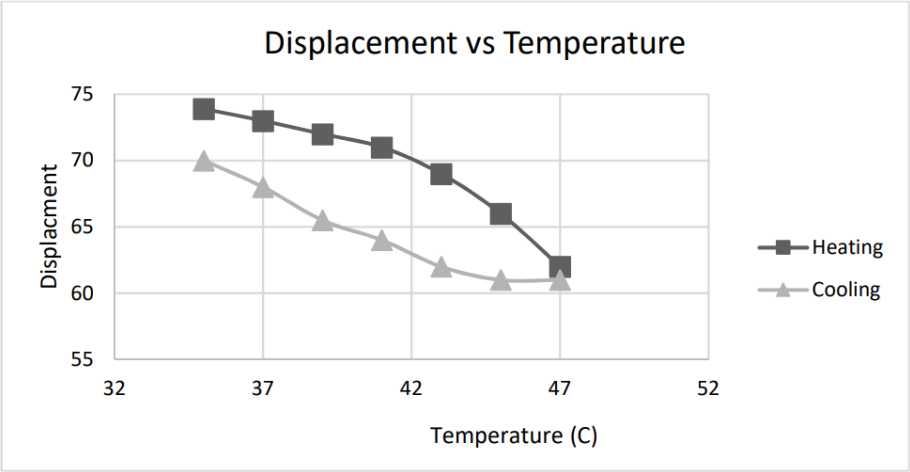

Figure 3-9 Displacement versus temperature required for FCD

Displacement generated by Nitinol as a function of temperature is plotted in the graph below. This plot corresponds to one combination of Nitinol and stainless-steel spring. Thermal cycling for numerous other spring combinations were also performed in the thermal chamber to identify the combination that would provide the highest displacements for the temperature range in which the FCD would have good functionality. The best combination is for acceptable total separation is tabulated below. The plot provided corresponds to the same spring combination.

Table 3-6: Nitinol Spring and Stainless-Steel Spring Properties

NITINOL SPRING	STAINLESS STEEL SPRING
• 1mm Wire diameter • 25mm Spring length • 4.75mm mandrel size DEFELECTION ACHIEVED FOR 140mm SEPARATION, 35°C to 47°C = **13mm**	• OD (in) 0.240 • Length (in) 1.130 • Rate (lbs/in) 0.870 • Initial Tension (lbs) 0.200 • Sugg. Max. Defl. (in) 1.600 • Sugg. Max. Load (lbs) 1.600 • Wire Dia. (in) 0.022 • Material Stainless Steel • Finish None

Hysteresis loops for temperature ranges that do not span the entire transition temperature ranges are plotted below after experimental testing. Hysteresis still exists even if transition temperature is not attained.

3.9 Preliminary Flow Control Device Design

The flow control device is responsible for housing the dual spring system. The springs are attached to a central block that can alter flow rate. Design considerations are made to obtain optimum flow rates and pressure drops across the FCD. The flow control device has an inlet and outlet that allows fluid flow along the vertical direction, with the spring system located perpendicular to the path of fluid flow.

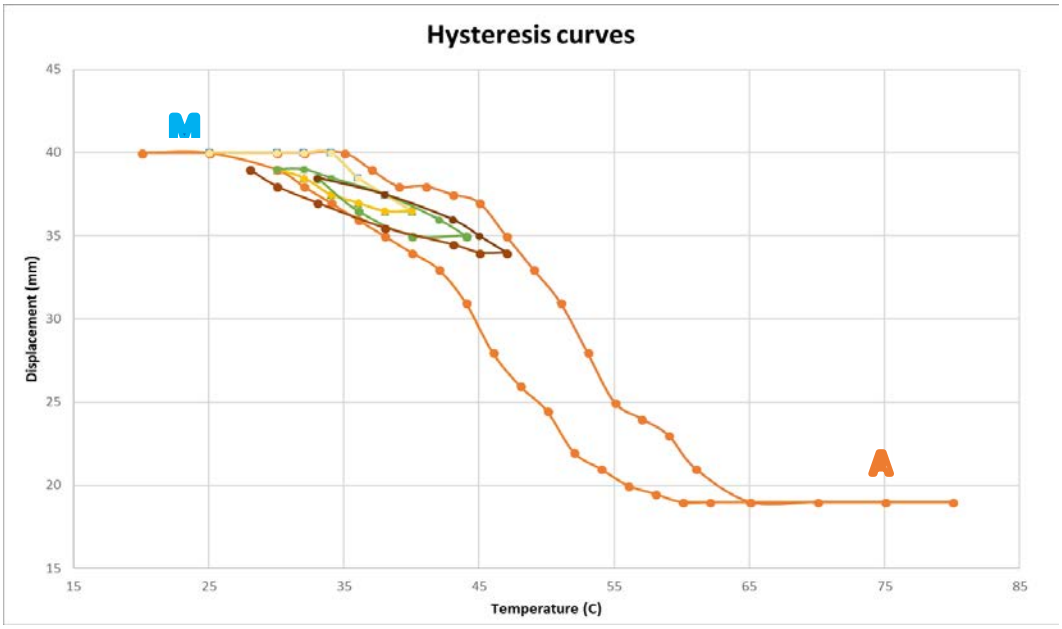

Figure 3-10 Nitinol hysteresis curve with full range

The springs move a solid block across the inlet and outlet orifice, thereby varying the hydraulic diameter of the flow. Since it is necessary for the nitinol spring to be in contact with the fluid, the inlet hydraulic diameter is made bigger than the outlet hydraulic diameter, ensuring that fluid fills up the horizontal housing that contains the dual spring system. The horizontal housing also has groves on all four sides. These grooves have two purposes: to reduce friction between the moving block and the walls, and to provide a non-zero fluid delivery from the FCD even when the block completely seals the exit.

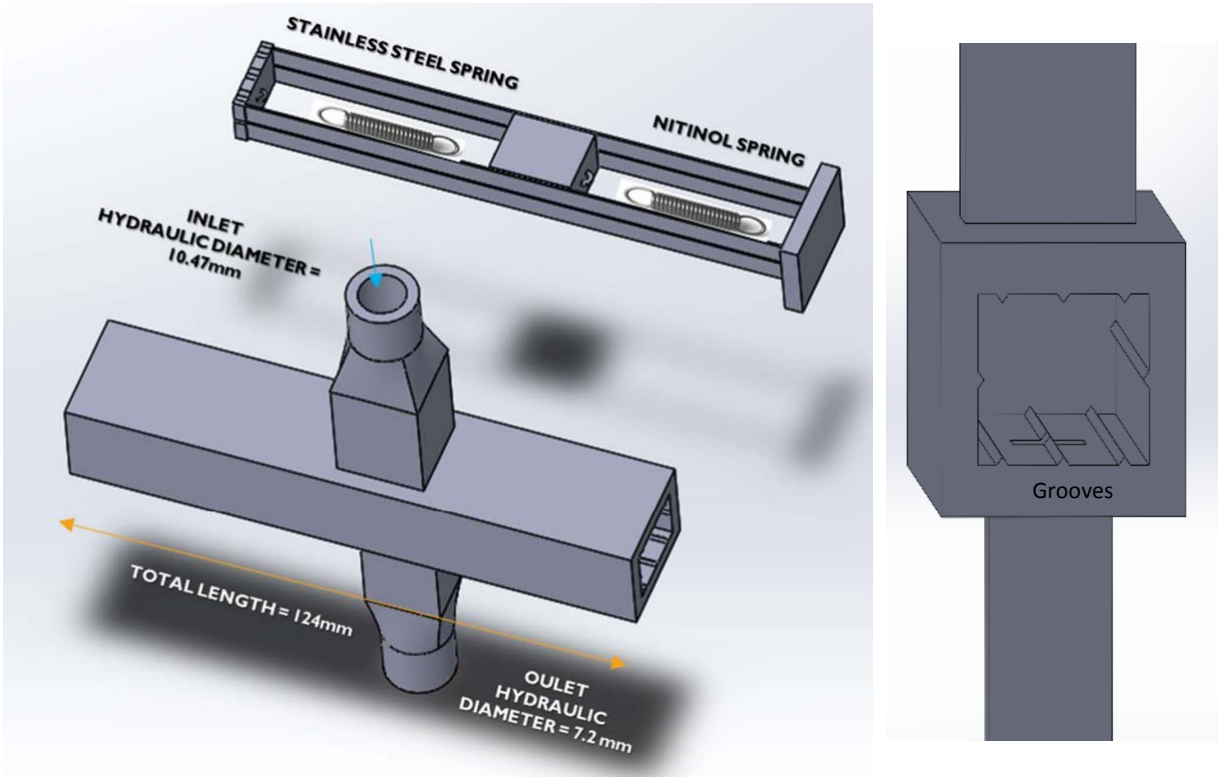

Figure 3-11 FCD Design

The flow control device has rectangular cross sections throughout its flow regions. This helps ensure linear change in hydraulic diameter with movement of the block. Experimental and CFD testing on the FCD was performed to validate linear change in flow rate with the change in block position.

3.10 FCD CFD Analysis

CFD analysis was done on the FCD to analyses the fluid flow rate for various position of the block. Linear change in flow rate is important to ensure that there are no sudden changes in flow rate with change in block position [11]. Change in

block position effectively reduces the hydraulic diameter of the outlet. The plot below shows linear change in flow rate with change in block position.

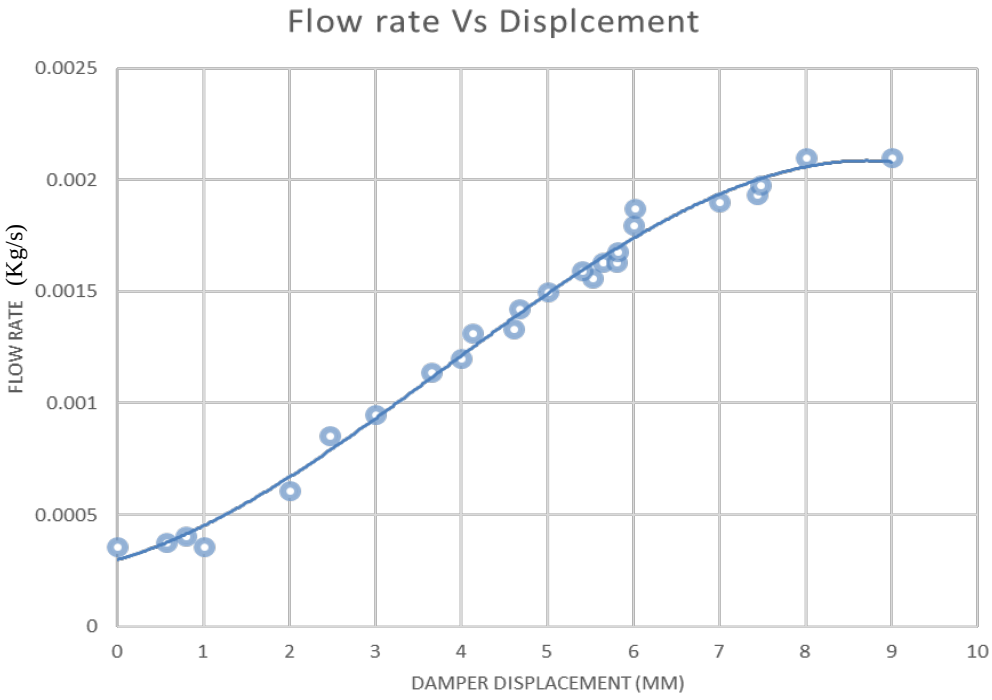

Figure 3-12 CFD results for flow rate based on damper displacement

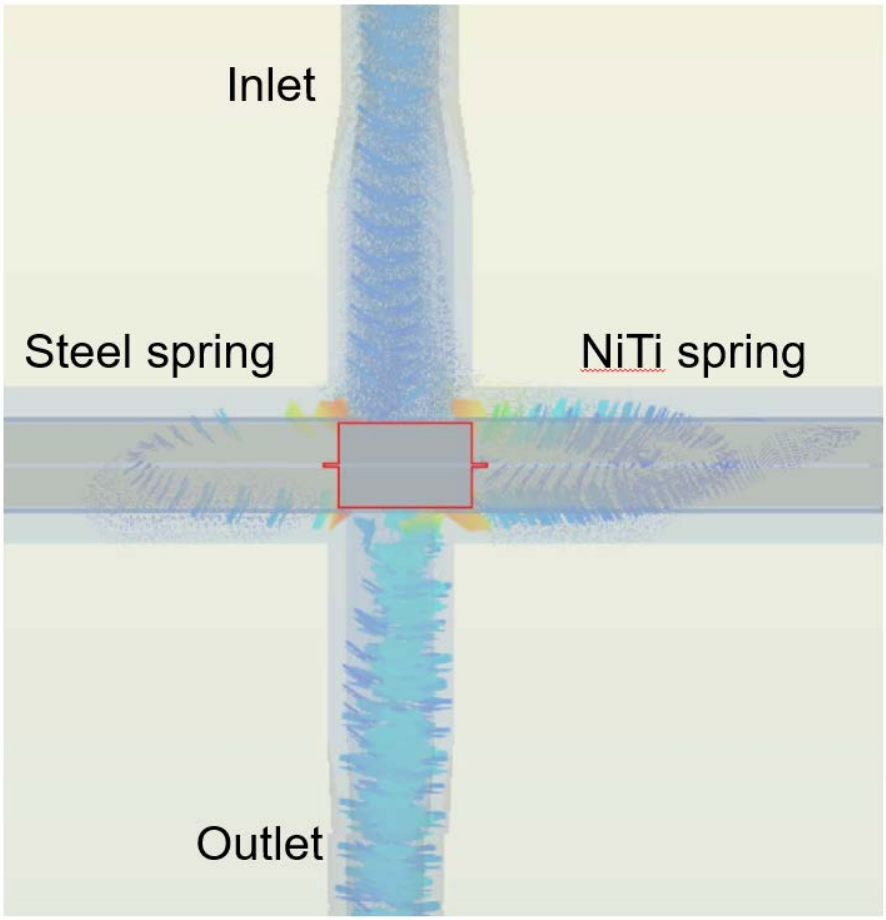

Figure 3-13 CFD snapshot of the FCD

CHAPTER 4

COLD PLATE CHARACTERIZATION AND FCD PROTOTYPE TESTING

4.1 Experimental setup preparation

A reference chip module platform as shown in Figure 4-1, is designed and manufactured. Careful consideration is paid to dimensional and power consumption constraints involved in employment of these devices in the solution. A bench setup is implemented to mount the cold plates on the chip module which serves to provide the delivery of coolant to different parts of the chip module based on the amount of heat being dissipated in respective active regions. Generating the cooling circuit and selection of heat transfer surfaces within the body of the solution are also required exercises. The steady-state performance of the solution is to determine its range and sensitivity. The cold plate's performance is studied by analyzing the pressure drop and temperature change across the cold plate. Also, the base thermal resistance of the cold plate is determined to improve the optimum performance of the cold plate.

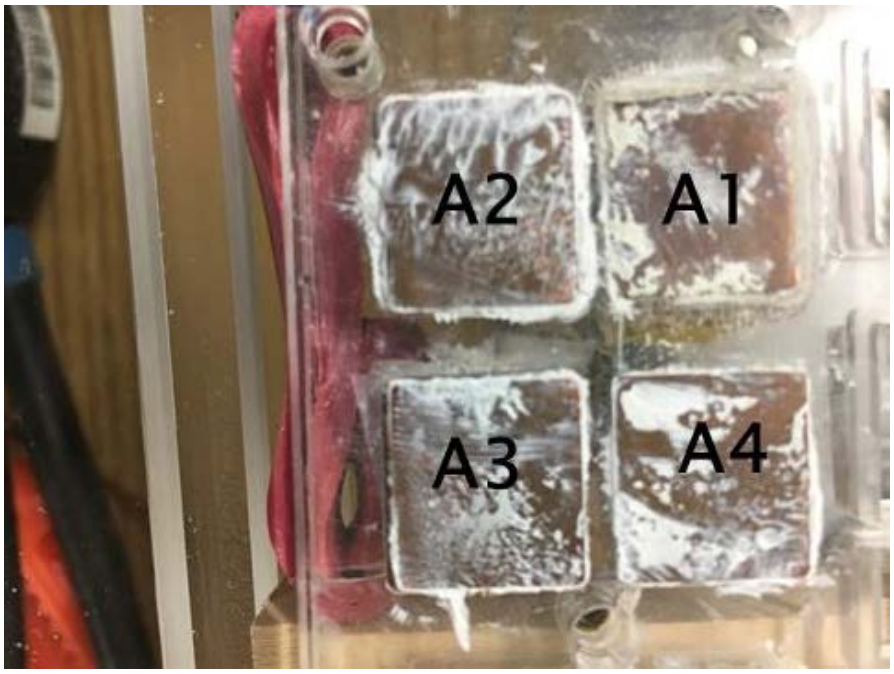

Figure 4-1 Copper blocks with resister heaters

4.2 Components in experimental setup

Present study experimentally investigates commercial cold plate that uses an impinging jet flow. Experiments were conducted without the impinging jet flow and by varying the flow rate and inlet power while maintaining the coolant temperature at 20°C. Heat transfer coefficient values were calculated from the obtained base thermal resistance and the literature-based relations. The temperature rise across the cold plate is measured for various coolant flow rate and chip power, the pressure drop across the cold plate is studied by varying the flow rate and keeping input power constant.

4.2.1 Heater elements

The base of the chip module is machined from acrylic consisting of two parts to hold the heater blocks. The top half ensures that the installed heater blocks only extend 0.8mm above the base while the bottom half prevents the heater blocks from moving when cold plate is attached with applied pressure. The holes in the bottom half of the base facilitate exit of heater leads and thermocouples from individual heater block.

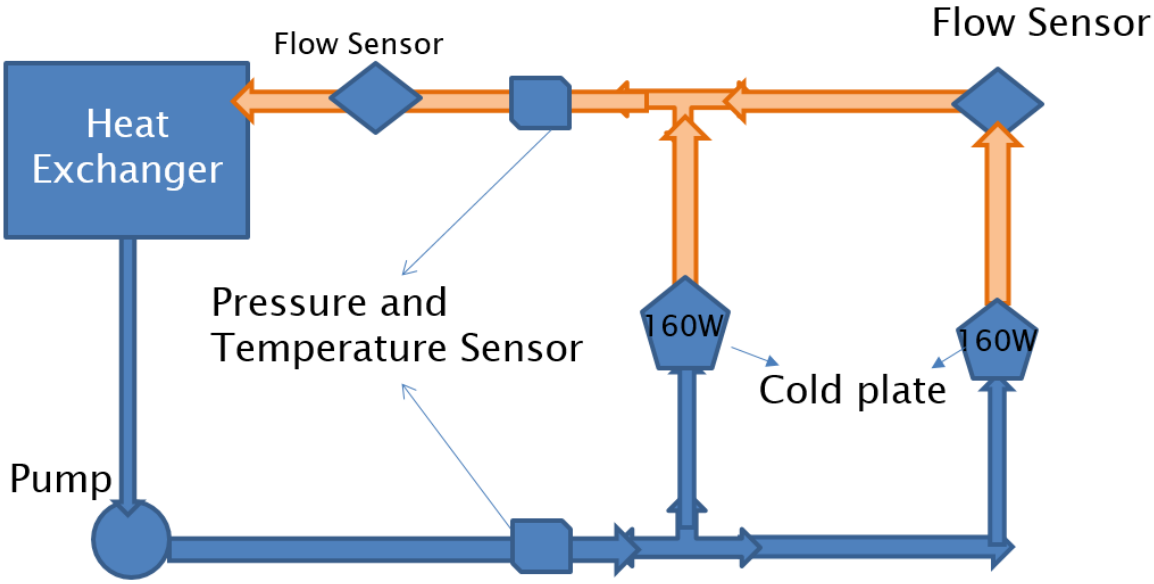

Figure 4-2 Experimental schematics

Controlling power dissipation of each heater block is achieved like details in Figure 3-2. The current drawn by the heater blocks are measured with the help of a shunt resistor based on the voltage drop readings through the data acquisition

unit (DAQ). A board with eight individual circuits was assembled for blocks in Sections A and B. Each section is populated with four heater blocks and was named starting from the top right and moving in a ‘C’ pattern. Both sections have a similar footprint and account for maximum power dissipation of 240W.

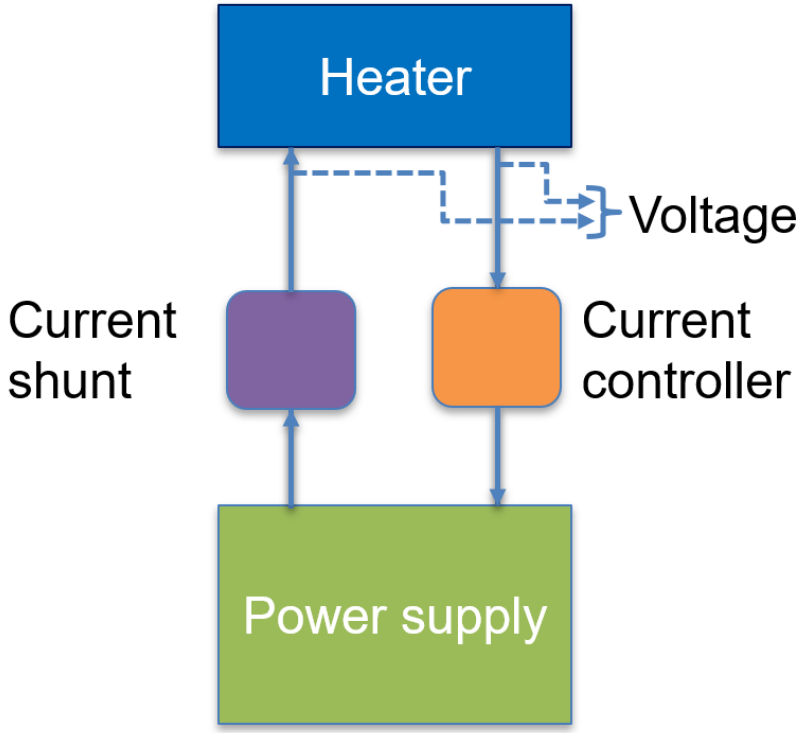

Figure 4-3 circuit block diagram

4.2.2 Cold plate Description

The experimental facility is built in-house to achieve high accuracy measurements, and it includes building a mock chip, taking measurements on the base of the cold plate, assembling the cold plate to the mock server (copper block) and a sanity

check for air voids at the Thermal Interface Material (TIM). Figure 4-4 shows the cold plate used for this study. The cold plates are used in Asetek Rack D2C to accommodate lower profile footprints such as custom chases. The cold plate employs microchannels with a split-flow technology as a solution to decrease the cold plate thermal resistance. The cold plate consists of two main parts; the plastic cover to provide the required impinging flow and the copper plate with microchannels.

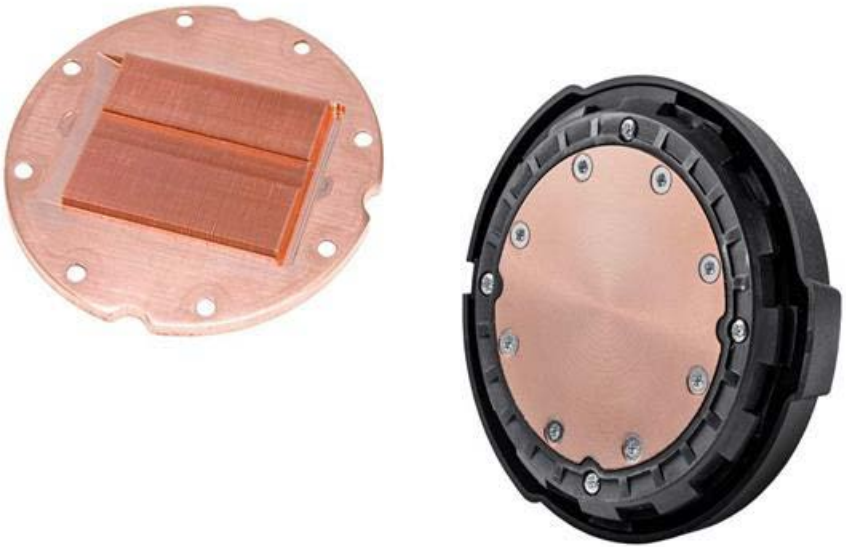

Figure 4-4 Cold plate in testing

Meticulous care was taken in assembling the cold plate on the heater block as uneven assembly would lead to formation of air voids at the interface, resulting in non-uniform power distribution. A syringe was used to evenly dispense the TIM

over the heater block, as shown in the Figure 4-1. The cold plate assembly on top of the heater block was done in multiple steps.

The control scheme was designed in LabVIEW to characterize the cold plate by studying the parameters such as temperature, pressure and flow across the cold plates. The mock chip module as mention earlier was designed and fabricated for the experimental testing. Details of liquid cooling test bench are also finalized and previewed. Finally, a series of tests are conducted on both cold plates and resultant parameters of interest are outlined.

4.2.3 The Centralized Pump

The selected Swiftech MCP50X pump as show in Figure 4-5, has pulse width modulated (PWM) control so it can be used to control the flowrate of distilled water (Coolant). This pump has a smaller footprint and higher-pressure head capacity with low power requirement. It works on centrifugal pumping mechanism and operates at low noise. It is powered by a DC supply through a SATA cable and has a 4-wired connector for PWM control. Also, the pump has an attached reservoir with a standard G1/4” ports which are compatible with large assortment of fittings. The PWM enables control of speed of the flow through an Arduino, for a wide range of speeds, from 1200 rpm for a silent operation to 4500 rpm for an ultra-high flow performance.

Figure 4-5 Centrifugal Pump

Figure 4-6 T-Type thermocouple

4.2.4 Thermocouple Probe

The thermocouple probes from OMEGA are selected as they have quick disconnected with miniature connectors. The glass filled nylon connector is rated for temperatures up to 220°C. The diameter of thermocouple probe is 3.0mm. These thermocouple probes are fitted into stainless steel vacuum fitting as shown in Figure 4-5 The vacuum fittings are then fitted into fluid line by use of Tee joint.

4.2.5 Flowmeter

The Omega FTB-421 flowmeter was selected as it has range of operation from 0.1 to 2.5 lpm. It has an accuracy of +-3% of reading normal range and

repeatability of 0.5% FS normal range. The flowmeter accuracy and repeatability were checked by recalibrating the flowmeter frequently. The lightweight turbine ensures fast startup and can mount in any orientation.

Figure 4-7 Pressure Sensor

Figure 4-8 Flow sensor

4.2.6 Pressure Sensor

The pressure sensors selected is Honeywell MLH050PGL06E works on silicon Piezo-resistive pressure sensing principle. The pressure sensor is equipped with four piezo-resistors suppressed in a chemically- etched silicon diaphragm. This diaphragm is being flexed together with the suppressed resistors whenever there is a change in pressure that induces stress. This result in an electrical output when the resistor value changes in proportion to the stress applied. These sensors were

selected as they are small, more reliable and economic. They report maximum repeatability, precision and reliability under different conditions. Also, they are highly consistent in operating characteristics and interchange without recalibration.

4.2.7 Data Acquisition Units (DAQ)

The Agilent 34972A DAQ unit has a 3-slot mainframe with built-in 61/2-digit DMM and eight optional switch and control plug-in modules. It measures and converts 11 different input signals: temperature with thermocouples, RTDs and thermistors; dc/ac volts; 2- and 4-wire resistance; frequency and period; dc/ac current. In stand-alone applications during the experiment, the temperature rises in heater blocks is instantaneously logged onto a USB flash drive. The Bench Link Data Logger software is used for logging data and controlling the process in the stand-alone mode.

Figure 4-9 Data acquisition unit

4.2.8 Liquid Cooling Test Bench

A simplified sketch of the test bench setup to evaluate both cold plates is depicted in

Figure *4-10*: Experimental Test Setup with 2 cold plates. A Kinetics RS33AO11 recirculating chiller drives flow through the external loop and cools the plate heat exchanger (HEX). The chiller is equipped with a positive displacement pump capable of pumping up to 1.6gpm of coolant at 100psi and a temperature range of -15°C to 75°C. As these units are known to drift (variation in temperature), the HEX provides substantial thermal capacitance to prevent transmission to subsequent loops. A DC 4-wire pump drives flow of distilled water through the two HEXs in the intermediate loop. Similarly, a separate pump controls flow of distilled water through all components in the internal loop. Turbine flowmeters measure the flow rate of water cooled by the plate HEX. Temperature and pressure differences across the cold plate are measured using T-type thermocouple probes and pressure transducers. The pump in the internal loop is primarily responsible for maintaining a fixed flow rate during testing. The pump in the intermediate loop controls the inlet temperature of water to the cold plate by modulating flow rate between the two HEXs. Temperature and flow rate readings are input to the LabVIEW code that in-turn controls both pumps by sending PWM signal through Arduino. Inlet temperatures to the cold plate is relatively high (35°C) to test for warm water cooling. Water and glycol mixture (50/50) are employed in external loops to have effective running of chiller. The Agilent 34970A Data Acquisition/Switch Unit is used to sense temperature, pressure, flow, voltage and current by compiling a LabVIEW program. There are thirteen case temperature readings measured from

the MCM as mentioned in earlier section through the LabVIEW program. Agilent E3632A 120W power supply is used to power the pressure sensor, flowmeter. A Corsair CX750M power supply unit is used to power the 4-wired DC pumps since they have a SATA cable.

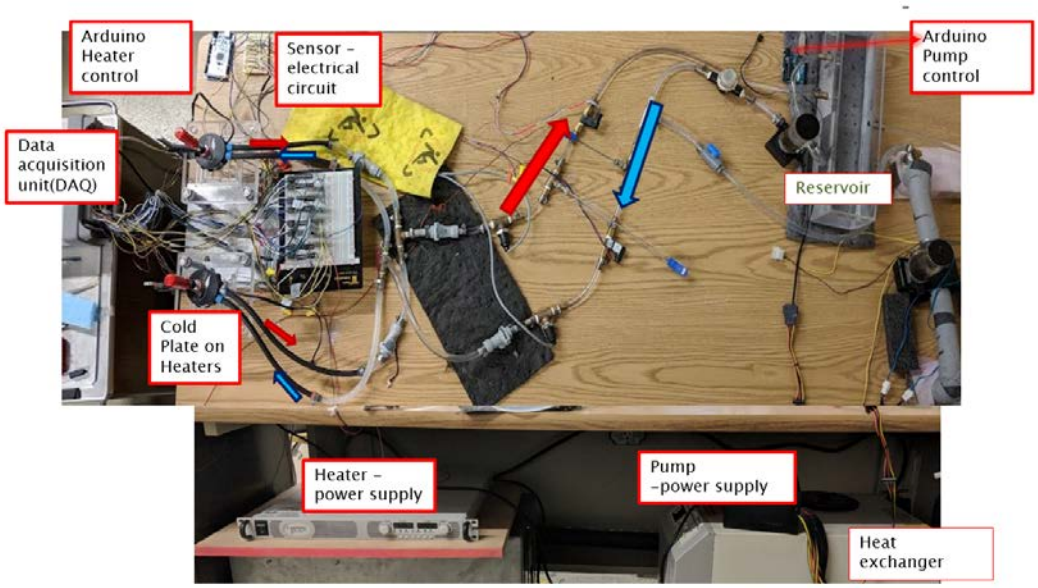

Figure 4-10: Experimental Test Setup with 2 cold plates

4.3 Experimental testing of Cold Plate

The experimental test setup was operated with an inlet temperature of 20˚C. The chip modules were subjected to uniform loading conditions during the testing of the liquid cold plate. There were six cases of uniform loading considered where all eight ASICs were subjected to uniform loads of 10W, 20W, 30W, 40W, 50W and 60W. All the loading conditions were studied at different flow rates varying the

PWM from 50 to 100 in the internal loop. Two flowmeters were used in parallel to make sure the flowmeter operates in its working range. The pressure drop across the cold plate is measured and utilized to calculate the pumping power.

The LabVIEW code written, and the data were monitored instantaneously using the Agilent Bench link Software as shown in Figure 4-11. The PWM signal to the pump is controlled by the LabVIEW program as shown in Figure 4-11. The base temperature is an important measurement to be determined with accuracy. The value depends on the geometrical shape and on the total amount of energy to be dispersed. A 1mm hole was drilled beneath the heater block and a T-Type Thermocouple was placed inside to measure the base temperature. T type thermocouples were calibrated using a precision oven by varying the oven temperature from room temperature to 45˚C.

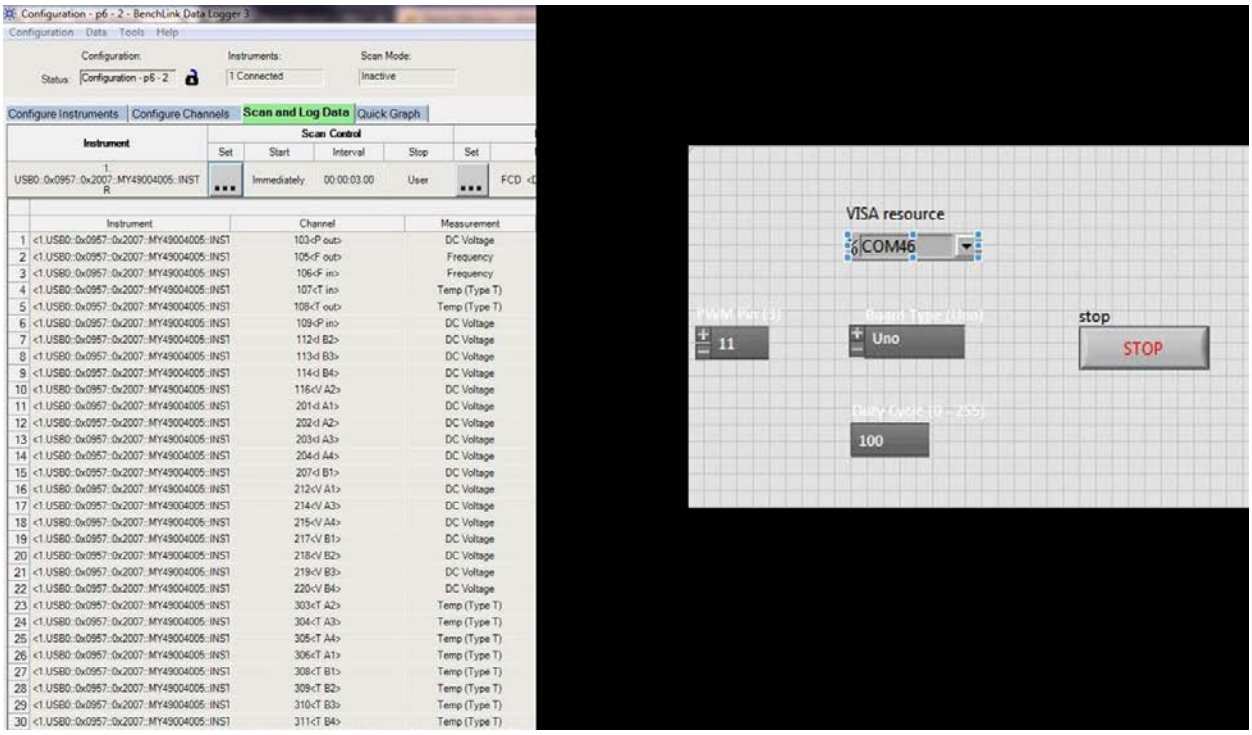

Figure 4-11 (a) Agilent Bench Link Data logger (b) LabVIEW Front Panel

4.4 Results

Firstly, the threshold temperatures of heater blocks are determined to have a safe operating region. The inlet temperature is maintained at 20oC using the Kinetics RS33AO11 recirculating chiller devices and the maximum flow rate is allowed through the water circuit. The pump PWM is given a duty cycle of 100 which generates a flowrate of 0.89lpm through the coolant circuit loop. Figure 7-1 shows the plot of Chip Temperature against the Power supplied to the heater blocks. Although, a constant power of 10W is supplied to each heater block, there is a deviation in the power pulled by each heater block, which is due to the resistance

change in resistors. Every resistive heater is measured using a multimeter for its resistance and there is an offset found on each resistor before operating.

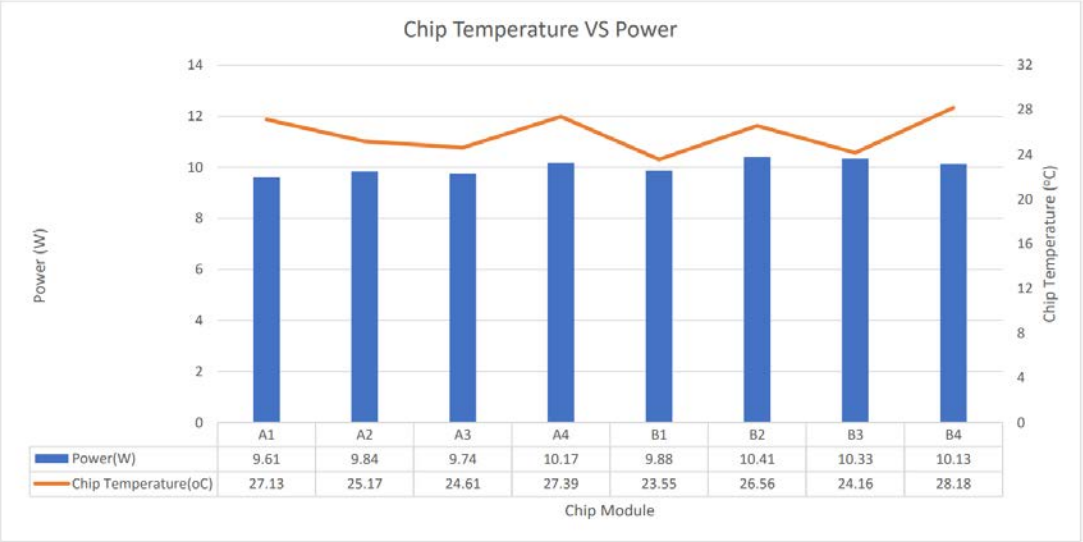

Figure 4-12 Temperature profile of the heaters

The change in temperature across the cold plate is monitored by varying the inlet temperature using the Heat exchanger. The input power to both sections of the heater blocks are maintained at 320W and a constant flow rate of 0.89lpm making water flow constantly in the loop. The Figure 4-13 shows a linear decrease in the temperature rise as the inlet temperature increases.

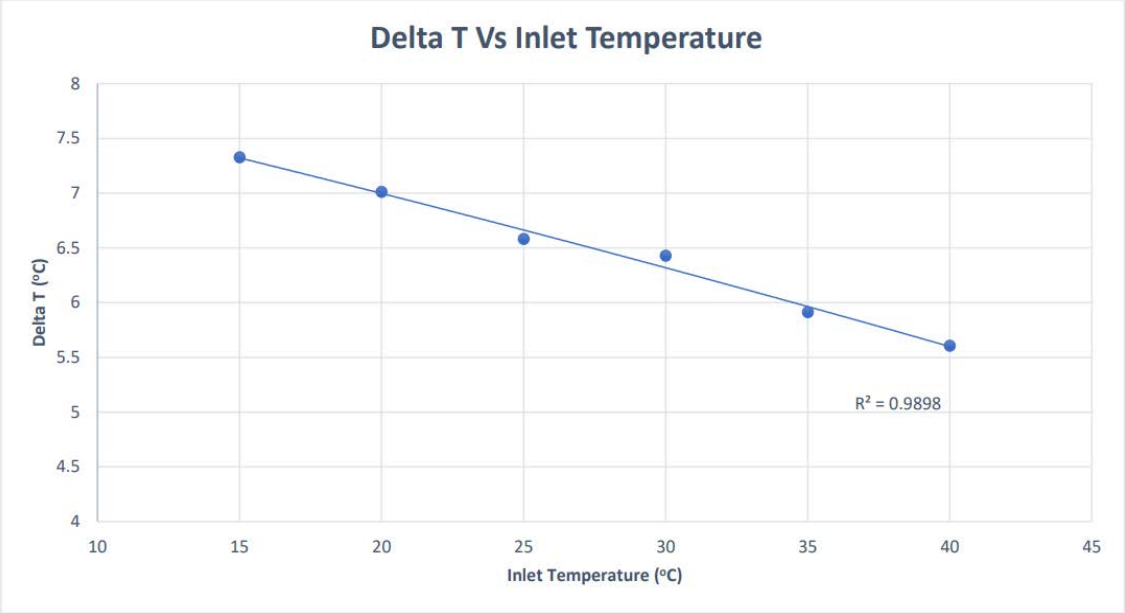

Figure 4-13 Temperature Difference as a Function of Coolant Inlet Temperature

4.4.1 Pressure drop Vs flowrates

To validate the energy equation, the pressure gradient across the cold plate is studied in the same fashion by keeping the input power constant at 320W and maintaining the coolant inlet temperature to the cold plate at 20˚C. The plot shows a linear increase in the change in pressure as the flow rate increases. The flow rate is varied by controlling the PWM signals. This satisfies the energy equation

$$Q=mCp\Delta T.$$

4.4.2 Temperature gradient at various flow rates

The change in temperature across the cold plate is studied by varying the flow rate and having the input power and the inlet temperature constant. The input power to the heater blocks is 320W and the inlet temperature is maintained at 20˚C. The plot is shown in Figure 4-15.

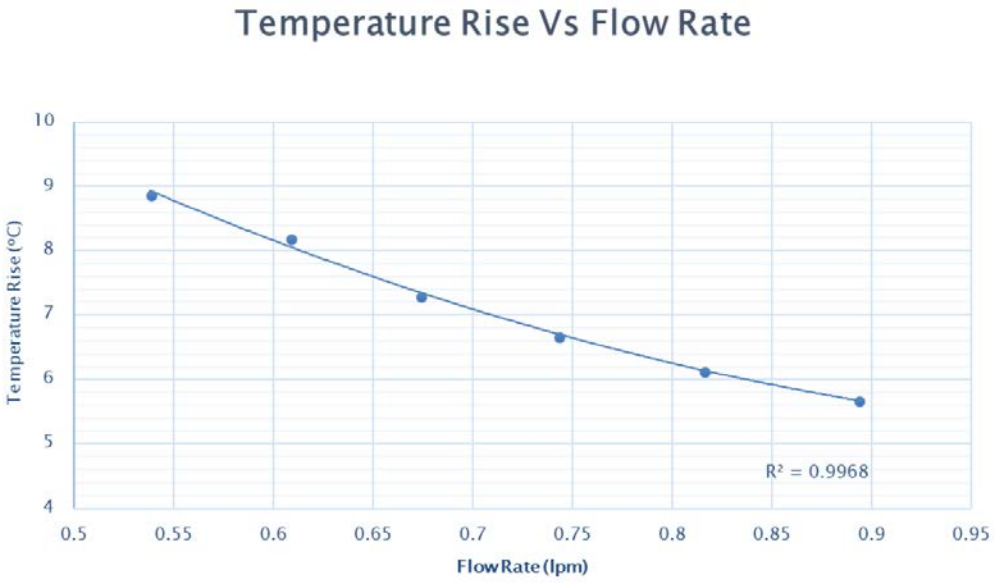

Figure 4-14 Temperature gradient at various flow rates

4.4.3 Thermal resistance calculation

The thermal resistance is calculated by the following formula. The inlet temperature of the coolant is maintained at 20°C and the maximum flow rate is allowed through

the coolant circuit. The input power to the setup is varied and the thermal resistance is calculated.

$$R_{TH}=\frac{T_b-T_{in}}{Q_{in}}$$

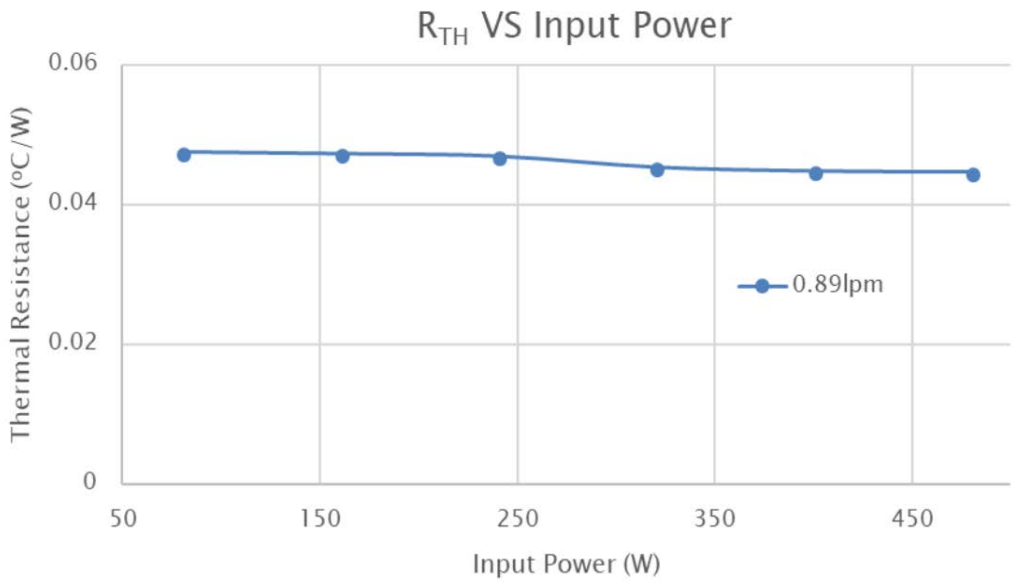

Figure 4-15: Thermal Resistance Vs Power

4.5 Flow Control Device Prototype Testing

The flow control device prototype is manufactured using 3D printing. The prototype consists of three individual components: The external housing, a holder and the block. The springs are loaded onto the holder with the block in the middle and then slid into the main housing. The holder is then sealed using a leak proof sealant. Photographs of the prototype are provided in the appendix. An

experimental test rig is used to analyses the performance of the FCD. A heat exchanger is used to control the temperature of the coolant being delivered to the FCD. The test rig is populated with flow, pressure and temperature sensors at various points on the circuit. A relief valve is connected in parallel to the FCD to allow for optimum pressure drop across the FCD. Data acquisition devices are used to log data from the various sensors. Flow rate changes for change in coolant temperature is recorded and documented.

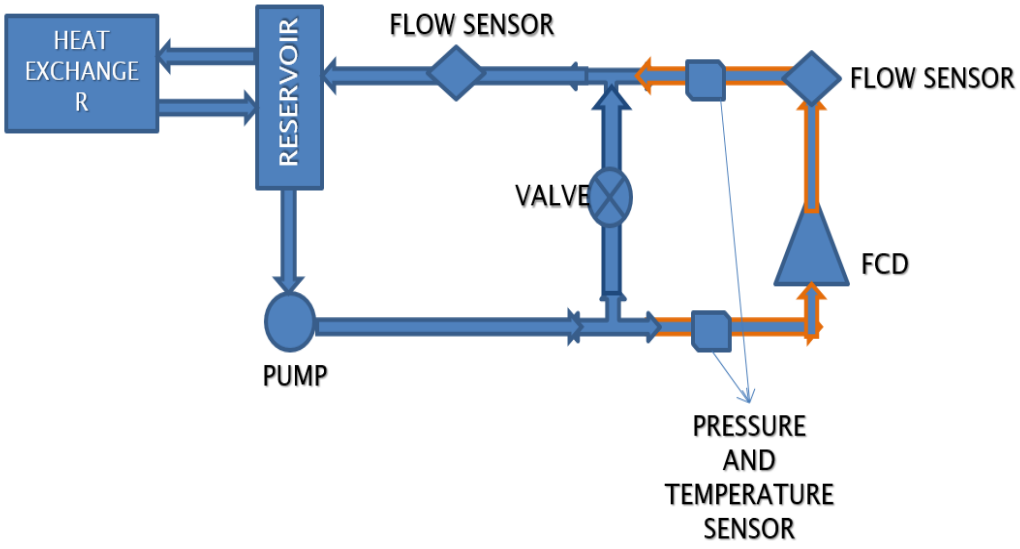

Figure 4-16 Flow control device prototype testing schematic

4.5.1 FCD Flow analysis

The experimental test rig explained in section 5.1 is used to quantify the performance of the FCD prototype. Data acquisition from various sensors in the

test rig was done for every three seconds. Constant flow rate was provided throughout the experiment by the pump. Temperature of the water was varied using the heat exchanger. From the experimental data obtained, a flow rate change of about 0.1 lpm was observed for a temperature change from 20°C to 45°C. The change in flow rate is linear with respect to temperature.

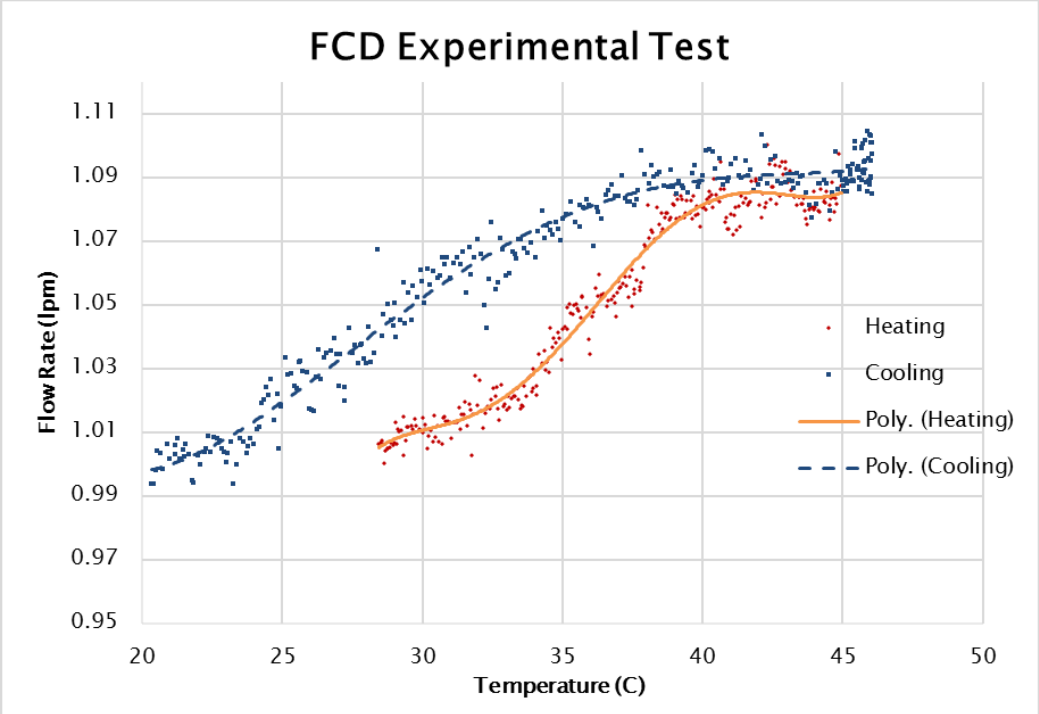

Figure 4-17 Change of flowrate with respect to temperature

The FCDs must be place closer to the exit of the cold plate to avoid response time. Also, the maximum performance can be achieved by placing the FCDs closer to the cold plate.

4.6 Power Savings with FCD

The performance characteristics of the FCD are studied by connecting them in the coolant loop without cold plate and heater blocks and an optimum working range is obtained. The Figure 8-2 shows the experimental test results of the FCD connected in the coolant circuit. Also, the plot of change in temperature against the inlet temperature is considered, where the inlet temperature of 35˚C give us a change in temperature of 6˚C. An inlet temperature of 35˚C is considered as we are dealing with warm water cooling.

Comparing that data with the FCD experimental setup, it is clearly seen that there is a variation in flow rate from 1.0 lpm to 1.09 lpm. These calculations are carried out for a 160 W power module and a pump savings of around 9% is calculated. By increasing the modules, the use of FCDs increases at the exit of the cold plates which results is more pumping power savings.

CHAPTER 5

MINIATURIZATION

The aforementioned FCD is proof that the selected material is an excellent fit for dynamic cold plate application. The experimental data is utilized to design the miniaturized version of the FCD that can be incorporated into the cold plate. The dynamic cold plate might have multiple sections as mentions in chapter 1 the proposed mini FCD will be attached to those sections at the outlet. The concept is intended to have FCD's incorporated in the cold plate as a part of it. As a part of that a two-piece FCD is designed to just mimic the scenarios in the top section of the cold plate. A rectangular butterfly valve is analyzed using ANSYS fluent to linearize the flow with respect to the damper angle.

5.1 Design Considerations

In order to most accurately emulate a typical processor a 160W heat source is considered as the test module. A 160 W module is chosen just to show that the concept works. Experimentally testing a 160W module was much more feasible than designing a high-power density module. It is to be noted that higher power will only further improve the performance of the FCD. The heat dissipation calculations were done based on the assumption that the thermal resistance offered by the cold plate is negligible. We assumed a ΔT of 10 degrees across the module for convenience. A hydraulic diameter of 10 mm is considered, which provides

optimum velocity for our flow control device and is adaptable over a range of heat sources. This design choice also keeps pressure drop due to losses minimal at various locations.

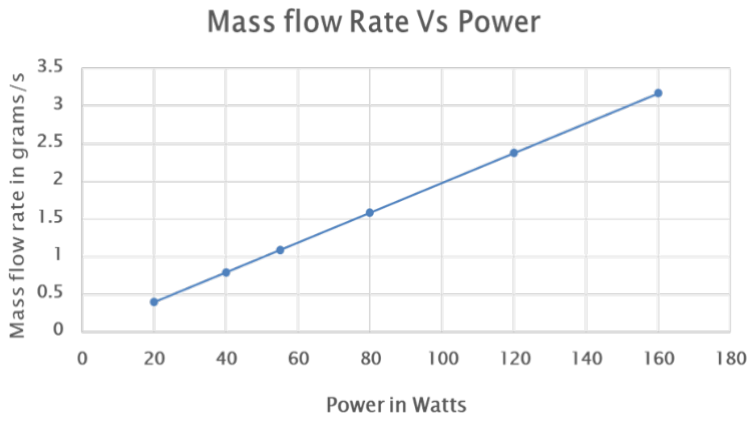

Figure 5-1 Variation of mass flow rate in grams/s with respect to power in watts.

Required hydraulic diameter is calculated for a fixed velocity and temperature difference for a range of power dissipations from 20W to 160W. It can be observed that there is an almost linear increase in hydraulic diameter from 3mm to 8mm with respect to power. Based on this deduction we designed a flow control device with butterfly valve to have variation in the flow rate for different power dissipations.

5.2 Valve design

Valve designing is done considering some factors that affect the overall system efficiency like pressure drop across the device, flow with respect to angle change

and flow rate range. The traditional circular butterfly valve design will meet most of these requirements except for the flow rate variation with respect

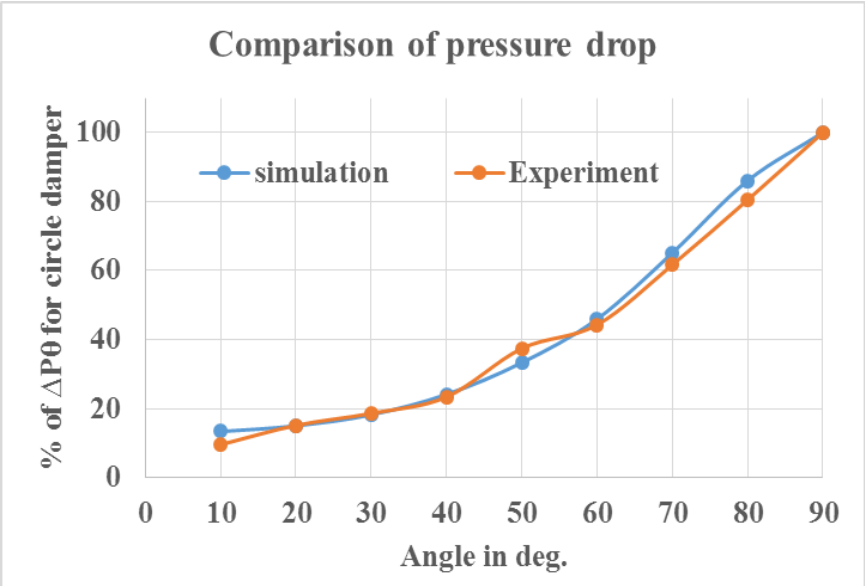

Figure 5-2 Pressure drop variation in percentage and damper angle, comparing experimental and simulated results.

to the damper angle, so to address this issue we changed the cross section of the damper from circular to rectangular. In rectangular cross section the length to breadth ratios are varied to find an optimized design.

A circular FCD is designed with the required hydraulic diameter to validate with available experimental data. As shown in the Figure 5-3 Plot between pressure drop variation in percentage and damper angle, comparing circular and rectangular cross sections. below the percentage of pressure drop verses angle is compared

between the simulation values and the experimental data taken from the thesis paper of Del Toro, A [29]. The maximum pressure value at 10 degrees is take as reference to calculate the percentage of pressure drop. These values are very close the maximum error is 3% at 20 degrees.

5.2.1 Circular vs Rectangular cross sections

Now we compare the circular cross section with the rectangular one to compare the change in the pressure drop with respect to the angle. The Figure 5-4 Mass flow rate and damper angle for circular and rectangular cross sections. below shows the pressure drop for a rectangular when compared to the circular cross section. We can observe that pressure losses are less in rectangular when compared with circular damper.

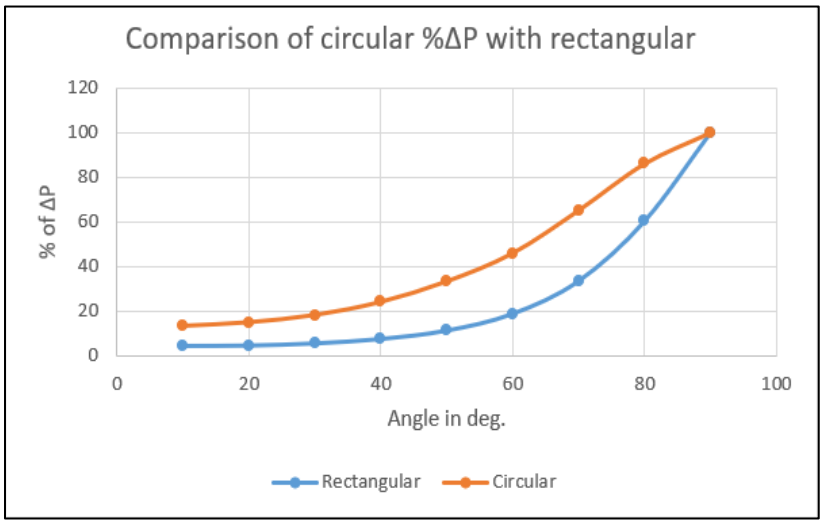

Figure 5-3 Plot between pressure drop variation in percentage and damper angle, comparing circular and rectangular cross sections.

Another useful comparison to help illustrate the advantage of using a rectangular cross section is given below. We compare the mass flow rate of both cross-section shapes for various damper angles. The rectangular design provides a wider range of flow rates, allowing much lower flow rates at angles nearing completely closed position. Hence the rectangular cross section allows us for use of the flow control device over a wider range of temperatures. Also, the linear trend is much more consistent with the rectangular design especially in angles nearing closed position when compared to the circular design which tends to saturate at these angles.

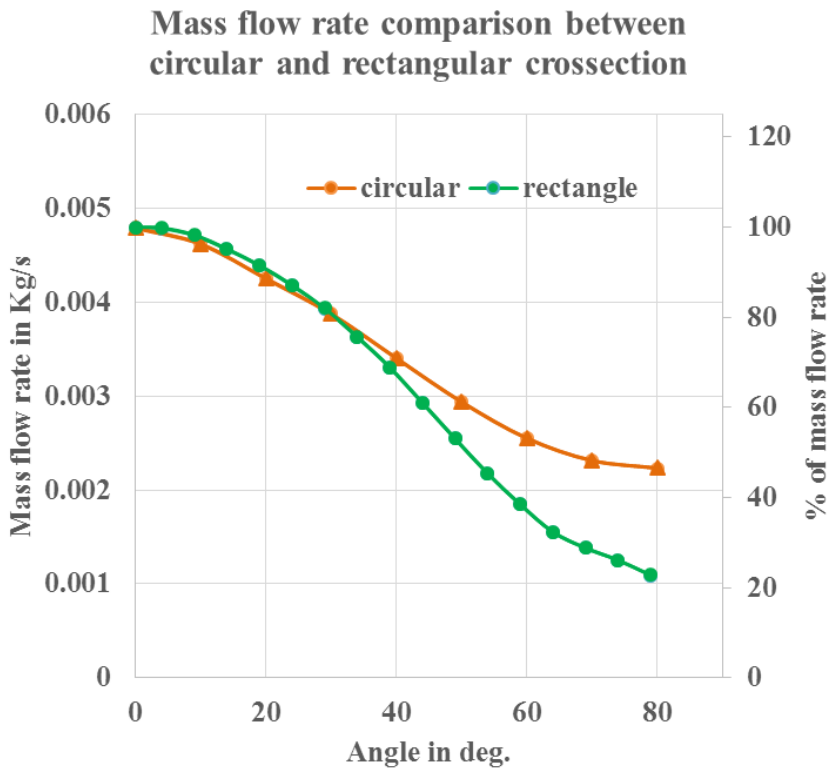

Figure 5-4 Mass flow rate and damper angle for circular and rectangular cross sections.

5.3 Design of flow control device

The flow control device consists of circular inlet and outlet. When we move closer towards the damper, the circular cross section tapers into a rectangular cross section. As discussed in the previous section a rectangular cross section at the damper allows us to have more control over the linearization of the flow, when compared to a circular cross section.

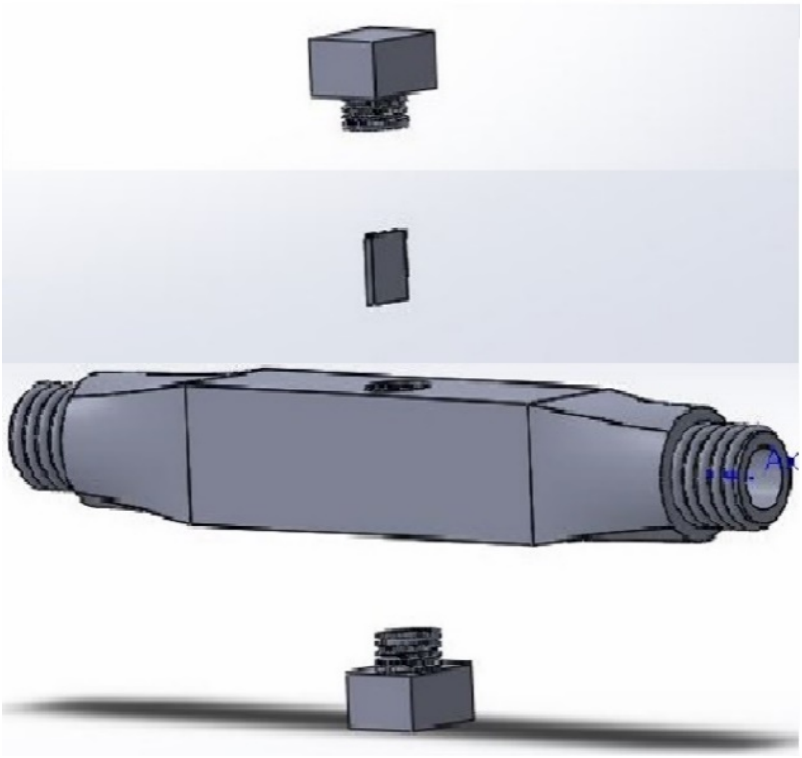

Figure 5-5 Illustration of flow control device design

The damper is controlled by an active material that is sensitive to temperature. In order to fit the flow control device in the server, the overall dimension of the FCD

are kept very small, with the cross sections in the order of 15mm and the entire length of the device around 80mm.

5.4 Meshing

To solve the Fluid model in CFD, the continuous fluid medium has to be partitioned into discrete volumetric cells vertices or nodes and elements. This process is called meshing. For any study using CFD solver, fluid properties like velocity, temperature, pressure etc. are calculated at every volumetric cell and are integrated and averaged to get a total value of all the properties for whole fluid [4]. Increase in the number of volumetric cells results in more refined results which imitate real life experimental results. In the present problem, CFX fine meshing is used with slow transition and a fine span angle center. The cell geometry features a minimum size of 2.5E-2 mm, max face size and max Tet size of 5mm. Inflation is used for fluid around the damper to capture highly refined flow features around the valve. Inflation is a meshing property which creates a fine and slowly growing mesh at a surface to capture more accurate fluid properties around that surface.

Mesh sensitivity analysis is done comparing the mass flow rate for different mesh size. We observed there is no significant change in the mass flow rate when mesh density goes above 50 elements per mm^3. The chosen cell geometry of 2.5E-2 mm results in much higher element density than the above-mentioned threshold and provides highly accurate results.

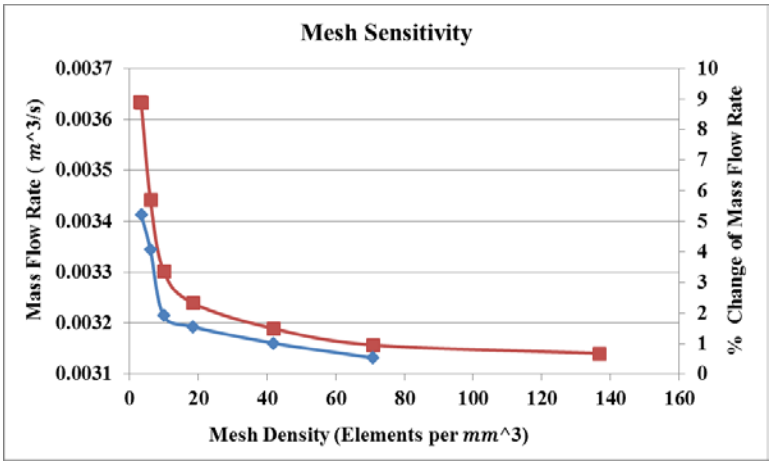

Figure 5-6 Mass flow rate vs Mesh density and

percentage change in mass flow rate vs Mesh Density.

5.5 Computational Fluid Dynamics

The equations that govern the motion of a Newtonian fluid are the continuity equation, the Navier-Stokes equations, the momentum equation and the energy equation. The set of equations listed below represents seven equations that are to be satisfied by seven unknowns [3]. Each of the continuity, energy, and momentum equations supplies one scalar equation, while the Navier-Stokes equations supply three scalar equations. The seven unknowns are the pressure, density, internal energy, temperature, and velocity components. The scope of our analysis predominantly lies in the laminar region of flow owing to low flow velocities and relatively simple geometries. The only instance where a k-Epsilon turbulence model is used is in the region between when the damper is completely closed and

when it is open by an angle of 10 degrees. The equations used for solving in the laminar as well as turbulent regions are listed below.

$$\text{Continuity}: \quad \frac{\partial \rho}{\partial t} + \vec{\nabla} \cdot (\rho \vec{u}) = 0$$

$$\text{Momentum}: \quad \rho \frac{D\vec{u}}{Dt} = -\vec{\nabla} p + \nabla(\mu \nabla \vec{u}) + \vec{f}_b$$

$$\text{Energy}: \quad \rho \frac{DE}{Dt} = -\vec{\nabla} \cdot (p\vec{u}) + \vec{\nabla} \cdot \left(k_t \cdot \vec{\nabla}(T)\right) + \Phi + S_E$$

$$\text{Turbulent kinetic energy}: \quad \frac{\partial(\rho k)}{\partial t} + \vec{\nabla} \cdot (\rho k \vec{u}) = \vec{\nabla} \cdot \left[\alpha_k(\mu + \mu_t) \cdot \vec{\nabla}(k)\right] + 2\mu_t E_{ij} \cdot E_{ij} - \rho\varepsilon$$

$$\text{Turbulent dissipation}: \quad \frac{\partial(\rho\varepsilon)}{\partial t} + \vec{\nabla} \cdot (\rho\varepsilon \vec{u}) = \vec{\nabla}\left[\alpha_\varepsilon(\mu + \mu_t) \cdot \vec{\nabla}(\varepsilon)\right] + C_{1\varepsilon}^{*} \frac{\varepsilon}{k} 2\mu_t E_{ij} \cdot E_{1j} - C_{2\varepsilon}\rho \frac{\varepsilon^2}{k}$$

where

$$\mu_t = \rho C_\mu \frac{k^2}{\varepsilon}, \quad C_\mu = 0.0845, \quad \alpha_k = \alpha_\varepsilon = 1.39,$$
$$C_{1\varepsilon} = 1.42, \quad C_{2\varepsilon} = 1.68$$

and

$$C_{1\varepsilon}^{*} = C_{1\varepsilon} - \frac{\eta\left(1 - \frac{\eta}{\eta_0}\right)}{1 + \beta\eta^3}, \quad \eta = (2E_{ij} \cdot E_{ij})^{1/2} \frac{k}{\varepsilon},$$
$$\eta_0 = 4.377, \quad \beta = 0.012$$

5.6 CFD Results

The damper ratios were varied parametrically on ANSYS fluent to obtain results for several other variables like pressure drop and mass flow rate. The height to width ratio of the damper cross section (damper ratio, r) is varied between 0.8 and 1.5 to determine the design which will provide linear change in flow with change in damper angle.

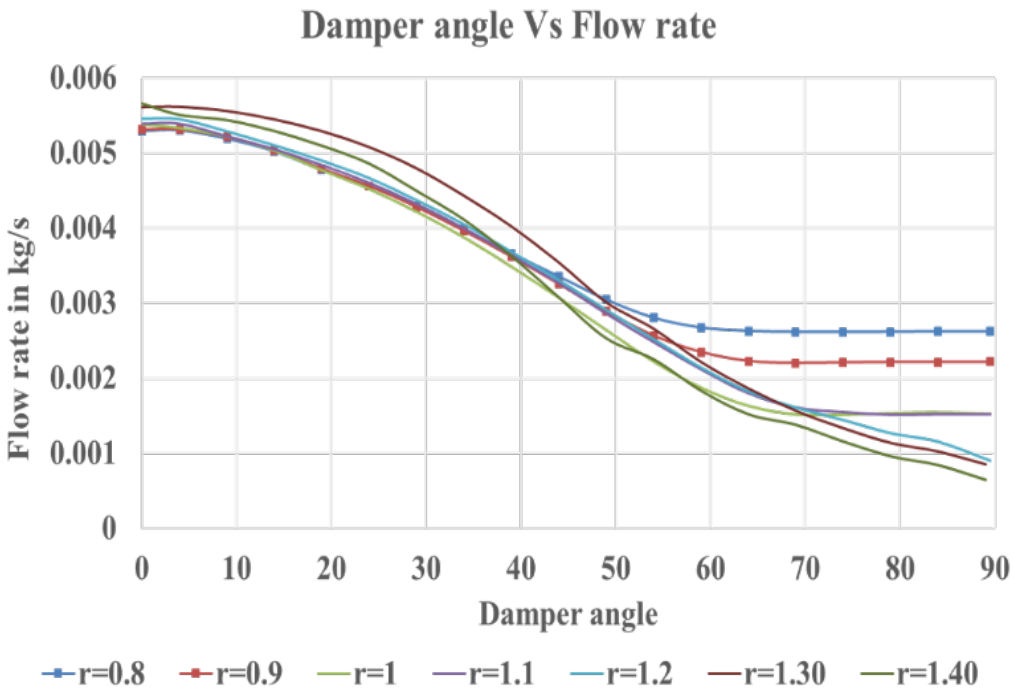

Figure 5-7 mass flow rate and the damper angle for various r ratios.

Figure 5-7 mass flow rate and the damper angle for various r ratios. shows the plot between mass flow rate and damper angle for various damper ratios(r). The

x axis shows the damper angle with 0 degrees indicating completely open position and 90 degrees indicating completely closed position; the y axis shows the mass flow rate in kg/s. We designed this flow control device to have a small non-zero flow rate even when the damper is completely closed.

Based on the flow rate required at idle condition of the server, we are able to modify above mentioned minimal flow at closed damper position to meet that requirement. From the graph we can observe that for r=0.8 the range of flow rates is very limited. When we increase r from 0.8 through 1.5, we observe increment in the flow rate range, saturating at r=1.2 above which there is no pronounced increment in flow rate range. We choose 1.2 as the optimum value for r, as higher r values tend to produce greater torque on the damper.

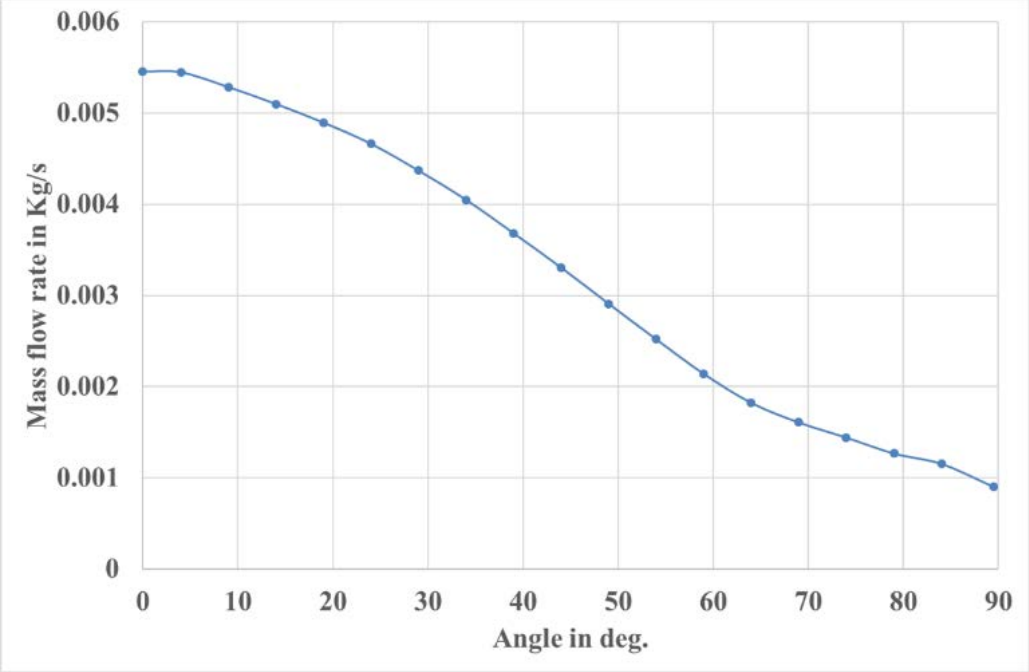

Figure 5-8 Plot between mass flow rate and damper angle for r=1.2.

Figure 5-9 shows the plot between mass flow rate and damper angle for r=1.2. We observe that the flow rate varies most linearly with change in damper angle compared to other ratios. Figure 5-9 Plot between Reynolds number and damper angle for r=1.2.indicates the change in Reynolds number with respect to change in damper angle.

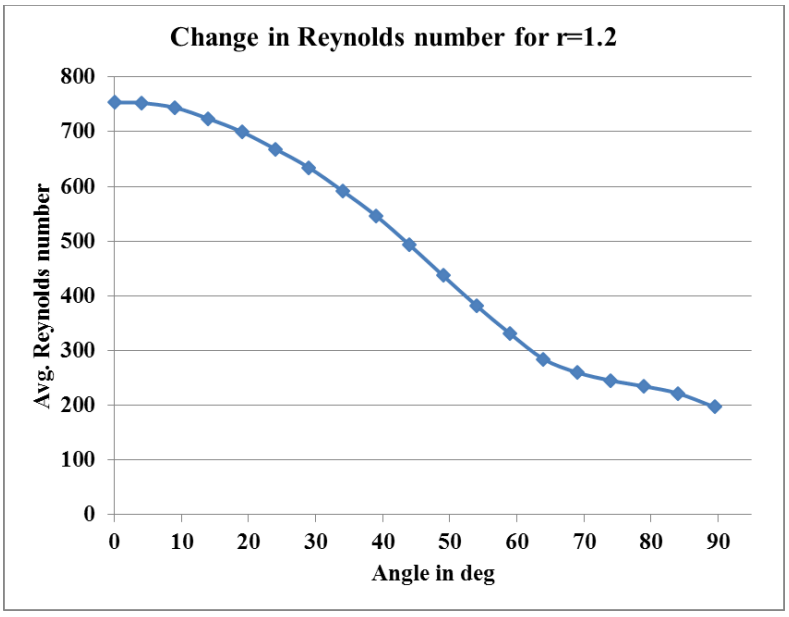

Figure 5-9 Plot between Reynolds number and damper angle for r=1.2.

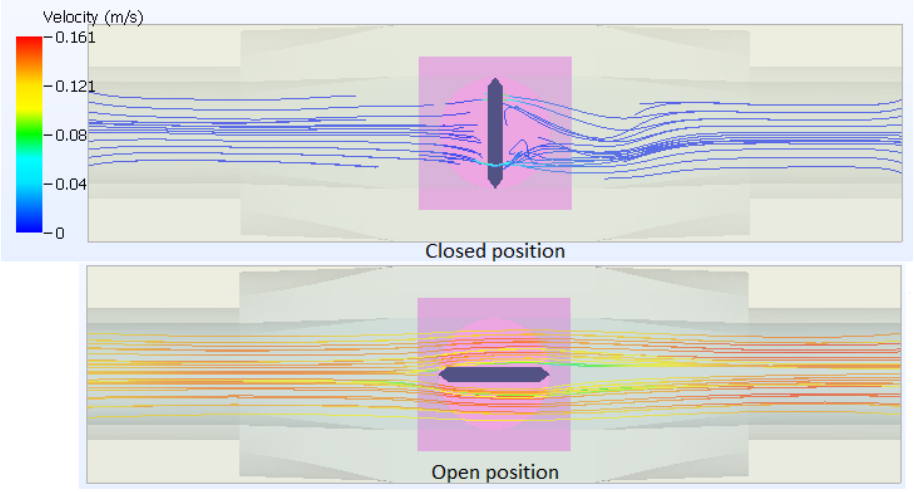

Figure 5-10 Cross sectional view of the FCD at closed and open position

In steady flow, the fluid passing a given point maintains a steady velocity. The motion can be represented with streamlines showing the direction of water flow in different areas. Fig 12. Shows the change in color of the streamlines as the velocity increases. Blue color of flow lines shows very less flow across the damper while the orange color shows high flow velocity in the range of 0.121 to 0.161 m/s.

5.7 Forces on the damper

Hydrodynamic moment on the damper is shown below with respect to angular change. The maximum hydrodynamic moment observed on the damper is about 5E-06 Nmm which is indicated as 100% in the plot below. We can observe that when the damper goes from completely open to closed position, the hydrodynamic moment increases until approximately 25 degrees from open position and goes back to zero when it is completely closed.

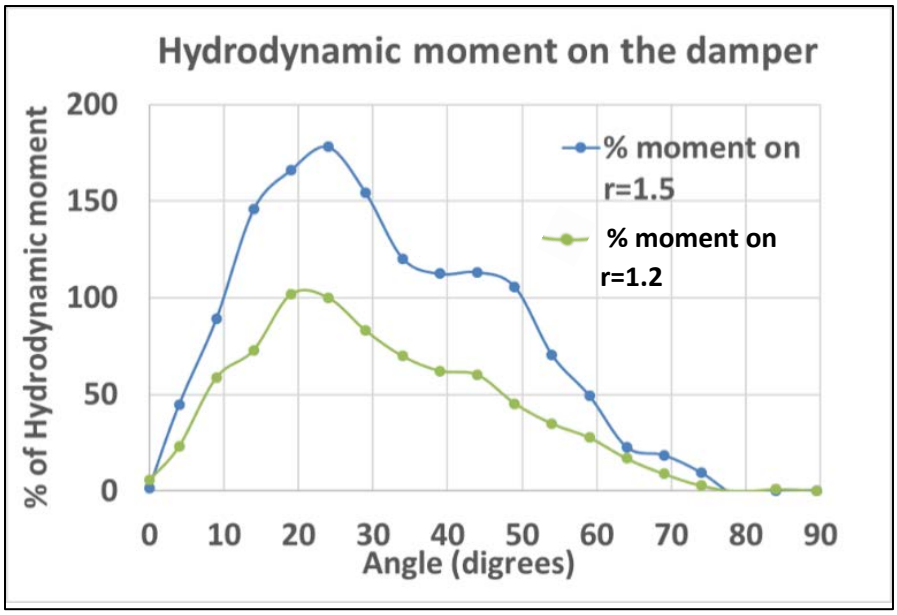

Figure 5-11 percentage of hydrodynamic moment and damper angle for two different r values.

The Figure 5-11 shows the ANSYS CFX result contours of force distribution on the damper at three different damper angles namely 24 degrees, 44 degrees and 89 degrees. We can observe that the 24-degree contour has more force on the side of the damper that moves with the flow. When the damper moves towards the closed position, the force concentration moves gradually from one side of the damper towards the center of the damper.

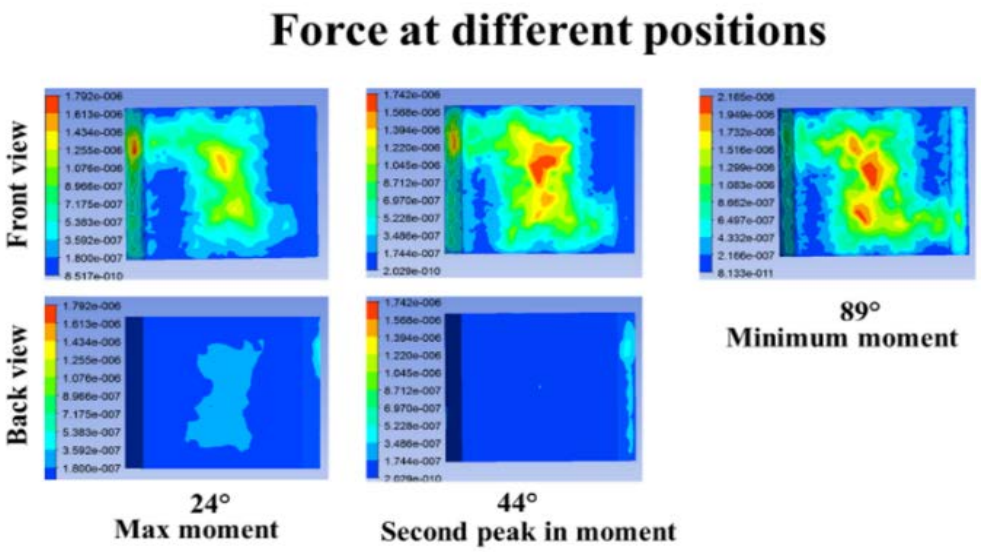

Figure 5-12 Contours of force acting on the damper

It is to be noted that these can basically be considered as a solid structure blocking a steady viscous flow. Hence the drag force equation is quite straightforward and is given by:

$$F_{Drag} = \frac{1}{2}\rho U^2 A C_D$$

The forces and a moment on the damper greatly influence the actuator selection for the FCD and the material selection for the damper. The FCD actuator must be selected in such a way that the moment it generates is either of a magnitude much larger than the peak hydrodynamic moments or is able to sufficiently compensate for it by providing non-linearly high moments at the peaks. The material selection

for the damper must be done in such a way that the damper always remains a rigid body at all positions and does not warp or bend dude under the force exerted by the fluid.

The dynamic cold plate works better with an array of smart flow control devices, which effectively does the job of the combination of a temperature sensor, control system and an actuator. In our flow control device, we use an active material which rotates the damper with respect to change in temperature. To have better control overflow rate, the rectangular butterfly valve design is better than the traditional circular butterfly valve because it varies flow rate more linearly with change of angle. Through CFD analysis we can conclude that a damper ratio of r=1.2 is good in linearizing the flow. This can also possibly find applications in different fields apart from data center water cooling as discussed before.

5.8 Future dynamic cold plate design

The analysis of miniaturized FCD is used to design the dynamic cold plate as shown in the Figure 5-13 the cold plate is made of three layers. Cold plate Base is a copper plate with fins fallowed by the second layer that can be incorporated with mini FCDs and the final top layer that covers the FCDs with required spacing. There is potential to analyze and optimize this cold plate design. The introduction of the FCDs needs good control strategy to utilize its best performance.

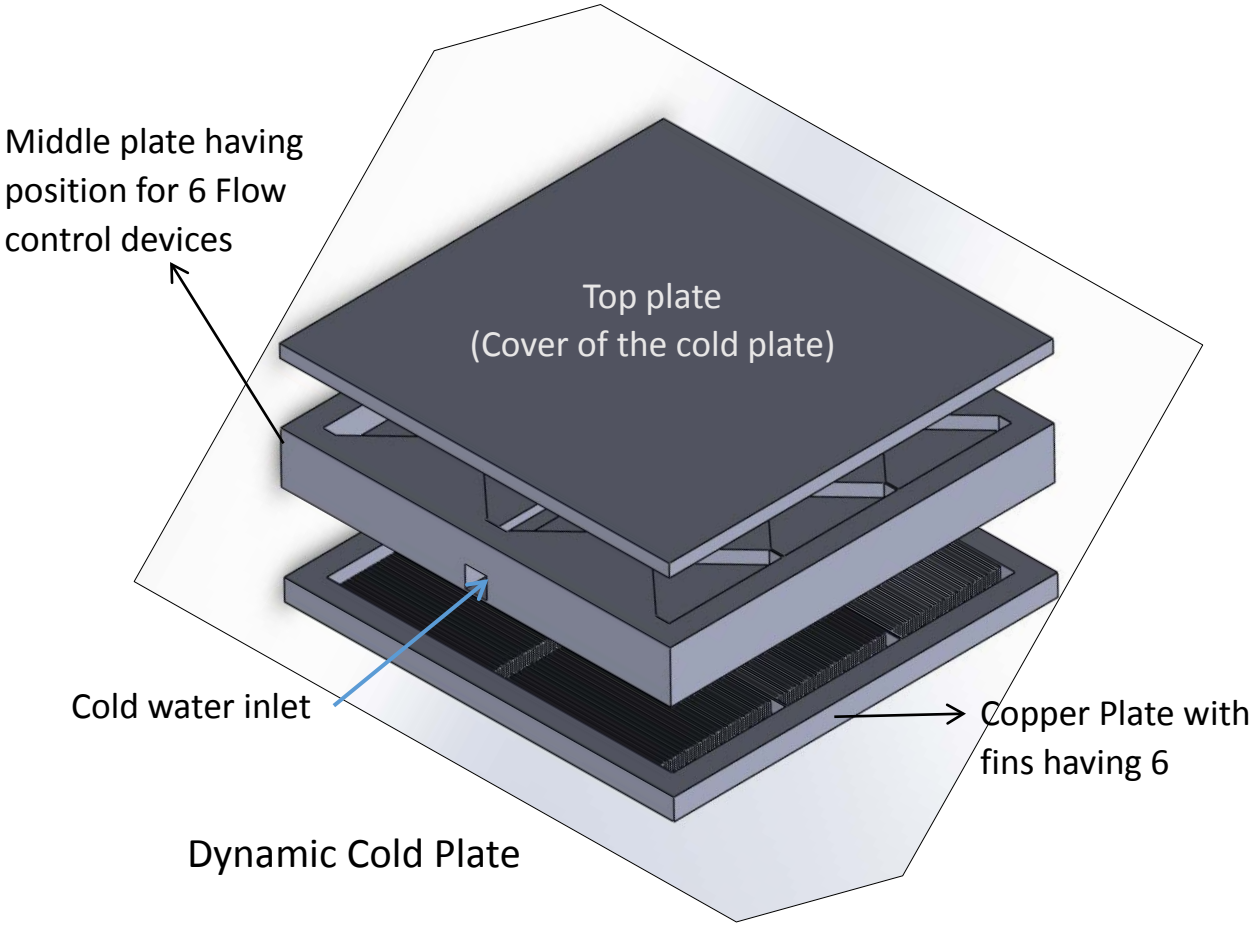

Figure 5-13 future dynamic cold plate assembly

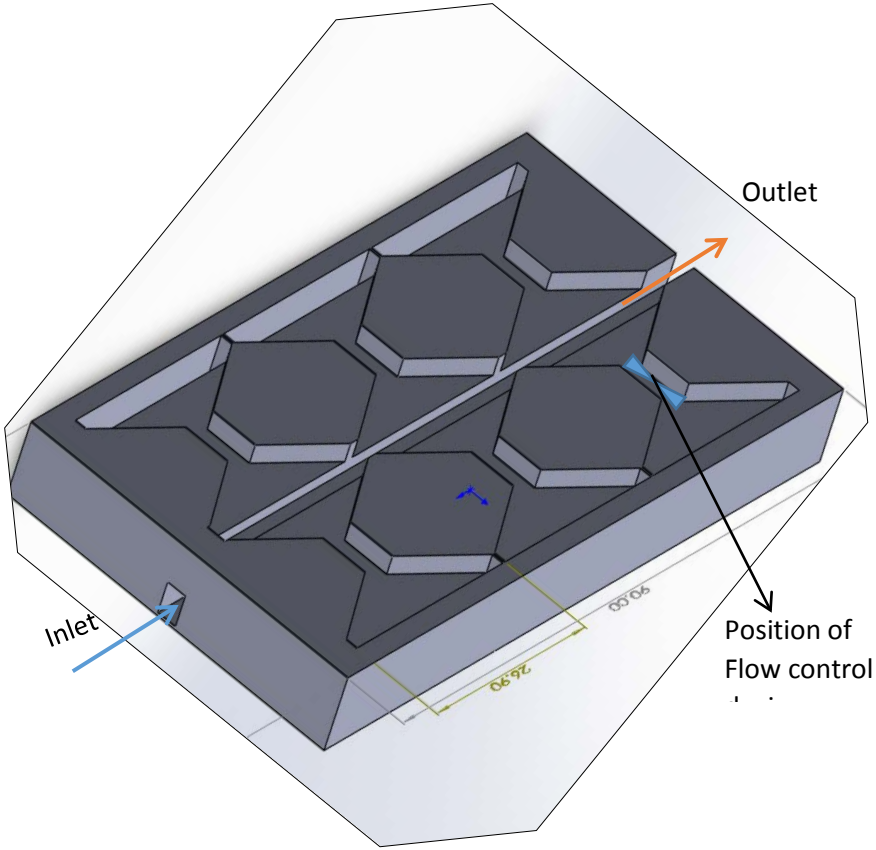

Figure 5-14 second dynamic cold plate layer with FCDs

CHAPTER 6

RACK AND DATA CENTER LEVEL DYNAMIC COOLING

The utilization of a server in the datacenter is determined by the total load on the data center. In a study done by earlier researchers found that only 25% of the data center is being used [30]–[32]. Introducing an FCD at server level have the potential to reduce the cooling energy for the servers running at idle conditions. The existing servers can be easily equipped with an FCD without changing the existing architecture of the server and the building.

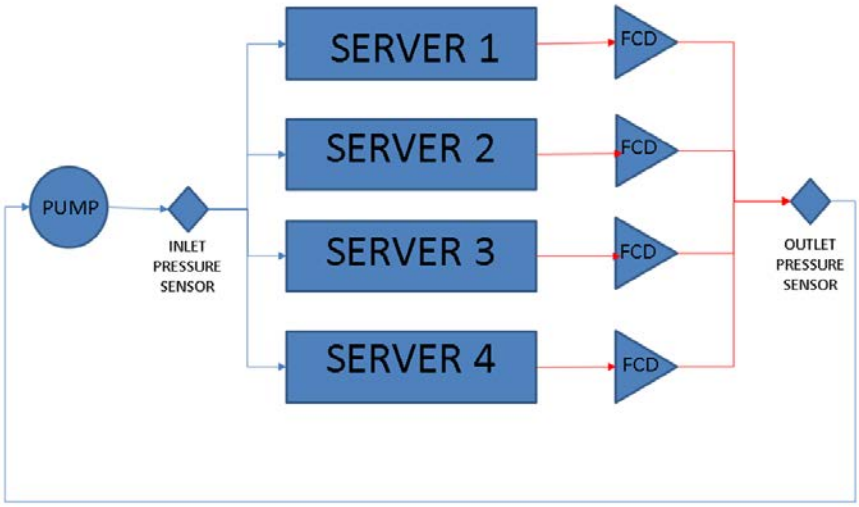

Figure 6-1 Schematic of Rack level flow control device

Each server is provided with an individual flow control device which senses the heat output and regulates the flow of coolant to each of the servers. A centralized

pump is used to pump the fluid to the cluster. This significantly reduces the pumping power consumption over distributed pumping.

The schematic Figure 6-1 represents centralized pumping of coolant to servers fitted with flow control devices. Temperature and Pressure sensors at the inlet and outlet manifold are used to control the pump.

6.1 Dynamic Cooling Control Strategy

Control strategy was developed in 6sigmaEt using the ducting feature. it is very difficult to mimic the model with the actual components in CFD and hence 6 sigma tools were used to replicate the model. In this model several major flows restricting and heat generating components are chosen. Components considered for modeling are a pump, 4 components and 4 Dampers which replicate the actual working of an FCD, 4 heat sinks replicated to act as cold plates as this control strategy was developed for liquid cooling purposes.

For this to be executed further, a control strategy is required. To have a good energy saving model control strategy plays important role besides DCP's and FCD's.

Hence the urge of developing a control strategy lead to a prominent path where pumping power savings using FCD and a DCP is attained.

- Pressure driven control
- Temperature and pressure-based control

6.1.1 Pressure driven flow

In this type of system, the inlet temperatures are maintained constant. Only pressure across the system is monitored. Inlet supply temperatures are maintained constant varying Loads on the servers due to which there will be pressure difference created in the whole system. But since the Pressure difference across the system is urged to be maintained constant, the system tries to attain the constant pressure input varying the flow rate. The flow distribution between the cold plates will be taken care by self-regulating FCD's will be used to monitor the overall pressure drop of the system and will be controlling the pump based on the utilization of the rack. The heat exchanger can or cannot be included in the system. We are monitoring pressure with the help of pressure sensors placed at inlet and outlet which are used to control the pump reducing its pumping power

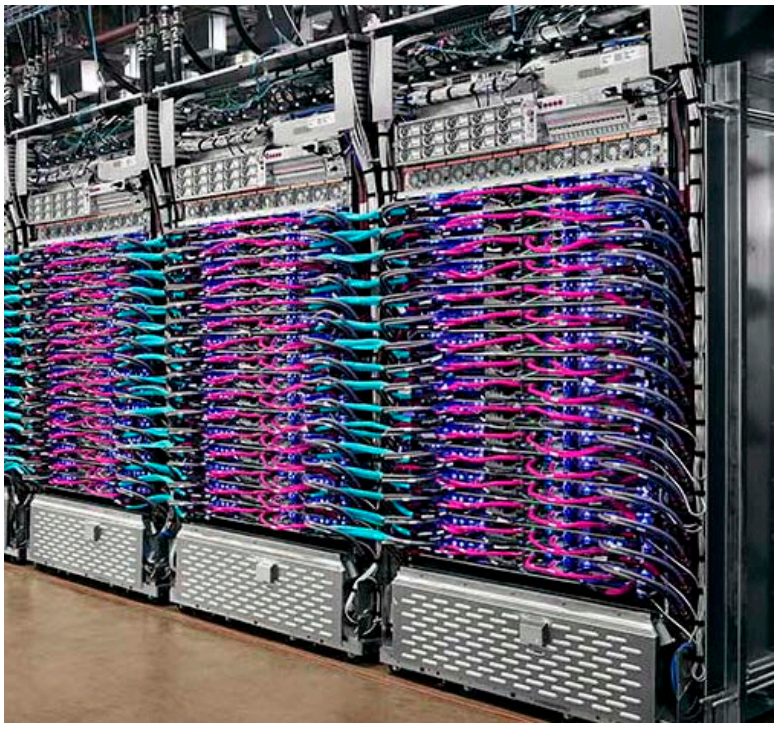

Figure 6-2 Google liquid cooled data center [33]

6.1.2 Temperature and pressure monitored flow

In this type of system, a constant heat extraction heat exchanger is used, Such as rack liquid to liquid heat exchanger. Here, both pressure drop across the system and outlet temperature are monitored giving the system enough flow rate at respective temperatures. Weights will be given to Temperature and pressure drop as the heat exchanger is also in in the system loop.

The same principle can be applied at the cold plate level in which we have a multi-chip scale module we can divide the cold plate into sections based on the design and requirement and this section can be attached with miniaturized FCD which acts

in similar manner. With this concept we can prioritize higher utilized servers which in return reduce pumping power and increase chiller efficiency.

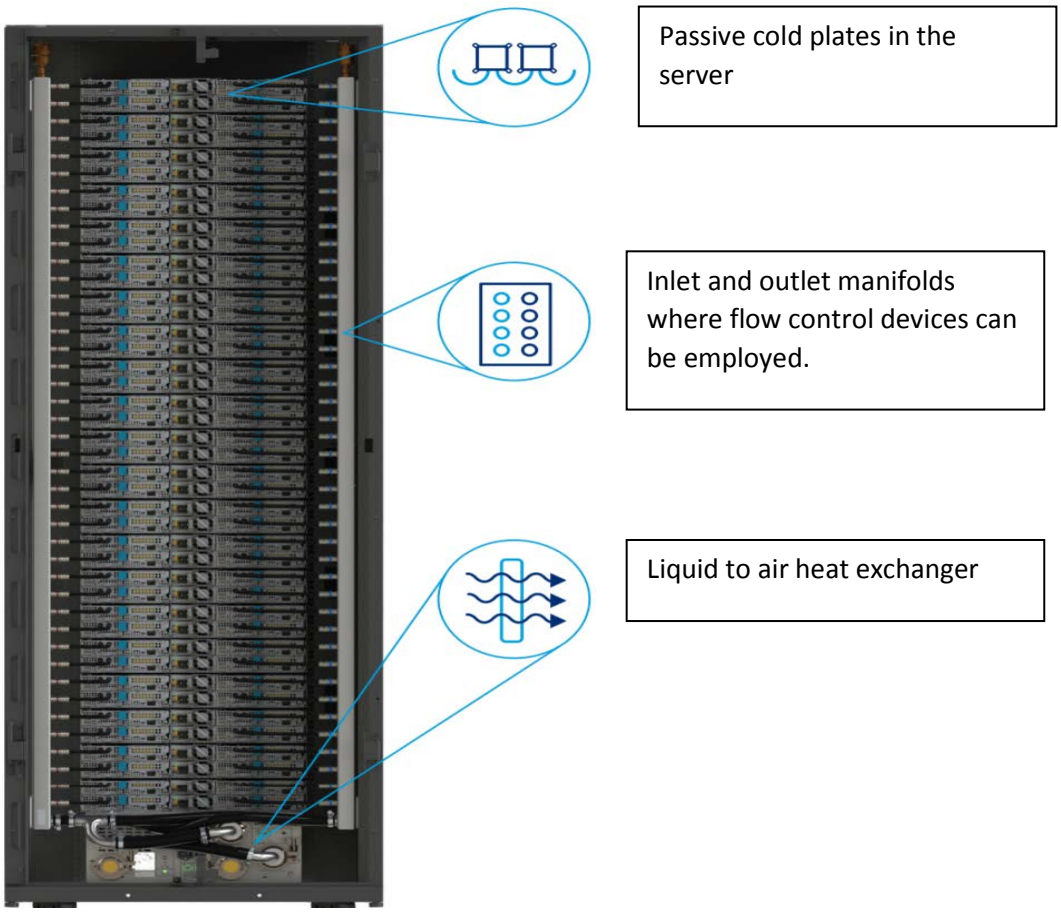

Figure 6-3 Cool IT DCLC rack [34]

6.2 6SigmaET Model

A CFD model is developed in 6Sigma to test and optimize the control strategy of FCDs. Figure 6-4 shows the 6Sigma model with four cold plates equipped with four different servers. The damper and temperature sensor represent the FCD in the

model. Experimental data from the temperature vs flow rate curve is used to regulated the damper. Presuure sensors at the inlet and outlet manifold regulated the flow of the coolant to maintain a constant pressure drop across the inlet and outlet during all positions of the damper.

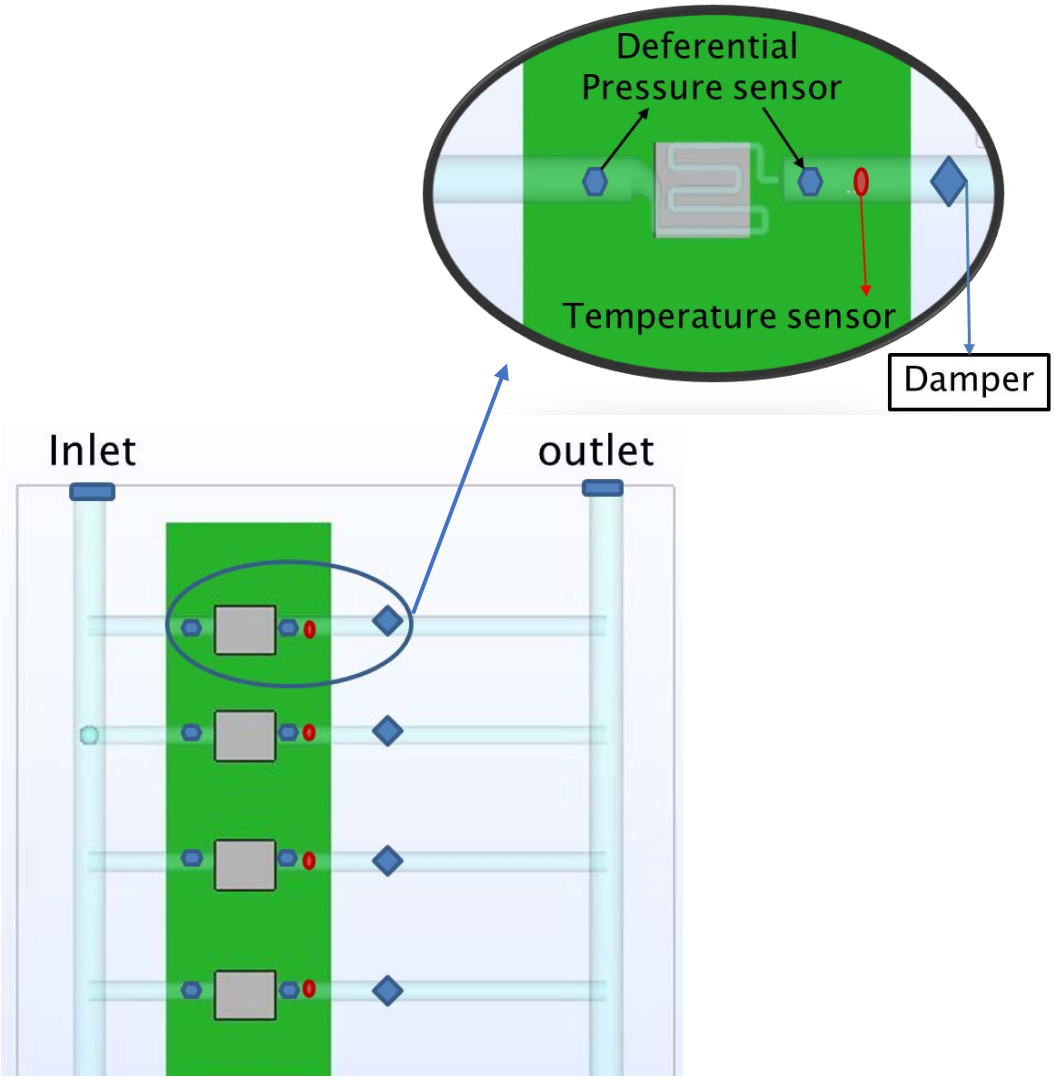

Figure 6-4 6Sigma model of 4 cold plates

6.3 MATLAB Integration

MATLAB is integrated with 6SigmaET to customize the two control strategies through which system is being controlled. For the Pressure Based Control, depending upon the pressure difference created in the system based on different loads, controller varies the PWM of the pump to attain the constant pressure input given to it. Dead Band width is set as 10 to have high accuracy for the Pressure and Temperature based control. The controller will change the opening area of the damper to regulate the flow rate. These Damper openings follow a hysteresis curve drawn from the experimental results of the FCD. Dead Band width is set as 0.1 to have high accuracy. Every iteration will report the temperature values to MATLAB and the output from the code is used by the solver as new inputs. All the MATLAB integrations are taken from 6Sigma user manual.

6.4 Modeling and Characterization of Cold Plate

6.4.1 Mesh Sensitivity Analysis

A grid analysis is carried out at different level to look at the grid sensitivity. 6SigmaET has the capability of adopting the grid based on the model. A local gridding feature in the software is used to create enough grid to capture the heat transport. From the Figure 6-5 Mesh sensitivity analysis it is evident that after 2

million nodes the change in the temperature and thermal resistance are insignificant. So, this model uses around 2 million nodes for all the simulations.

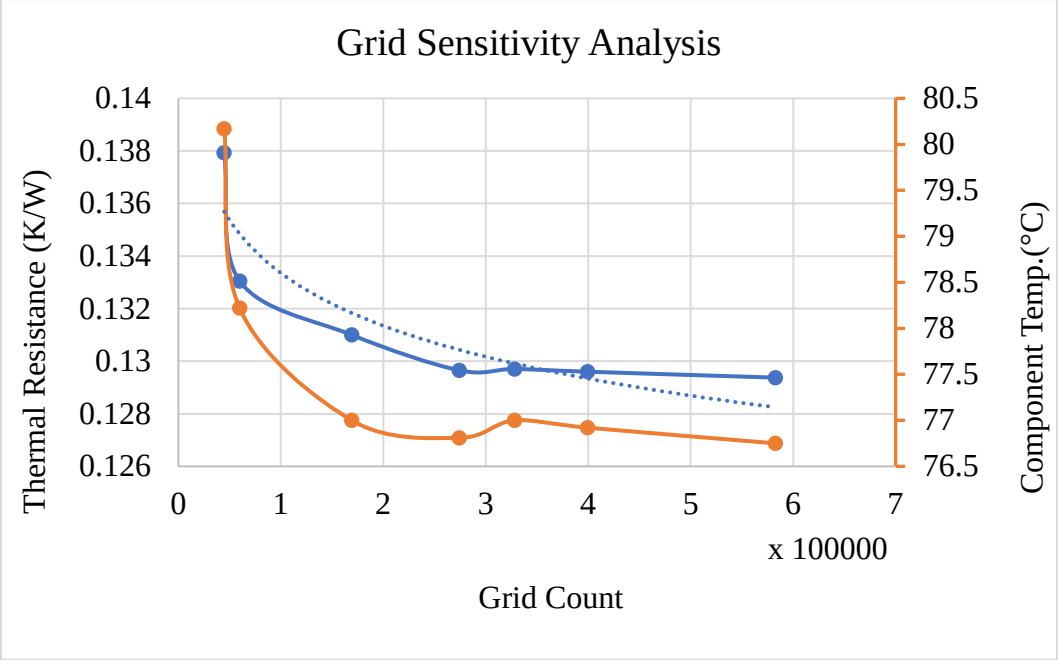

Figure 6-5 Mesh sensitivity analysis

6.4.2 Multi-variable optimization

The cold plated designed is a jet flow impingement type which impinge the cooling fluid into the fins in the form of small jets. The cooling fluid then passes through the fins of the cold plate and carry the heat out of the component.

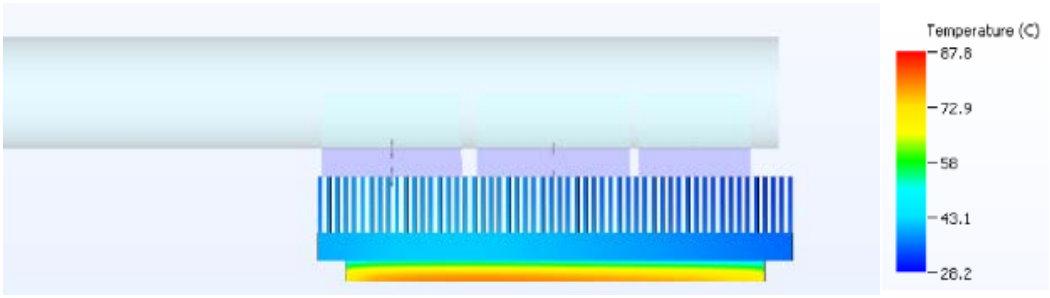

Figure 6-6 Impingement cold plate side view

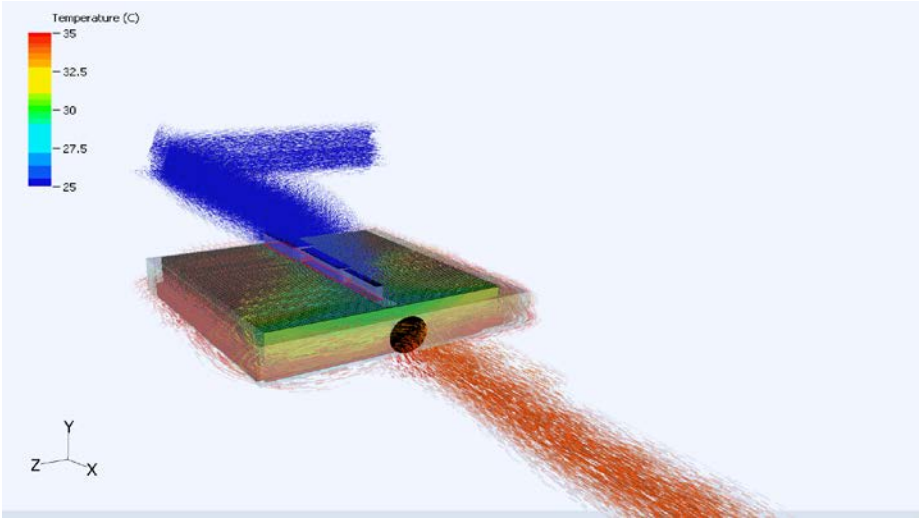

Figure 6-7 impingement cold plate with streamlines in isometric view

A multi variable study was done to optimize the cold plate design by varying fin thickness, fin separation therefore number of fins, and fin height inside the cold plate.

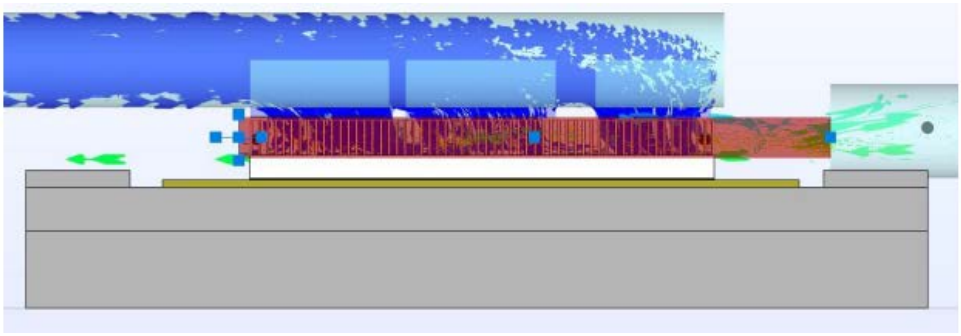

Figure 6-8 Impingement and flow direction

Table 6-1 Optimization results with all the variables

Power W	Fin thickness mm	Number of fins	Fin separation mm	Flow rate L/min	Supply temperature ^{0}C	Component temp ^{0}C	Pressure Difference pa	Temp difference ^{0}C
500	***0.1***	***101***	***0.3004***	***1***	***15***	***52.81***	***1035.9***	***7.92***
500	0.1	51	0.7008	1	15	58.95	919.81	7.32
500	0.1	37	1.0122	1	15	64.22	1114.8	7.45
500	***0.3***	***67***	***0.3036***	***1***	***15***	***52.32***	***997.18***	***7.26***
500	0.3	40	0.7215	1	15	61.14	945.4	7.29
500	0.3	31	1.028	1	15	62.8	1059.4	7.3
500	0.5	50	0.309	1	15	53.32	1057.51	7.26
500	0.5	34	0.7012	1	15	62.33	933.2	7.29
500	0.5	27	1.0246	1	15	71.76	952.3	7.27

The characterization by fin thickness and fin separation is shown in Table 6-1. the fin thickness is chosen as 0.1, 0.3 and 0.5 mm. and separation of fins chosen are 0.3, 0.7 and 1 mm. The flow rate of fluid is 1 L/min. The supply temperature of the fluid Is 15°C. the TDP of the chip is 500Watts. As we can see from the results that two cases of fin geometry are highlighted. These two cases have relatively low component (chip) temperature. Pressure difference shown is between inlet and outlet of the cold plate which contributes in pumping power. The temperature difference between inlet to outlet is remain almost similar for all the cases.

Now case of fin thickness 0.1 and fin thickness 0.3 with component temperature 52.81°C and 52.32°C are to be characterized further by using different fin height.

Table 6-2 Fin height optimization

Fin height mm	Fin thickness mm	Number of fins	Component temperature ^{0}C	Pressure Difference Pa	Temperature difference ^{0}C	Return temperature ^{0}C
3	0.1	101	52.81	919.81	7.26	22.26
4	0.1	101	52.3	964	7.3	22.3
5	0.1	101	58.8	816.4	7.3	22.3
3	0.3	67	52.32	997.18	7.92	22.92
4	***0.3***	***67***	***51.4***	***914.5***	***7.3***	***22.3***
5	0.3	67	54.3	788.4	7.4	22.4

As it can be seen from the obtained results from Table 6-2 that when the fin height is 4 mm, fin thickness is 0.3 mm and number of fins is 67 mm we get the best possible temperature for the component. Which is 51.4°C. the cold plate with this geometry is used for simulations.

6.5 Model for Testing Controls

The schematics shows 4 cold plates connected in parallel representing the cold plate sections as shown in Figure 6-9. Damper is attached at the outlet of the cold plate which will regulate the flow rate based on the temperature sensor which is located in front of it. The pressure sensors at each are just to monitor the pressure drop across the cold plate. There are pressure sensors at the inlet and outlet to look at the overall pressure drop across the system. The flow rate is monitored for every cold plate. Inlet temperature of the coolant is kept constant. Cold plates are used to cool 400W component with 1insq area. This component will be maintained at designed range of temperatures. We will not be reporting the component temperature as it is proportional to the flow rate and temperature rise of the coolant. The coolant considered in the study is water. Initial flow rate of water is set based on the 400Watts power per each component.

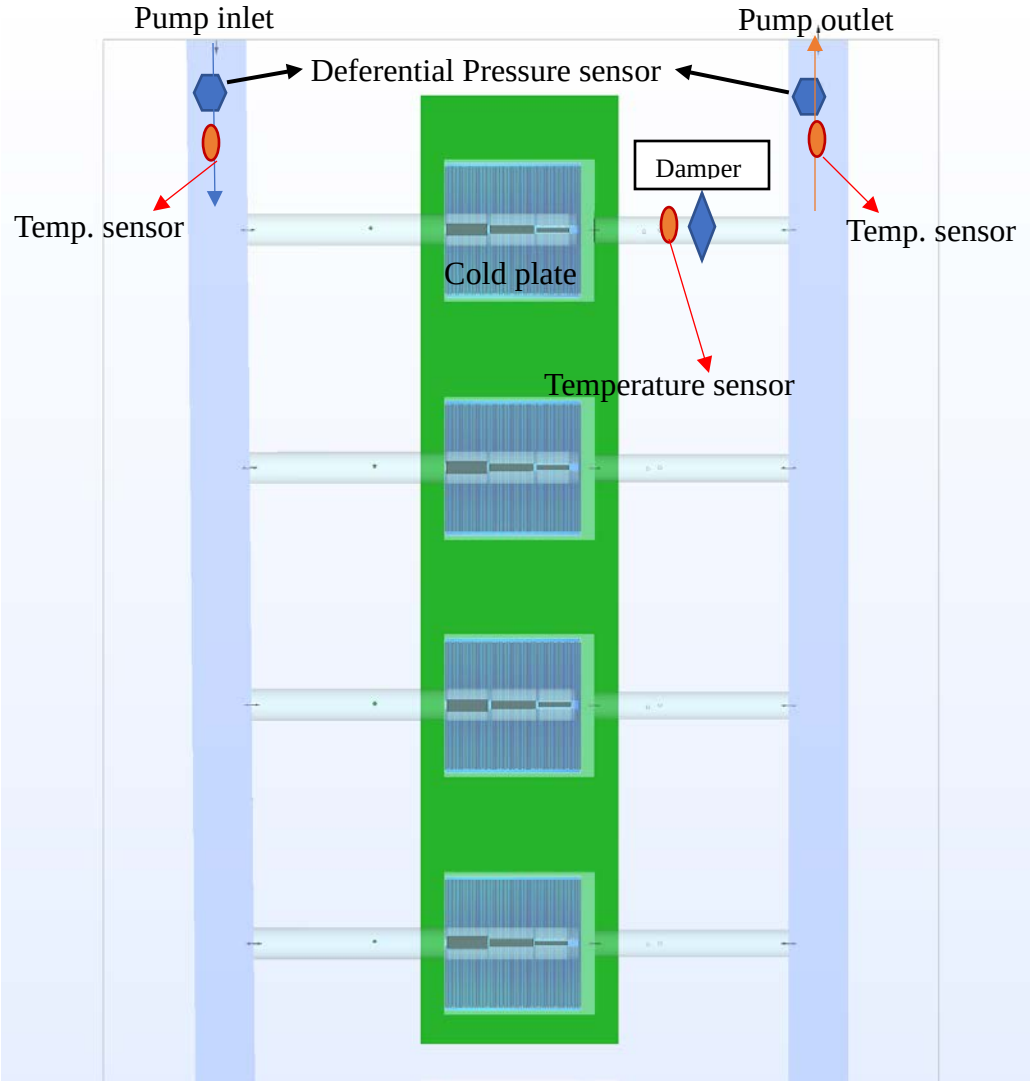

Figure 6-9 6SigmaET model of the model used in testing control strategy

6.6 MATLAB Controls

An initial Control strategy tested is a constant pressure with variable frequency drive pump. This type of pumps will save energy by reducing the

electricity consumption. The flow chart shown in figure 3 shows that the pressure difference across the system will be taken into MATLAB and processed as shown based on the set value. The set value is dependent on the system and varies from system to system.

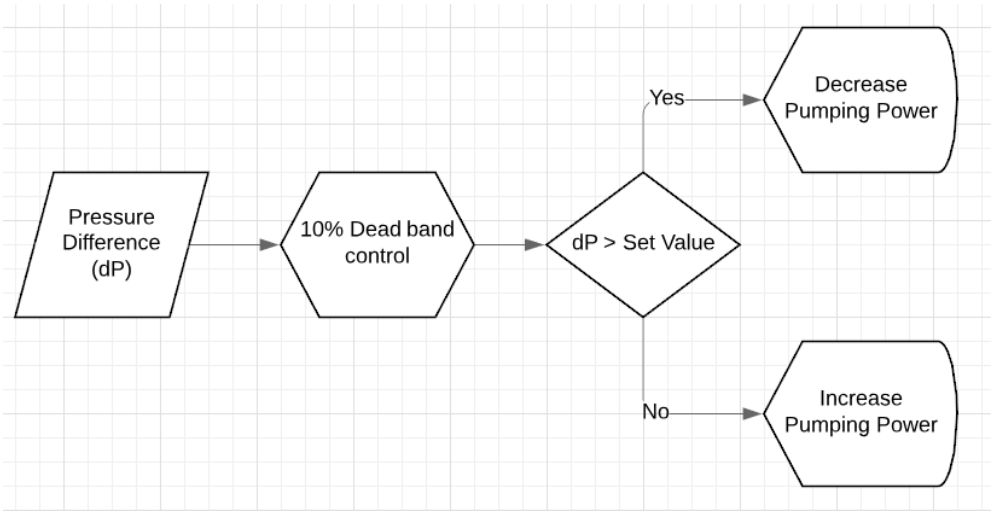

Figure 6-10 Control System Flow Chart

Nitinol FCD experimental results are used to wright the MATLAB coding that mimics the functionality in 6Sigma. The Figure 6-11 shows FCD hysteresis curve that is plotted from MATLAB code. This code is integrated with 6SigmaET to test the control strategy. A separate code in MATLAB is designed just for the controlling the pump by sensing the pressure changes in the system. More than 100 simulations are carried out just to initiate the perfect multi control integration.

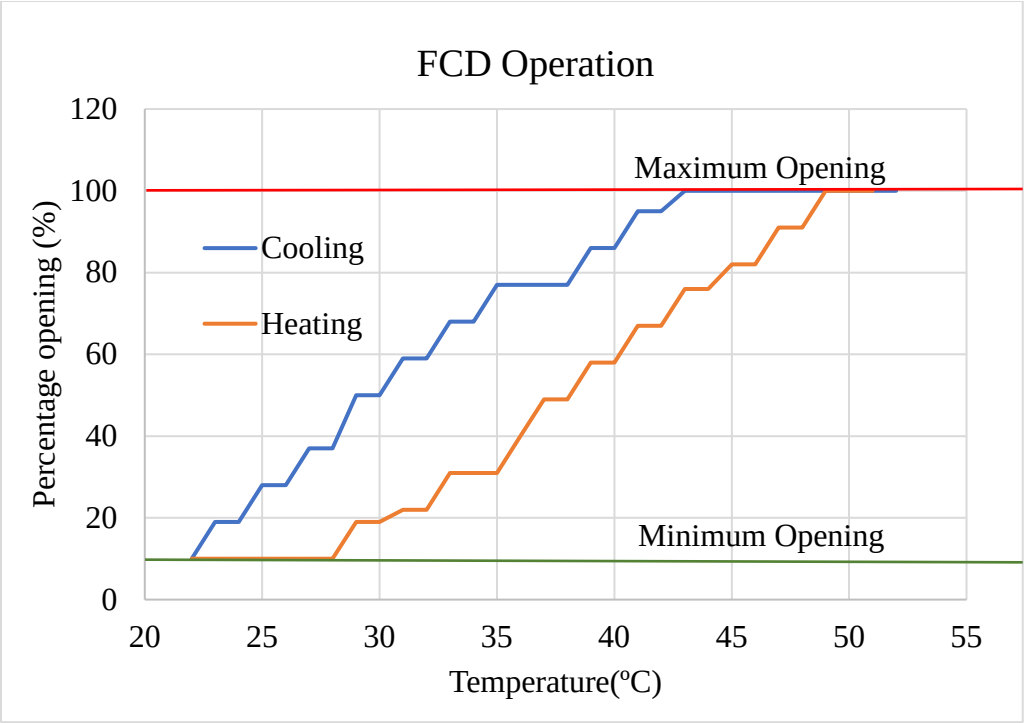

Figure 6-11 FCD hysteresis curve using MATLAB

6.7 Results

6.7.1 System pressure calculation

An initial parametric study was conducted to determine the supply pressure drop to the system. In Table *6-3* supply pressure is varied from 300 to 600 pascal. D1 through D4 represent dampers concerning to different components. The outlet temperature is maintained at a constant 37 degrees Celsius. Red color indicates that box with high damper opening value with same power, whereas green indicates the

least value. Four different of pressure are tested to find out the best pressure. The values D1, D2, D3, D4 indicate respective dampers at the cold plates 1, 2, 3, 4.

Table 6-3 Damper open ratio and pressure drop across the system

Damper % area opening

Pressure (Pa)	D1	D2	D3	D4
300	28.31	40.12	69.98	64.86
400	18.02	20.25	24.3	24.08
500	13.42	14.64	17.69	17.63
600	10.84	11.33	13.96	13.97

Temperature of outlet liquid at the damper

Pressure (Pa)	T1	T2	T3	T4
300	37.11	37.12	37.38	37.28
400	36.92	37.02	37.11	37.12
500	36.99	36.93	36.94	36.95
600	36.95	36.97	37	37.01

It is observed that the damper opening is proportional to component power. The values T1, T2, T3, T4 indicate the outlet temperatures of coolant at the respective cold plate1,2,3,4. Figure shows that at 300 Pa dampers open at different percentages. Once the pressure is more than 400Pa the damper openings are relatively close to each other with a maximum difference of 6% which is good to able to consider 400Pa as the set value for the pressure difference. The temperature values also agree with the damper openings. Only 300Pa pressure drop has elevated outlet temperatures more than 37˚C.

Table 6-4 Simulation Variable samples

Sample No.	Component U1	Component U2	Component U3	Component U4	Total Power
1	100	100	100	100	400
2	100	100	100	200	500
3	100	100	100	300	600
4	100	100	100	400	700
5	100	100	300	300	800
6	100	100	300	400	900
7	100	200	300	400	1000
8	200	200	300	400	1100
9	200	300	300	400	1200
10	200	300	400	400	1300
11	200	400	400	400	1400
12	300	400	400	400	1500
13	400	400	400	400	1600

6.7.2 Control system simulation variables

Control strategy was tested using the sample set provided in Table 6-4 which covered all the possible powers in the taken scenario. There might be 256 number of possible combinations and arrangements with duplicates but, all of them will have a similar power with the selected sample set. This samples are simulated and the data on flow rate, temperature, damper openings and pressure drops are collected for processing.

6.8 Pumping Power

Pumping power is calculated using the flow rate change in the overall system due to the control strategy applied and the pressure drop of the system. Using theoretical calculations that pumping power is equal to the product of flow rate and pressure drop pumping power is calculated for all the samples sets. A shown in Figure 6-12 the pumping power changes based on the system power as FCDs are installed. Pump flow rate will be changes according to the overall system requirements whereas the FCDs will take care of the individual flow rate at the cold plate level. In a no FCD scenario the pumping power will be constant and is directly proportional to the maximum junction temperature of the component in the whole fleet of servers. The green line on top of the chart in Figure 6-12 represents the fixed pumping power line.

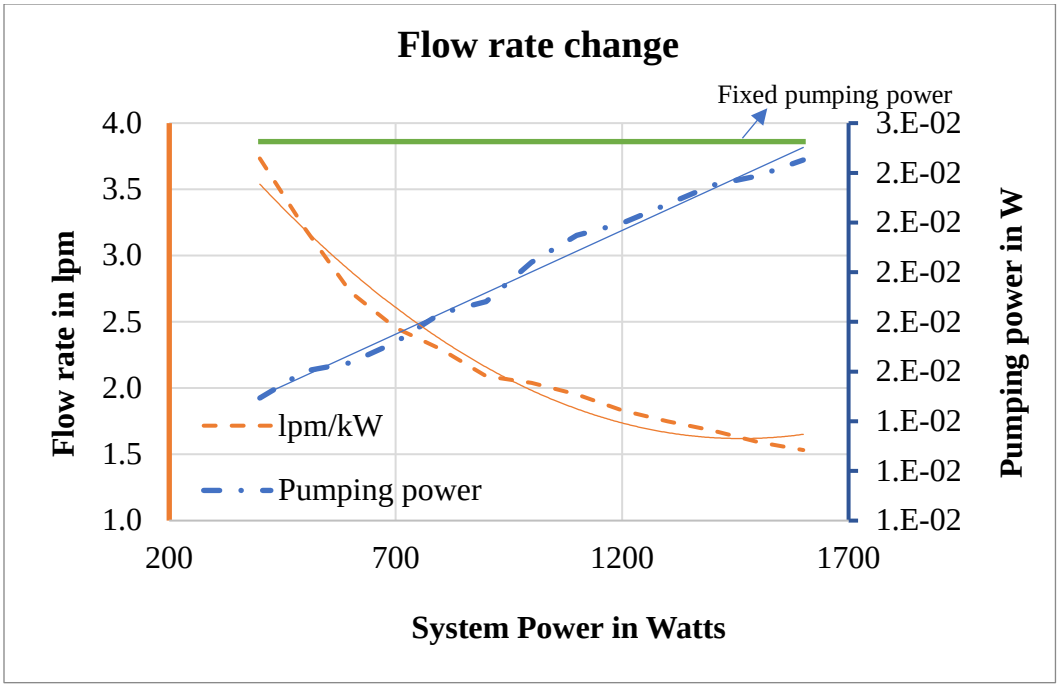

Figure 6-12 Pumping power Vs System power

In an actual application centrifugal pump with a variable frequency drive (VFD) should be able to change the flow rate. The PWM-type VFD normally uses a constant voltage which is pulsed with integrated bi-polar power transistors (IGBT). The sine wave is generated by varying the width of the pulses. The frequency which the transistors are turned on and off by, is called switching frequency. The higher the switching frequency, the better the reproduction of the ideal sine wave [35]. Using this PWM signal we can maintain the required flow rate all times as well as reduce the pumping power during less demand for cooling.

6.9 Dynamic Cooling Savings

6.9.1 Pump savings

This shows that there is potential to save up to 64% pumping power when compare with fixed pumping power. When lpm/kW is compared between the two cases with and without FCD. It is clear that with FCD flow rate requirement is less. This reduces the pumping power by utilizing PWM control on the pumps.

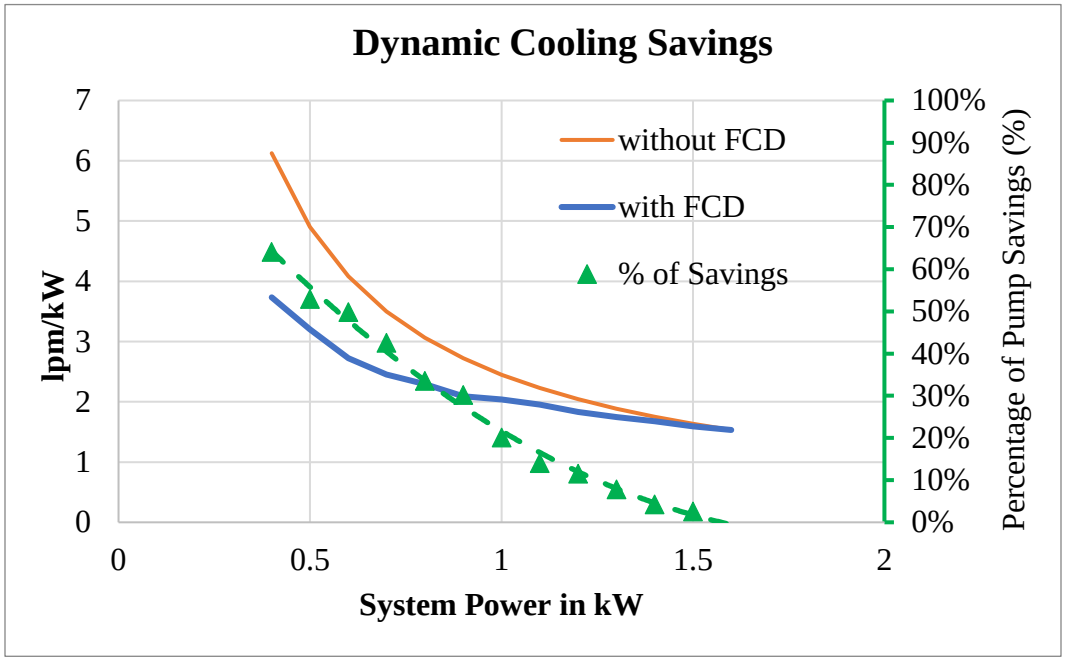

Figure 6-13 Savings due to dynamic cooling

6.9.2 Dynamic cooling PUE

Based on the power consumption of the pump the PUE will be varying. With the test scenarios shown in the results. PUE will be varying between 1.007-1.01. This is only due to pumping power change.

6.10 Experimental Design for Control Strategy Validation

This dynamic control strategy is tested only using CFD analysis. The fallowing experimental setup will can validate it through experiments.

6.10.1 Liquid schematics

A simplified description of the test bench setup to evaluate both cold plates with and without FCDs is depicted in Figure 6-14. A Kinetics RS33AO11 recirculating chiller drives flow through the external loop and cools the plate heat exchanger (HEX) highlighted by the dotted green. The chiller is equipped with a positive displacement pump capable of pumping up to 1.6gpm of coolant at 100psi and a temperature range of -15°C to 75°C. A DC 4-wire pump highlighted in yellow, controls flow of 25% glycol water mixture through all components in the internal loop. Turbine flowmeters arranged in parallel measure the flow rate of water cooled by the plate HEX. Temperature and pressure differences across the cold plate are measured using K-type thermocouple probes and pressure transducers. The pump in the internal loop is primarily responsible for maintaining a flow rate during testing. The pump in the reservoir is responsible to control the

inlet temperature of water to the cold plate by modulating flow rate between the heat exchanger and reservoir. Temperature, Pressure and flow rate readings are input to the LabVIEW code that in-turn controls both pumps. Flow control device at the outlet of each cold plate is responsible for controlling flow rate to each cold plate. Inlet temperatures to the cold plate as low as 15°C are targeted during testing. Water and glycol mixture (50/50) is employed in external loops to enable near zero temperatures to account for heat loss.

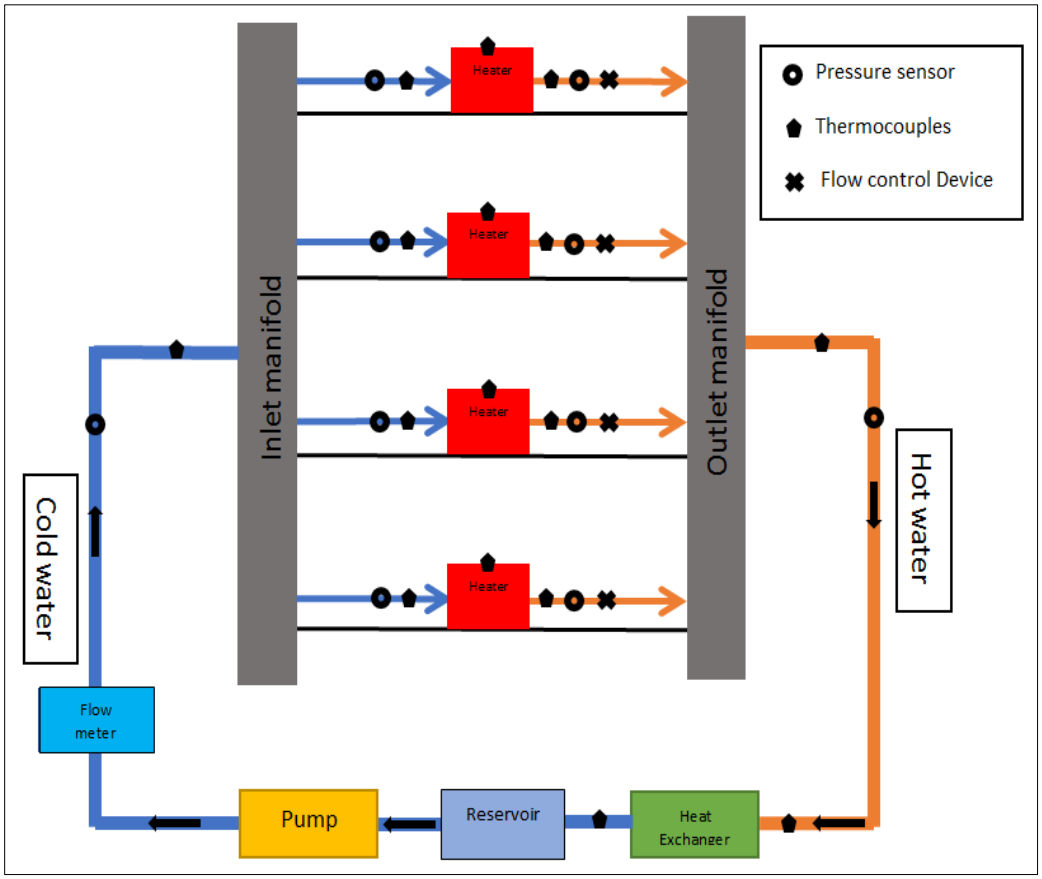

Figure 6-14 Water Circuit schematics and sensor locations

6.10.2 Heater circuit and data collection

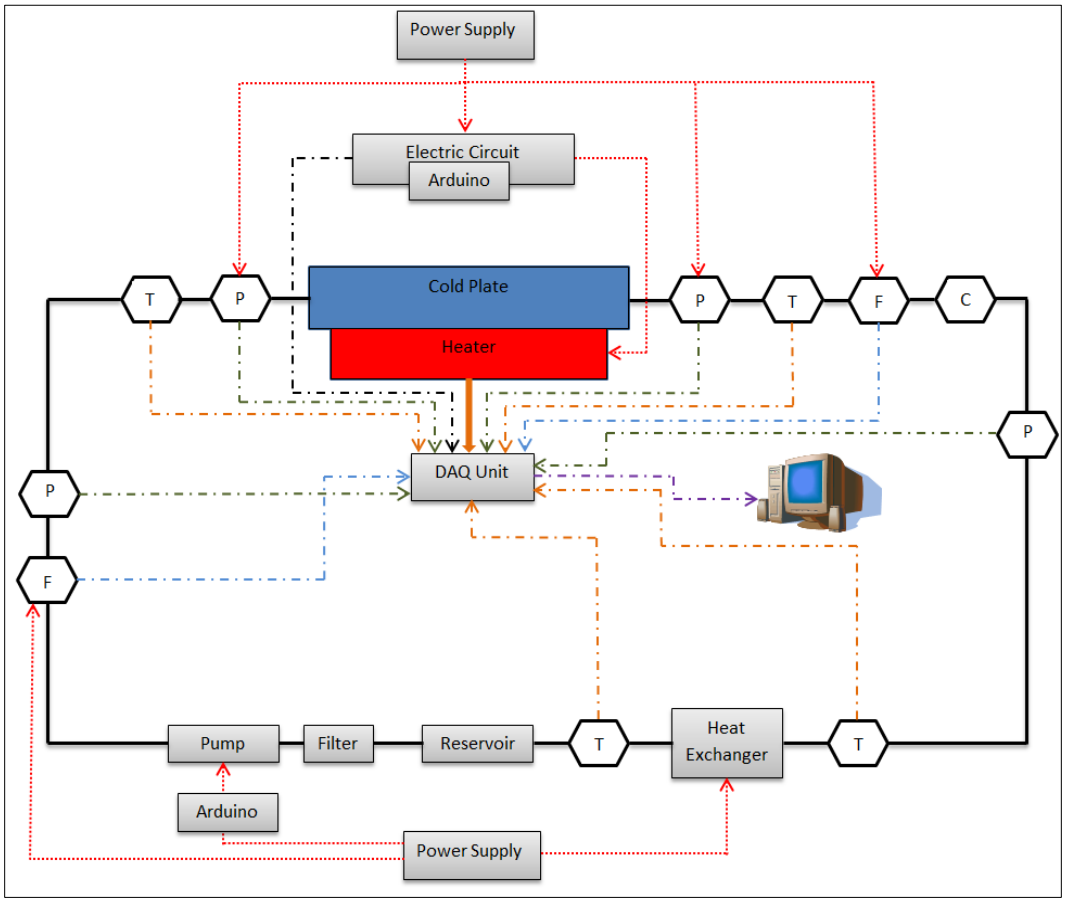

Figure 6-15 Heater electronic circuit and data collection

Figure 6-15 is a detailed simple description of all the inter relation between sensors and control. Figure 4-3 shows the block diagram for the heater circuit. Arduino is used to control the PWM signal for the heater which decides the power generated by the heater. The shunt in series with heater is a current sensor which can be read by the DAQ and to LABVIEW. The designed heater for each cold plate

contains four 1cmsq TTV's, all of these can be controlled using the same PWM signal. On the contrary they can be controlled individually when required.

6.10.3 Test matrix

The TTV's should be subjected to different loads and test the dynamic cooling control strategy. The 13 different cases that are illustrated in Table *6-4* Simulation Variable samples Table *6-4* should be tested. The 4 heaters that are attached to each cold plate should be controlled collectively but the 4 cold plates should have different powers to achieve required load conditions. The cooling power consumption should be quantified for all the cases in Table *6-4*. This should be compared with no FCD condition which will quantify the saving due to dynamic cooling.

6.10.4 FCD future work

FCD optimization is made easy with this experimental setup. There is still some scope for improvement in the FCD design in terms of bypass flow. The gaps between the block and the side walls can be optimized to have more flow towards the nitinol spring. Reliability of the FCD is also a big concern which can be tested and quantified on the reputability and accuracy.

CHAPTER 7

DATA CENTER AIR FLOW OPTIMIZATION

7.1 Open Compute Data Center Design

Figure 7-1 Open compute data center airflow path [36]

The model data center chosen for study is Open computer data center [36] as shown in Figure 7-1. Entire building is used for the movement of cold air through the servers instead of using ductwork. Outside air enters the intake corridor and then the mixing room where the dampers modulate to vary the proportion of outside air and return air depending on temperature and humidity of the outside air. Further the pre-filter followed by a MERV 13 filter, filter the air from contaminants. Air conditioning equipment are used to condition the upstream air to the data center

conditions. Fans are employed to pull the air and send it towards the data center. Fourteen vertical shafts located 16 feet down the center spine of the main aisle open into the data center through which the cold air is guided towards the center cold aisle. The server cabinets are arranged in rows in hot aisle containment configuration. The contained hot aisles extend up to a return air plenum. The return air is directed towards the mixing chamber as well as outside from there.

A case study was taken up to study the airflow pattern and energy consumption of the data center cooling. The main interest is vested in airflow and distributed inside the data center. The 6Sigma room model of supply shaft and cold aisle showed uneven distribution of air in the cold aisle.

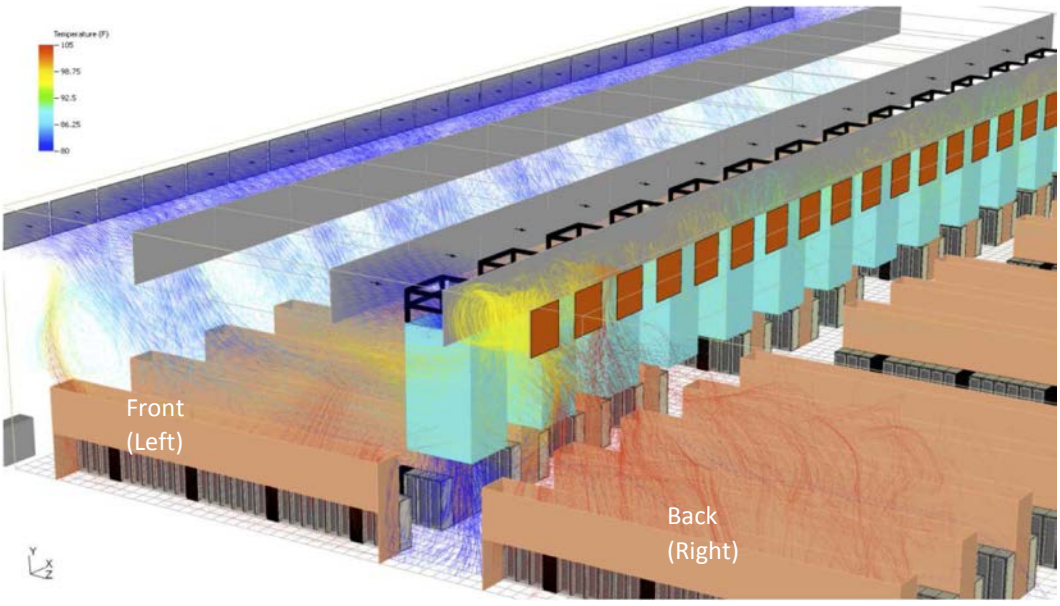

Figure 7-2 data center design in 6Sigma Room CDF tool [36]

7.2 Problem Identification

From the Figure 7-3 it is evident that the right cold aisle receives considerably more air in comparison to the front cold aisle. Approximately 14% difference is observed in the total cooling air received by each aisle.

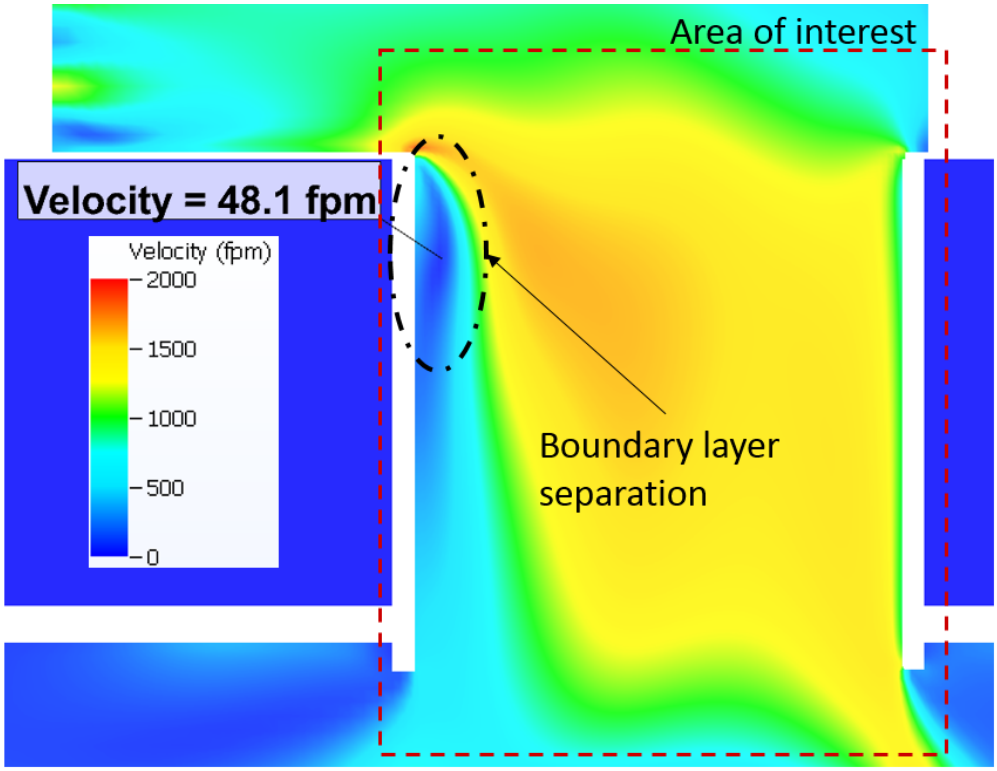

Figure 7-3 original design showing velocity couture

This difference occurs due to the position of the fan arrays. A boundary layer separation can be observed in the inlet shaft which may be the propagating factor of the uneven distribution. This uneven distribution of cooling could hurt the overall

PUE of the datacenter. To understand and eliminate this issue a 6Sigma Room model is designed.

7.3 Simulation Setup

The model with 14 air supply vents is huge and takes at least 10 hours to solve with more 50 million optimized grid nodes. To simplify the problem statement three inlet shafts were modelled in which center supply shaft is studied for the airflow pattern. Three fan arrays were modelled to supply the air to the inlet shaft. This inlet shaft opens into the main cold aisle from where air flows in two opposite directions as shown in Figure 7-5.

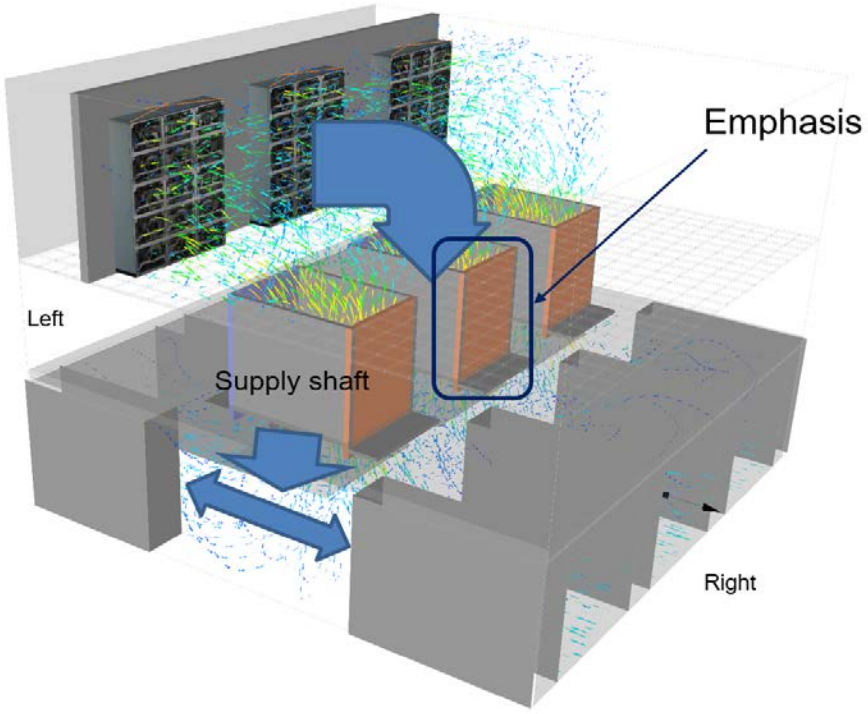

Figure 7-4 Iso-metric view of simulation setup

7.3.1 Optimization variables

Impotent but simple variables in play are left and right angles ɵ and ϕ respectively. These variables are utilized to reduce the non-uniform flow distribution at the supply shaft. Using these variables different parametric studies are conducted to understand the effect of each of them on the air flow distribution in the cold aisle.

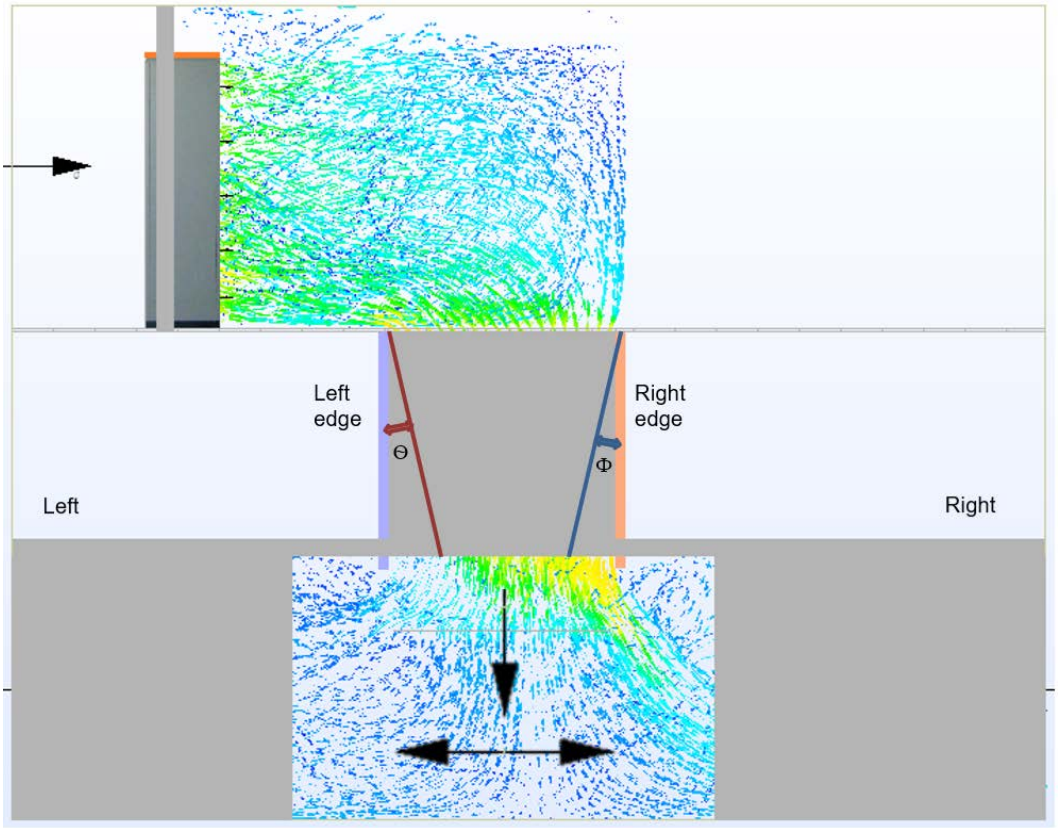

Figure 7-5 Test case experimental model

7.4 Results

Three different parametric studies are promising over the others. One of them is only left angle variation, then right angle variation, finally both angle variation. Each variable has its own impact on the air flow distribution in the cold aisle. As the boundary layer separation occurred towards the left side of the shaft changing the ɵ angle has more beneficial effects on the air flow pattern.

7.4.1 Impact of changing left angle only on airflow

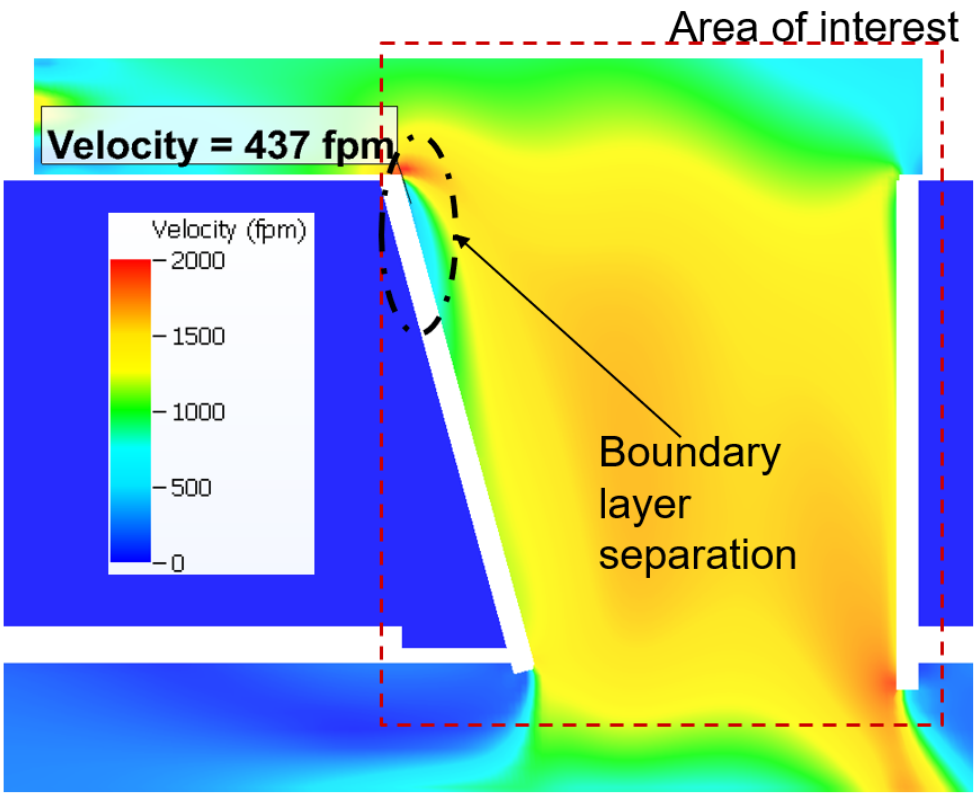

Figure 7-6 Velocity contour when left angle is changed (ɵ= 10º)

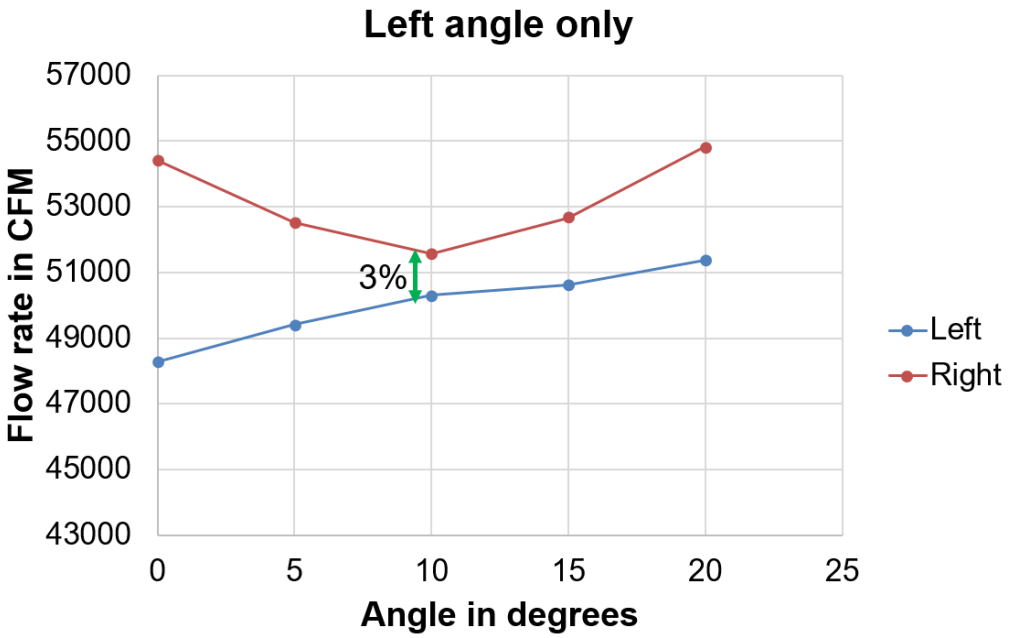

Figure 7-7 Effect of left angle on air flow

Air flow rate difference between the two aisles converge and diverge as the angle change from 0 to 25 degrees. As shown in Figure 7-7 flow difference reduces until 10 degrees which is only 3% between left and right. We can also observe in Figure 7-6 that the flow separation reduced.

7.4.2 Impact of changing right angle only on airflow

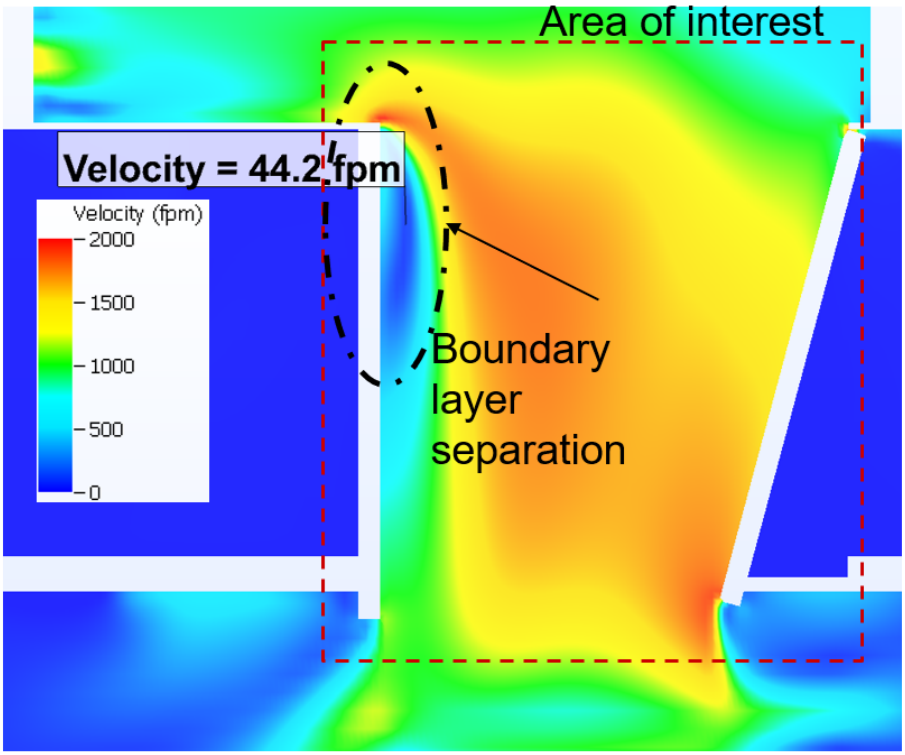

Figure 7-8 Velocity contour when right angle is changed (ϕ = 10º)

Even with the change of the right angle there is no effect on the boundary layer separation. As shown in Figure 7-9. the flow rate between the front and back is on an average of 17%. This implies that the change in the back angle has more impact on the flow distribution. From Figure 7-8 it is evident that the flow separation did not changed. Even the velocity at the separation reduced from the original shaft with-out angle change.

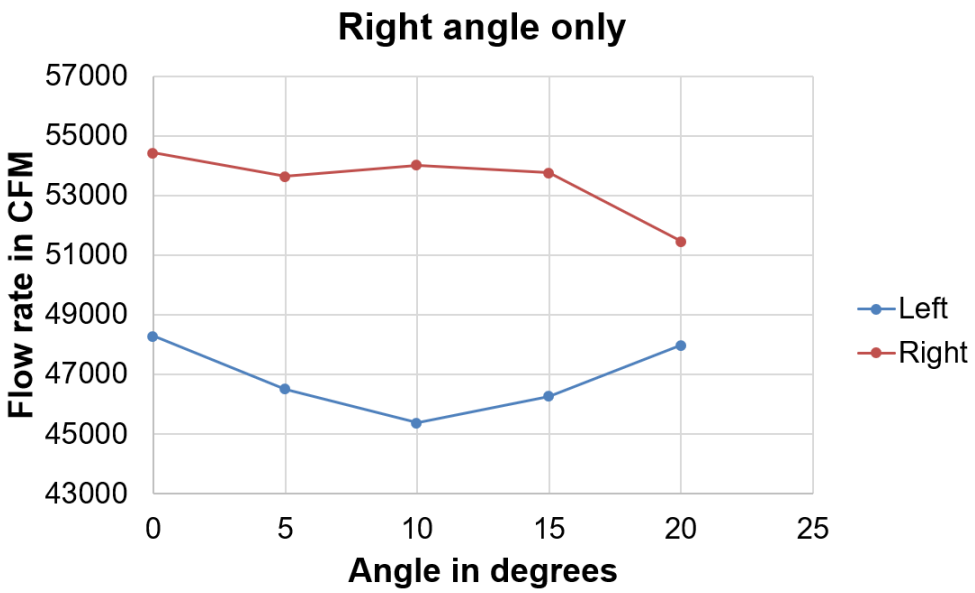

Figure 7-9 Effect of change in right-angle on-air flow

7.4.3 Impact of changing both angles change on airflow

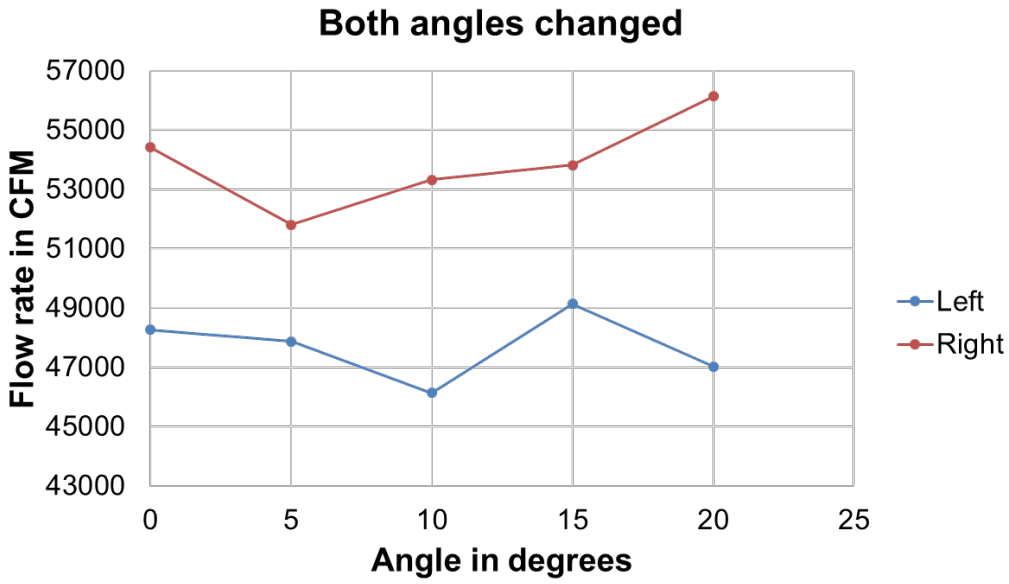

Figure 7-10 effect of change in both the angle on-air flow

Changing both the angles did not help in reducing the flow deference. As shown in Figure 7-10 the flow difference varied without a trend. This imply that changing both angles doesn’t give us much benefit.

Table 7-1: Summary table with parametric study on air flow effect due to change in angles

Left angle (Φ)			Right angle (Θ)			Left(CFM)	Right(CFM)	Left (CFM)	Right (CFM)	Left (CFM)	Right (CFM)
0	0	0	0	0	0	45527	53471	48270	54416	40591	49406
5	5	5	5	5	5	45963	50098	47865	51805	45517	50090
10	10	10	10	10	10	45694	50628	46139	53324	44531	51520
15	15	15	15	15	15	47766	47686	49138	53822	45063	48660
20	20	20	20	20	20	42555	48492	47025	56142	44697	51812
								Left (CFM)	Right (CFM)		
0	0	0	0	0	0	45527	53471	48270	54416	40591	49406
5	5	5	0	0	0	44512	50975	46513	53639	44262	50554
10	10	10	0	0	0	44736	51342	45368	54012	43854	51050
15	15	15	0	0	0	46238	50716	46271	53753	44043	50915
20	20	20	0	0	0	48001	48121	47996	51449	45225	49567
								Left (CFM)	Right (CFM)		
0	0	0	0	0	0	45527	53471	48270	54416	40591	49406
0	0	0	5	5	5	45641	50173	49415	52516	44993	49984
0	0	0	10	10	10	45730	48654	50306	51562	45389	48607
0	0	0	15	15	15	45083	48957	50614	52669	44812	48413
0	0	0	20	20	20	44569	48952	51373	54821	45150	48163

Both angles change Left angle change Right angle change Dark indicates high flow rate

7.5 Future work

However, there are other optimizations possible which require additional structure build into the existing structure to have a uniform air distribution.

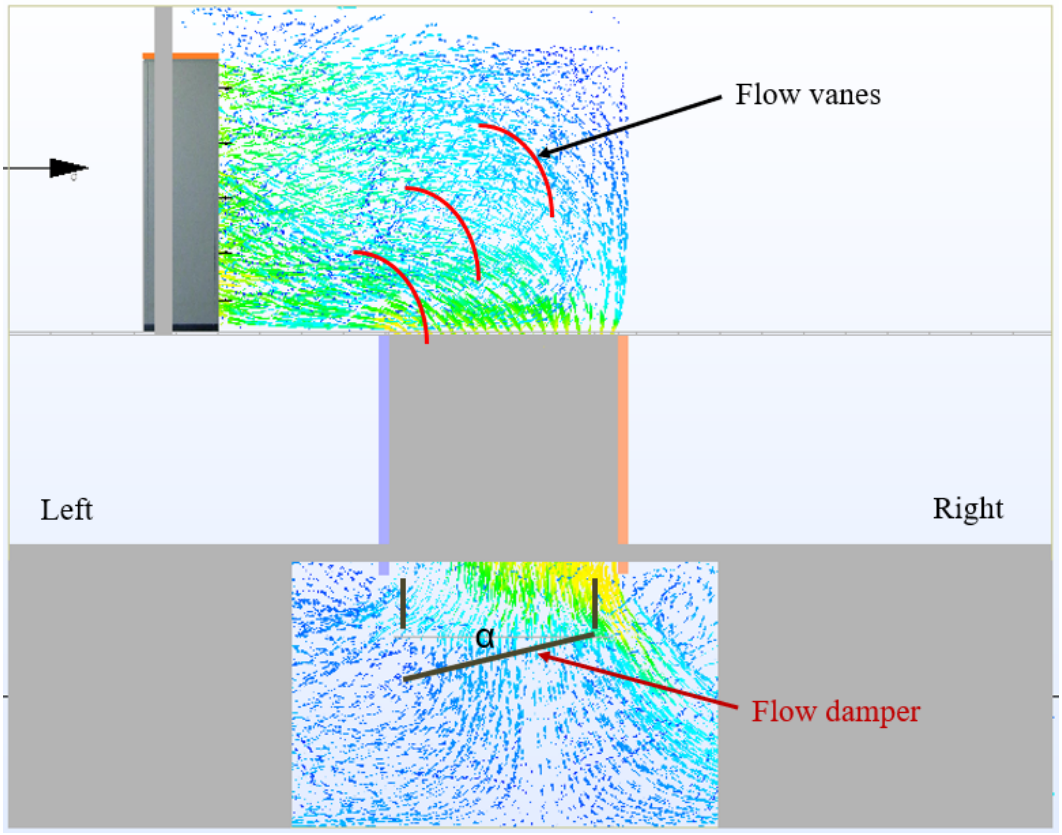

Figure 7-11 Supply shaft future optimization

7.5.1 Flow vanes

Introducing flow vanes will create a good streamline flow without any recirculation's at the top of the supply duct. The number of vanes depend on the

dimensions of the supply shaft. For the existing design can have three to five vanes to have a good flow distribution. A multi-variable analysis can be performed on the vane x and y positions to optimize the even flow at the bottom of the supply shaft. The length of the vane can be optimized to reduce the recirculation's in the supply duct.

7.5.2 Dampers

The damper after the supply duct could be potentially an alternative solution. In this a perforated damper can be built at the bottom of the duct to achieve the uniform distribution between the left and right cold aisles. This solution can potentially be used to divert the air to the required aisle between left and right based on the IT load. A dynamic control could be developed to control the damper angle proportional to the IT load of the aisle.

CHAPTER 8

CONCLUSION

To deal with the continued growth of the data center industry which increases the load on the national electricity grid, there is a need to boost energy-efficiency within such facilities. Specifically, targeting improvements in cooling systems at different levels with the data center is necessary. In the reported series of studies, module, server, rack and data center level evaluations of single-phase air and liquid cooling solutions are outlined as follows.

8.1 Dynamic single-phase liquid Cooling

The dynamic cold plate works better with an array of smart flow control devices, which effectively does the job of the combination of a temperature sensor, control system and an actuator. The flow control device uses an active material which rotates the damper with respect to change in temperature. From detailed experimental study it is observed that one-way nitinol is better than two-way nitinol owing to lower hysteresis. The novel dual spring setup allows for one-way nitinol to be mechanically loaded at room temperature. From extensive experimentation on Nitinol springs to estimate force during phase change and displacement characteristics optimum spring selection was possible. An FCD was designed and manufactured to vary flow rates based on required temperature difference. The FCD prototype was able to produce 0.1 lpm change in flow rate when operated

between 25°C and 45°C. This concept can be scaled to required use and operated for the required temperatures between 35°C and 65°C.

Miniaturization of FCD is required for the dynamic cold plate form factor fallowed by the material characterization. To have better control over the flow rate, the rectangular butterfly valve design is better than the traditional circular butterfly valve because it varies flow rate more linearly with change of angle. Through CFD analysis a damper ratio of 1.2 is good in linearizing the flow. This can also possibly find applications in different fields apart from data center water cooling. The hydrodynamic forces on the damper helped to understand the optimized damper ratio. With the selected damper ratio 24% more flow rate change can be achieved.

It is very important to have a good control strategy in order to implement the dynamic cooling solution. In this study, a novel control strategy was developed and tested to save overall pumping power at a rack and data center level. Implementation of dynamic cooling along with Flow control device is effective with a good control strategy. The control strategy developed is tested using simulations in 6sigmaET. Pressures are calculated for individual components at 100% possible flow rate, and then cumulative pressure is given as a pressure boundary condition to the system for the first methodology adopted whereas maximum temperature that a cold plate can bare for a given area is an addition to the former in the second methodology. The controls are optimized to have only

single sensor input to control the VFD pump. Various possible powers are varied and tested to show how Dynamic cooling and FCD help saving pumping power. It is proven that the control strategy is fully functional with the test setup developed in 6SigmaET. A 64% variation of pumping power is observed in the iterations performed.

8.2 Data center airflow optimization

Open compute data center design is analyzed and identified uneven air flow distribution. The air flow distribution between left and right aisles is optimized by changing the angle of the supply shaft. As mentioned in 7.3 the angles are changed between 0° to 25° and flow is analyzed. Airflow distribution between the left and right aisles was reduced 14% to 3%. This will reduce the over-all energy consumption in the data center cooling.

APPENDIX A

NOTES AND SUPPLEMENTARY FIGURES

Funding

Work presented here is supported by the National Science Foundation Industry/University Collaborative Research Center for Energy Smart Electronic Systems (ES2) under Grant No. IIP - 1134821. Any opinions, findings, and conclusions or recommendations expressed in this material are those of the author(s) and do not necessarily reflect the views of the National Science Foundation.

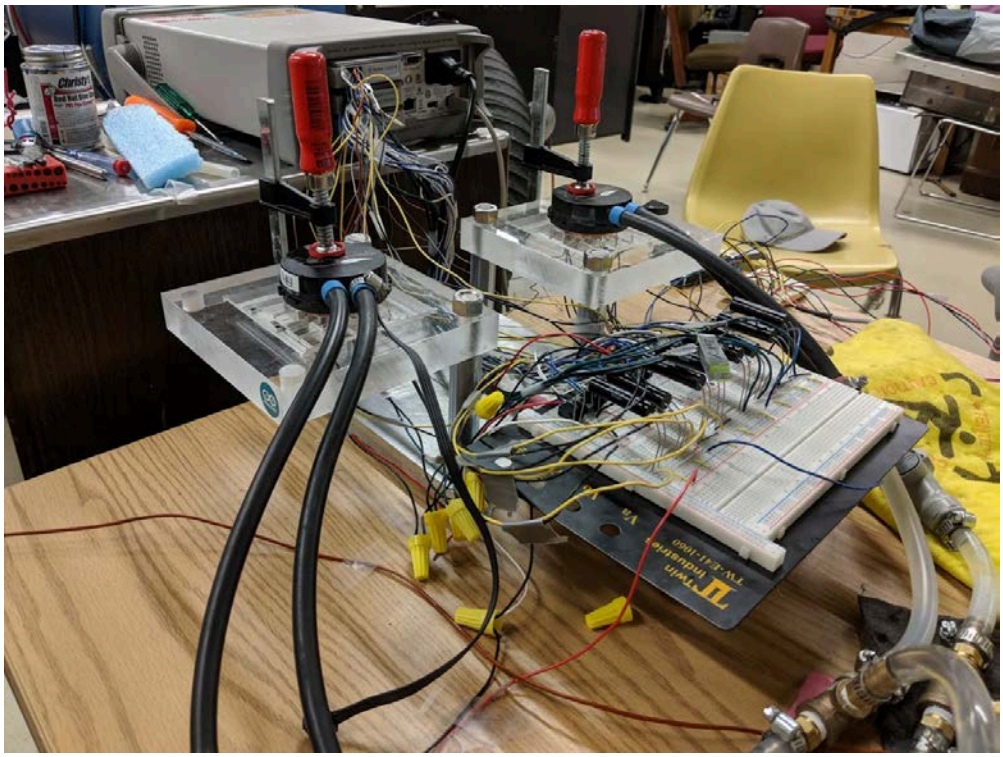

Figure 0-1 Heater circuit

Figure 0-2 Experimental setup in progress for Control Strategy Validation

REFERENCES

[1] M. Rouse, “What is internet of things (IoT)_ - Definition from WhatIs,” *Tech Target*. p. TechTarget, 2016.

[2] A. Shehabi *et al.*, “United States Data Center Energy Usage Report,” 2016.

[3] J. Whitney and P. Delforge, “Data Center Efficiency Assessment,” 2014.

[4] H. Geng, *Data Center Handbook*. Wiley Blackwell, 2014.

[5] V. Avelar, S. Electric, D. Azevedo, A. French, and E. Network Power, “PUE^{TM}: A COMPREHENSIVE EXAMINATION OF THE METRIC EDITORS.”

[6] “Harmonizing Global Metrics for Data Center Energy Efficiency Harmonizing Global Metrics for Data Center Energy Efficiency Global Taskforce Reaches Agreement Regarding Data Center Productivity,” 2014.

[7] UptimeInstitute, “Annual Data Center Survey Results,” 2019.

[8] ASHRAE, “Best Practices for Datacom Facility Energy Efficiency,” 2016.

[9] T. C. ASHRAE, “2011 Thermal Guidelines for Data Processing Environments–Expanded Data Center Classes and Usage Guidance,” *Data Process.*, pp. 1–45, 2011.

[10] B. Agostini, M. Fabbri, J. E. Park, L. Wojtan, J. R. Thome, and B. Michel, “State of the art of high heat flux cooling technologies,” *Heat Transf. Eng.*, vol. 28, no. 4, pp. 258–281, 2007.

[11] L. A. Barroso and U. Hölzle, “The Case for Energy-Proportional Computing,” *Computer (Long. Beach. Calif).*, vol. 40, no. 12, p. 33, Dec. 2007.

[12] R. C. Chu, U. P. Hwang, and R. E. Simons, “Conduction Cooling for an LSI Package: A One-Dimensional Approach,” *IBM J. Res. Dev.*, vol. 26, no. 1, pp. 45–54, 1982.

[13] D. J. Delia *et al.*, “System cooling design for the water-cooled {IBM Enterprise System\slash 9000} processors,” *IBM J. Res. Dev.*, vol. 36, no. 4, pp. 791–803, 1992.

[14] R. C. Chu, R. E. Simons, M. J. Ellsworth, R. R. Schmidt, and V. Cozzolino, “Review of cooling technologies for computer products,” *IEEE Trans. Device Mater. Reliab.*, vol. 4, no. 4, pp. 568–585, 2004.

[15] J. Fernandes, S. Ghalambor, D. Agonafer, V. Kamath, and R. Schmidt, “Multi-design variable optimization for a fixed pumping power of a water-cooled cold plate for high power electronics applications,” *Intersoc. Conf. Therm. Thermomechanical Phenom. Electron. Syst. ITHERM*, pp. 684–692, 2012.

[16] U. P. Hwang, K. P. Moran, and R. G. Kemink, “Cold Plate Design for IBM ES/9000 TCM Electronic Modules,” *Proc.Advances Electron. Packag.*, p. 1, 1992.

[17] J. Fernandes *et al.*, “Combining Computational Fluid Dynamics (CFD) and Flow Network Modeling (FNM) for design of a Multi-Chip Module (MCM) cold plate,” in *ASME 2013 International Technical Conference and Exhibition on Packaging and Integration of Electronic and Photonic Microsystems*, 2013, p. V002T08A053.

[18] R. Mahajan, C. P. Chiu, and G. Chrysler, “Cooling a microprocessor chip,” *Proc. IEEE*, vol. 94, no. 8, pp. 1476–1485, 2006.

[19] M. Sahini *et al.*, “Rack-level study of hybrid cooled servers using warm water cooling for distributed vs. centralized pumping systems,” *Annu. IEEE Semicond. Therm. Meas. Manag. Symp.*, pp. 155–162, 2017.

[20] D. B. Tuckerman and R. F. W. Pease, “High-Performance Heat Sinking for VLSI,” *IEEE Electron Device Lett.*, vol. EDL-2, no. 5, pp. 126–129, 1981.

[21] H. Y. Zhang, D. Pinjala, T. N. Wong, K. C. Toh, and Y. K. Joshi, “Single-phase liquid cooled microchannel heat sink for electronic packages,” *Appl. Therm. Eng.*, vol. 25, no. 10, pp. 1472–1487, Jul. 2005.

[22] S. Lee, S. Song, V. Au, and K. P. Moran, “cONSTRICTION/SPREADING RESISTANCE MODEL FOR ELECTRONICS PACKAGING.”

[23] W. Qu and I. Mudawar, “Experimental and numerical study of pressure drop and heat transfer in a single-phase micro-channel heat sink,” *Int. J. Heat Mass Transf.*, vol. 45, no. 12, pp. 2549–2565, Apr. 2002.

[24] “i3 electronics – Discover the Latest Technology with i3.” [Online]. Available: http://i3electronics.com/. [Accessed: 19-Dec-2019].

[25] J. E. Fernandes, “MINIMIZING POWER CONSUMPTION AT MODULE, SERVER AND RACK-LEVELS WITHIN A DATA CENTER THROUGH DESIGN AND ENERGY-EFFICIENT OPERATION OF DYNAMIC COOLING SOLUTIONS,” 2015.

[26] P. Soni, “Performance Evaluation of Plate-fin and Pin-fin Heat Sinks for The Application of Oil Immersion Cooling and Design Optimization of Dynamic Cold Plate for The Application of Warm Water cooling,” 2016.

[27] R. K. Kokate, “EXPERIMENTAL ANALYSIS VALIDATING A CONTROL SCHEME TO DEVELOP A DYNAMIC COOLING SOLUTION FOR NON-UNIFORM HIGH POWERED ELECTRONIC DEVICES IN DATA CENTER,” 2015.

[28] U. Chowdhury, M. Sahini, A. Siddarth, D. Agonafer, and S. Branton, “Characterization of an isolated hybrid cooled server with failure scenarios using warm water cooling,” in *ASME 2017 International Technical Conference and Exhibition on Packaging and Integration of Electronic and Photonic Microsystems, InterPACK 2017, collocated with the ASME 2017 Conference on Information Storage and Processing Systems*, 2017.

[29] A. Del Toro, M. C. Johnson, and R. E. Spall, “Computational Fluid Dynamics Analysis of Butterfly Valve. Performance factors.,” *J. Am. Water Work. Assoc.*, no. 1957, pp. 243–255, 2015.

[30] S. Ruth, “Reducing ICT-related carbon emissions: An exemplar for global energy policy,” *IETE Tech. Rev. (Institution Electron. Telecommun. Eng. India)*, vol. 28, no. 3, pp. 207–211, May 2011.

[31] S. Forge, “Powering down: remedies for unsustainable ICT The problem of sustainable ICT.”

[32] M. Pawlish, A. S. Varde, and S. A. Robila, “Analyzing utilization rates in data centers for optimizing energy management,” *2012 Int. Green Comput. Conf. IGCC 2012*, no. June, 2012.

[33] Miller Rich, “Google Shifts to Liquid Cooling for AI Data Crunching,” 2018. [Online]. Available: https://datacenterfrontier.com/google-shifts-to-liquid-cooling-for-ai-data-crunching/. [Accessed: 21-Dec-2019].

[34] CoolIT, “CoolIT Rack DCLC: Reliable Direct Liquid Cooling for the world’s most demanding Data Centers.”

[35] ITT Industries, “Variable Frequency Drive Recommendations.”

[36] E. Frachtenberg, D. Lee, M. Magarelli, V. Mulay, and J. Park, “Thermal design in the open compute datacenter,” *Intersoc. Conf. Therm. Thermomechanical Phenom. Electron. Syst. ITHERM*, vol. 94025, pp. 530–538, 2012.

[37] Pravin A Shinde, Pratik V Bansode, Satyam Saini, Rajesh Kasukurthy, Tushar Chauhan, Jimil M Shah and Dereje Agonafer, 2019, Experimental analysis for optimization of thermal performance of a server in single phase immersion cooling, *ASME Conference Paper No. IPACK2019-6590*

[38] Gautham Thirunavakkarasu, Satyam Saini, Jimil Shah, Dereje Agonafer,2018, Airflow pattern and path flow simulation of airborne particulate contaminants in a high-density Data Center utilizing Airside Economization, *ASME Conference Paper No. IPACK2018-8436*

[39] Kumar, A., Shahi, P., & Saha, S. K. Experimental Study of Latent Heat Thermal Energy Storage System for Medium Temperature Solar Applications.

[40] Sarker, Md Rashedul H, ASM Raufur Chowdhury, and Norman Love. “Prediction of Gas–Solid Bed Hydrodynamics Using an Improved Drag Correlation for Nonspherical Particles.” Proceedings of the Institution of Mechanical Engineers, Part C: Journal of Mechanical Engineering Science 231, no. 10 (May 2017): 1826–38. doi:10.1177/0954406215622652.

[41] Chaudhari, Mugdha, A S M Raufur Chowdhury, Unique Rahangdale, Abel Misrak, Pavan Rajmane, Aniruddha Doiphode, and Dereje Agonafer. 2019. "Reliability Assessment of BGA Solder Joints - Megtron 6 VS FR4 Printed Circuit Boards." SMTA International. Rosemont, IL, USA: SMTA International

BIOGRAPHICAL INFORMATION

Rajesh Kasukurthy received his bachelor's degree (B. Tech) in Mechanical Engineering from Jawaharlal Nehru Technological University Kakinada, University College of Engineering Vizianagaram (JNTU-Vizianagaram), Andhra Pradesh, India. He began his graduate school at The University of Texas at Arlington in August 2014. He worked on data center evaporative cooling as a part of his master's thesis. He earned his MSc in Mechanical Engineering in August 2016. His interest in the field of electronic cooling made him continue this doctoral degree from the fall 2016. He conducted research on liquid cooling at the component and server level and air cooling at the data center during his time at UTA. He worked on NSF funded projects in collaboration with several industries. He interned two times at Facebook Inc. He received his PhD degree in Mechanical Engineering from The University of Texas at Arlington in December 2019.